ABSTRACT

Extremal Conditions in Early Universe Cosmology

Jeffrey S. Lee, Ph.D.

Mentor: Gerald B. Cleaver, Ph.D.

Some aspects of Special Relativity have remained largely unresolved and unexplored even after more than a century since its formulation; this is particularly true in the case of relativistic thermodynamics. Attempts to derive a relativistic temperature transformation have met with limited success, particularly when trying to transform a scalar temperature. Much more credible results have emerged when the inverse temperature (a van-Kampen Israel future-directed timelike 4-vector) was invoked. In this dissertation, the first self-consistent formulations of the relativistic Wien's Displacement Law and the relativistic Stefan-Boltzmann Law are presented. Also examined is the use of occupation number and the inverse temperature 4-vector to justify temperature inflation of the Cosmic Microwave Background for any relativistic observer. The interaction of the Hawking spectrum of a 1 attometer (10^{-18} m) primordial black hole with an incoming composite particle reveals that when a primordial black hole reaches the Planck scale, its absorptivity and emissivity cause it to effectively become a white hole for the final instant of its existence.

Extremal Conditions in Early Universe Cosmology

by

Jeffrey S. Lee, H.B.Sc., B.Ed., M.Sc., M.A.

A Dissertation

Approved by the Department of Physics

____

Lorin Swint Matthews, Ph.D., Chairperson

Submitted to the Graduate Faculty of
Baylor University in Partial Fulfillment of the
Requirements for the Degree
of

Doctor of Philosophy

Approved by the Dissertation Committee

____

Gerald Cleaver, Ph.D., Chairperson

____

Anzhong Wang, Ph.D.

____

Lorin Swint Matthews, Ph.D.

____

Dwight Russell, Ph.D.

____

Peter James, Ph.D.

Accepted by the Graduate School
December 2021

____

J. Larry Lyon, Ph.D., Dean

Page bearing signatures is kept on file in the Graduate School.

TABLE OF CONTENTS

LIST OF FIGURES

LIST OF TABLES

LIST OF ABBREVIATIONS

CMB	Cosmic Microwave Background (Radiation)
DSR	Doubly Special Relativity
LAB	Luminous Astrophysical Body
PBH	Primordial Black Hole
QCD	Quantum Chromodynamics
QED	Quantum Electrodynamics
QFT	Quantum Field Theory
RWDL	Relativistic Wien's Displacement Law
TPP	Trans-Planckian Problem
WH	White Hole

ACKNOWLEDGMENTS

I would like to acknowledge my dissertation advisor, Dr. Gerald Cleaver, and my dissertation committee members Dr. Anzhong Wang, Dr. Lorin Swint-Matthews, Dr. Dwight Russell, and Dr. Peter James.

DEDICATION

To my late mother Joan Lee whose steadfast support of me throughout my life made this dissertation possible.

ATTRIBUTIONS

J. S. Lee and G. B. Cleaver, “Apparent Ultra-Relativistic Energy Density Inflation of Astrophysical Bodies into Apparent Black Stars," *Journal of Applied Physical Science International*, vol. 9, no. 2, pp. 51-53, 2017.

In this paper (Chapter Two), Jeffrey S. Lee conceptualized the idea for the paper, performed the calculations, and wrote the paper. Gerald B. Cleaver verified the calculations, proofread the paper, and was the corresponding author with the journal. Corrections requested by the journal were made by Jeffrey S. Lee.

J.S. Lee and G. B. Cleaver, “The Relativistic Blackbody Spectrum in Inertial and Non-Inertial Reference Frames,” New Astronomy, Volume 52, 9 October 2016. arXiv:1507.06663

In this paper (Chapter Three), Jeffrey S. Lee conceptualized the idea for the paper, performed the calculations, created the graphs, and wrote the paper. Gerald B. Cleaver verified the calculations, proofread the paper, suggested edits for the graphs, and was the corresponding author with the journal. Corrections requested by the journal were made by Jeffrey S. Lee.

J.S. Lee, and G.B. Cleaver, “Black Sun: Ocular Invisibility of Relativistic Luminous Astrophysical Bodies,” Journal of High Energy Physics, Gravitation and Cosmology, 2, pp. 562-570., 12 September 2016. http://dx.doi.org/10.4236/jhepgc.2016.24048.

In this paper (Chapter Four, Jeffrey S. Lee conceptualized the idea for the paper, performed the calculations, performed the simulations, created the graphs, and wrote the paper. Gerald B. Cleaver verified the calculations, proofread the paper, suggested edits for the graphs, and was the corresponding author with the journal. Corrections requested by the journal were made by Jeffrey S. Lee.

J.S. Lee and G. B. Cleaver, "Relativistic Drag and Emission Radiation Pressures in an Isotropic Photonic Gas," Modern Physics Letters A, Volume 31, Issue 19, 21 June 2016. arXiv:1508.00534.

In this paper (Chapter Five), Jeffrey S. Lee conceptualized the idea for the paper (including selecting the published paper to be challenged), performed the calculations, created the graphs, and wrote the paper. Gerald B. Cleaver verified the calculations, proofread the paper, suggested edits for the graphs, and was the corresponding author with the journal. Corrections requested by the journal were made by Jeffrey S. Lee.

J.S. Lee and G. B. Cleaver, "Ultra-relativistic Thermodynamics and Aberrations of the Cosmic Microwave Background Radiation," Modern Physics Letters A, Volume 30, Issue 09, 21 March 2015.

In this paper (Chapter Six), Jeffrey S. Lee conceptualized the idea for the paper, performed the calculations, created the graphs, and wrote the paper. Gerald B. Cleaver verified the calculations, proofread the paper, suggested edits for the graphs, and was the corresponding author with the journal. Corrections requested by the journal were made by Jeffrey S. Lee.

J.S. Lee and G. B. Cleaver, "White holes as the asymptotic limit of evaporating PBHs," International Journal of Modern Physics A, Volume 31, Number 30, 24 October 2016.

In this paper (Chapter Seve), Jeffrey S. Lee conceptualized the idea for the paper, performed the calculations, performed the simulations, created the graphs, and wrote the paper. Gerald B. Cleaver verified the calculations, proofread the paper, suggested edits for the graphs, and was the corresponding author with the journal. Corrections requested by the journal were made by Jeffrey S. Lee.

CHAPTER ONE

Introduction

The Special Theory of Relativity has fascinated physicists since its 1905 elucidation in Einstein's seminal paper *On the Electrodynamics of Moving Bodies* [1]. It firmly established the speed of light as "nature's speed limit" and dispatched Lord Kelvin's certitude that "one thing we are sure of, and that is the reality and substantiality of the luminiferous ether." [2] Special Relativity (SR) quickly provided, in a cogent framework, a consistent and seemingly irrefutable description of numerous physical quantities (e.g., distance, velocity, momentum, kinetic energy, etc.) under relativistic conditions. A Lorentz covariant 4-vector in frame X is related to its equivalent in frame X' by $X' = B(v)X$, where the boost matrix $B(v)$ given by

$$B(v) = \begin{bmatrix} \gamma & -\gamma\frac{v_x}{c} & -\gamma\frac{v_y}{c} & -\gamma\frac{v_z}{c} \\ -\gamma\frac{v_x}{c} & 1+(\gamma-1)\frac{v_x^2}{v^2} & (\gamma-1)\frac{v_x v_y}{v^2} & (\gamma-1)\frac{v_x v_z}{v^2} \\ -\gamma\frac{v_y}{c} & (\gamma-1)\frac{v_y v_x}{v^2} & 1+(\gamma-1)\frac{v_y^2}{v^2} & (\gamma-1)\frac{v_y v_z}{v^2} \\ -\gamma\frac{v_z}{c} & (\gamma-1)\frac{v_z v_x}{v^2} & (\gamma-1)\frac{v_z v_y}{v^2} & 1+(\gamma-1)\frac{v_z^2}{v^2} \end{bmatrix}. \tag{1.1}$$

Also, $v = \left(v_x^2 + v_y^2 + v_z^2\right)^{\frac{1}{2}}$ is the velocity magnitude, and $\gamma = \left(1 - v^2\right)^{-\frac{1}{2}}$ is the Lorentz factor. For a Lorentz boost in the *x* direction, the $X' = B(v)X$ transformation can be written as

$$
\begin{aligned}
t' &= \gamma\left(t - \frac{vx}{c}\right) \\
x' &= \gamma\left(x - vt\right) \\
y' &= y \\
z' &= z
\end{aligned} \quad . \tag{1.2}
$$

In the limit that the velocity of the observer with respect to the source (and vice versa) approached zero, this framework was shown to reproduce flawlessly the accepted and long-established Galilean transformation equations. Thus, for $v \approx 0$, $\gamma \approx 1$, and eq. (1.2) reduces to

$$
\begin{aligned}
t' &= t \\
x' &= x - vt \\
y' &= y \\
z' &= z
\end{aligned} \quad . \tag{1.2}
$$

Even after Einstein's 1915 publication of the General Theory of Relativity, SR appeared to be largely complete, so long as both the observer and source remained in Minkowski spacetime. The emergence of a Poincaré covariant formulation of quantum mechanics (relativistic quantum mechanics) continues to be a highly successful description of "nature at high speed" at the atomic and subatomic levels.

However, to this day, there have remained unresolved issues in SR. For instance, a gedanken experiment in which a relativistic object's length-contracted dimension reaches its Schwarzschild radius had not been performed. In chapter 2, such a scenario is described in which the observed object would become a "black star" with a postulated emissivity of truly unity. Additional increases in speed would further decrease the observed linear dimension of the object, and the observed density would correspondingly increase. This would continue until the observed length was the Planck length $\left(\sqrt{\frac{\hbar G}{c^3}}\right)$ and the observed density was the Planck density $\left(\frac{c^5}{\hbar G^2}\right)$, where c is the speed of light, G is Newton's Gravitation Constant, and $\hbar$ is the reduced Planck's constant. At speeds that would supposedly produce shorter lengths and greater densities than these, the Trans-Planckian Problem (TPP) is encountered.

1.1 A Comment about the Trans-Planckian Problem in SR

Clearly, an observer approaching a real (albeit hypothetical) spherical object at a finite subluminal speed greater than that which is required to observe the Planck density (given by eq. (2.13)) should, in classical terms, produce an observed density greater than the Planck density. However, since such a density is thought not to exist physically, an apparent dichotomy – the Trans-Planckian Problem in SR – results.

In 1927, Robert Lévi postulated the existence of the *chronon*, the hypothetical time taken by a photon to twice cross the classical electron radius (~ 10^{-24} s) [3]. In Quantum Field Theory (QFT), it is conjectured that SR and Quantum Mechanics will unify within the chronon.

Furthermore, String Theory has demonstrated the irresolvability of particle structures of arbitrarily small but finite size [4], [5], [6], [7]. Consequently, *cut-off* regularization became one methodology by which singularities in fundamental theories can be avoided. Issues in SR (SR), specifically with Lorentz invariance, emerge because the cut-off is not frame independent.

However, it has been long argued that regardless of its frame dependence, the cut-off must be equal to the fundamental unit of spacetime (i.e., Planck length, Planck time, etc.) [8].

1.1.1 A Statement of TPP in SR

One possible statement that avoids the Trans-Planckian Problem in SR is: for an observable Q,

$$Q = L\left[Q_o\right]\delta_{\gamma\le\gamma_P} + Q_P\delta_{\gamma>\gamma_P} \tag{1.4}$$

where $L\left[Q_o\right]$ is the Lorentz transformation applied to the observable Q in its rest frame, Q_P is the Planck value of the observable Q, $\delta_{\gamma>\gamma_P} = \begin{cases} 1 & \text{for } \gamma > \gamma_P \\ 0 & \text{otherwise} \end{cases}$, $\delta_{\gamma\le\gamma_P} = \begin{cases} 1 & \text{for } \gamma \le \gamma_P \\ 0 & \text{otherwise} \end{cases}$, $\gamma = \dfrac{1}{\sqrt{1-v^2}}$ is the Lorentz factor, and v is the normalized (to the speed of light) speed.

However, eq. (1.4) could be interpreted as being "self-servingly circular" because it defaults to SR up to the Planck scale, and it defaults to the Planck value of the observable for velocities which would try to "force" the value of the observable beyond the Planck scale. Nonetheless, although an underlying physical justification appears to be missing from eq. (1.4), it should arguably describe the sub-Planck and super-Planck results for the transformation of an observable if the Planck scale is to be preserved as the fundamental scale of spacetime.

1.1.2 Doubly SR

One proposed solution to the Trans-Planckian Problem in SR is the Theory of Doubly SR (DSR) which has two postulates [9]:

1. The principle of relativity holds, and there is an equivalence of all observers.
2. There exist two observer-independent scales:
   i. The speed of light (c).
   ii. An (invariant) energy scale (E).

Smolin and Magueijo [10] have proposed a nonlinear Lorentz transformation (E, p) with respect to the invariant length ℓ. By introducing geometric rotations which are linearly dependent on the scale of the linear dimension [11], two parametrizing functions, f and g, produce nonlinear Lorentz transformations. Expectedly, Lorentz transformations are recovered when $lE \ll 1$ and $l^2 p^2 \ll 1$. As such, f and g are given by [12],

$$f = \frac{1}{2\ell E}\left[\left(1+\ell^2 p^2\right)e^{\ell E} - e^{-\ell E}\right], \tag{1.5}$$

$$g = \ell E . \tag{1.6}$$

For a tardyon (subluminal particle) [13], [14],

$$\left(1-\ell^2 p^2\right)e^{\ell E} + e^{-\ell E} = e^{\ell m} + e^{-\ell m}, \tag{1.7}$$

where m is the particle mass.

Also, solving eq. (1.7) for $e^{\ell E}$ and writing in terms of the hyperbolic cosine function gives

$$e^{\ell E} = \frac{\cosh(\ell m) + \sqrt{\cosh^2(\ell m) - (1 - \ell^2 p^2)}}{1 - \ell^2 p^2}. \tag{1.8}$$

Eq. (1.8) produces a momentum upper bound of $p_{\max}^2 < \frac{1}{\ell^2}$ [12]. It is now arguable that momentum can assume an arbitrary value which is restricted by a finite length. The discrete structure of spacetime at the Planck scale places an upper bound on the value of a particle's momentum.

For tardyons (subluminal particles), it is then possible to form a generalized uncertainty principle for generalized position and momentum operators which is given by [10],

$$[X_i, P_j] = i\hbar\left(e^{-\ell E}\delta_{ij} + \frac{\ell^2 p_i p_j}{\cosh(\ell m)}\right). \tag{1.9}$$

Clearly, $\lim_{m\to\infty}\left[i\hbar\left(e^{-\ell E}\delta_{ij} + \frac{\ell^2 p_i p_j}{\cosh(\ell m)}\right)\right]$ demonstrates that a transition from a quantum phase space to a classical phase space must occur. This occurs because $\frac{\ell^2 p_i p_j}{\cosh(\ell m)} \to 0$ as $m \to \infty$, and $e^{-\ell E} \to 0$ due to $E \to \infty$ as $m \to \infty$.

The discussion above is for tardyons. For luxons (luminal particles), a similar strategy applies for eq. (1.8) becomes

$$e^{\ell E} = \frac{1}{1 - \ell|\vec{p}|} \tag{1.10}$$

because the hyperbolic cosine terms are equal to 1 for massless particles. Additionally, eq. (1.9) becomes the generalized uncertainty principle for massless particles given by

$$\left[X_i, P_j\right] = i\hbar\left(\left(1-\ell\left|\vec{p}\right|\right)\delta_{ij} + \ell^2 p_i p_j\right). \tag{1.11}$$

1.2 Contentions on the Relativistic Transformation of Temperature

Perhaps most elusive among the unresolved relativistic descriptions is a relativistic transformation of temperature.

Contentions have emerged supporting three published transformations under the Lorentz group: Temperature Deflation [15], [16]; Temperature Inflation [17], [18], [19], and Temperature Invariance [20], [21], [22], [23]. Temperature inflation and deflation can be specified operationally by means of a relativistic Carnot cycle [24], [25], [26].

A universal approach for determining the Lorentz transformations of heat and temperature considers a bounded volume V_0 of an ideal fluid moving relativistically with respect to the laboratory frame [27], [28]. The clear phenomenological advantage of this approach is that pressure p is a Lorentz invariant, and the work done by the fluid is simply pV_0.

The confusion that arises regarding temperature in relativistic thermodynamics can be clarified by elucidating the respective differences between empirical and absolute temperatures. The *empirical temperature* is a frame-independent, relativistic scalar that depicts (for instance) the CMB rest frame and the moving frame as being in thermal equilibrium [29]. It follows from the Zeroth Law of Thermodynamics and can be related to the absolute temperature in the rest frame of a thermodynamic system. The Zeroth Law holds without invoking any thermodynamic property (including energy and entropy) [30].

The *absolute temperature* of a thermodynamic system follows from the Second Law of Thermodynamics and is defined as the product of the Lorentz factor and the absolute temperature in the rest frame (eq. (1.9)). Although potentially perceptible in non-relativistic thermodynamics, the difference between empirical and absolute temperatures becomes cogently elucidated in relativistic thermodynamics.

Unique insights into the problem of the Lorentz transformations of heat and temperature are offered by two alternative approaches. The solid angular number density of photons, as described by a Planck distribution, defines a *directional* temperature. However, it arises from purely mathematical manipulations, and therefore, its thermodynamic relevance is questionable.

Chapters three to five discuss previously undescribed relativistic phenomena by means of the inverse temperature. A van-Kampen Israel future-directed timelike 4-vector, inverse temperature β is defined as $\beta_\mu = \frac{v_\mu}{T_0}$, where v_μ is the 4-velocity, and T_0 is the temperature in the rest frame. Such an approach retains the thermodynamic relevance of the empirical and absolute temperatures, and at the same time, the necessary angular distribution description (as described by the thermodynamically questionable directional temperature) is preserved. Illumination of this idea is most easily provided with a simple example.

Consider an observer relativistically approaching an isotropically radiating heat source.

$$T = \gamma T_0 \tag{1.12}$$

where T is the temperature of the source in the observer's frame, T_0 is the temperature of the source in the rest frame, $\gamma = \dfrac{1}{\sqrt{1-v^2}}$, and v is the normalized speed expressed in units of the speed of light, is very likely an incorrect relativistic transformation of temperature because even though the source is an isotropic radiator, the direction of the observer's approach is a parameter for which the transformation of temperature must account. Furthermore, a simple Doppler shift of the incident-upon-the-observer photons applied to the rest frame temperature does not provide an adequate relativistic transformation of temperature because it clearly lacks a thermodynamic relevance.

1.2.1 Other Attempts at Defining a Relativistic Blackbody Spectrum

In a 1995 gedanken experiment, Costa and Matsas [31] used an Unruh-DeWitt detector to obtain the distribution of photons (of angular frequency ω) in a relativistic inertial frame (given by eq. (1.13)).

$$n(\omega) = \frac{T_0\sqrt{1-v^2}}{4\pi v}\ln\left[\frac{1-\exp\left(-\dfrac{\omega\sqrt{1+v}}{T_0\sqrt{1-v}}\right)}{1-\exp\left(-\dfrac{\omega\sqrt{1-v}}{T_0\sqrt{1+v}}\right)}\right] \tag{1.13}$$

Eq. (1.13) is not a Planck distribution[1], and this caused Landsberg and Matsas [32], [33] to suggest that a relativistic transformation of temperature is not possible. A more precise statement would be that a relativistic transformation of a Lorentz-invariant *scalar* temperature is not possible. However, when inverse temperature is considered as a van Kampen-Israel future-directed timelike 4-vector, a meaningful relativistic transformation of temperature is possible.

In 1992, Aldrovandi and Gariel attempted a relativistic temperature transformation by considering the thermodynamically questionable directional temperature. However, they preferred to "avoid an 'inside' thermodynamical discussion" [34]. They do contend that an object moving in a heat bath (e.g., the Cosmic Microwave Background (CMB)) will experience temperature inflation. However, this is not entirely correct. The forward and rearward surfaces of an object moving through an isotropic photon field will experience temperature inflation and temperature deflation, respectively. If these surfaces are not thermally isolated from each other, an induced Carnot cycle becomes possible, as discussed in chapter 5.3.4.

1.3 Black Holes (BHs)

In 1916, Karl Schwarzschild established the first metric for a region of spacetime containing a point of infinite curvature [35]. The Schwarzschild metric (in spherical coordinates), given by

$$ds^2 = \left(1 - \frac{1}{r}\right)dt^2 - \frac{dr^2}{\left(1 - \frac{1}{r}\right)} - r^2 d\theta^2 - r^2 \sin^2\theta d\phi^2, \tag{1.14}$$

[1] It is noteworthy that distribution functions change shape when expressed in terms of only energy.

provides a purely classical description of a spherically symmetric, non-rotating, electrically neutral spacetime expanse; the concept of a black hole had been born.

In 1974, the first theoretical demonstration that black holes are not truly black (i.e., objects whose emissivity ~ 1, but not equal to 1) was set forth by Stephen Hawking [36]. Stellar mass and supermassive black holes were shown to produce entirely photonic Hawking radiation, and their lifetimes were approximately the ratio of the initial mass energy to the rate of photon emission from a blackbody spectrum[2].

So long as the black hole's curvature remains sufficiently small that the Hawking radiation is entirely describable by a blackbody spectrum, the above-mentioned lifetime calculation is valid. However, toward the end of the black hole's lifetime, as its curvature increases, Hawking radiation is no longer wholly photonic. Supersymmetric models become important because not only is particle production occurring in the Quantum Electrodynamics (QED) vacuum, but it is also occurring in the Quantum Chromodynamics (QCD) vacuum and energies beyond.

1.3.1 Primordial Black Holes

Although Schwarzschild demonstrated that a sufficient mass density would create a horizon and become self-trapped, the Einstein Field Equations do not require that the necessary energy density result from the gravitational compaction of mass (such as in the case of stellar mass and supermassive black holes). In 1966, Zel'dovich and Novikov

---

[2] Although simplistic, this approximation is valid for stellar (and greater) mass black holes because for most of the black hole's lifetime, the rate of emission is approximately constant, and higher energy particle production can be neglected. This assumption becomes invalid for Primordial Black Holes.

proposed that during the radiation dominated era in Big Bang cosmology, primordial black holes (PBHs) could have formed due to the required density fluctuations in the early universe [37]. Since PBHs would not have been formed by gravitational collapse, they are expected to have masses significantly smaller than one solar mass. Harada, Yoo, and Khori demonstrated the required minimum energy density fluctuation for PBH formation to be given by [38]

$$\frac{\delta\rho}{\rho} \sim 0.1, \tag{1.15}$$

where ρ is the energy density of the universe, and $\delta\rho$ is the local energy density fluctuation.

Kashlinsky postulated that if the abundance of PBHs is comparable to that of dark matter, PBHs may be responsible for unresolved gamma ray emissions and background x-ray radiation [39]. However, this appears to be highly unlikely in light of a 2019 study which ruled out Stephen Hawking's speculation that dark matter is primarily PBHs smaller than 10^{-4} m (7×10^{22} kg) [40]. Even more speculative is Scholtz's and Unwin's 2019 contention that 5-15 $M_\oplus$ [3] PBHs may lurk in the Kuiper Belt and are responsible for the orbital anomalies suggesting a 9th planet in the Solar System [41].

The extreme curvature of a PBH suggested a Hawking radiation spectrum that is not purely photonic. This led MacGibbon and Webber, in 1990 and 1991, to perform the first calculations of the instantaneous and lifetime spectra, respectively, of PBHs [42],

[3] This is one Earth mass.

[43]. For attometer (10^{-18} m) PBHs, three established particle species emerge from the QED vacuum $\left(\gamma, e^{\pm}\right)$ and four from the QCD vacuum $\left(p, \bar{p}, \nu, \bar{\nu}\right)$.

The particle energy and flux of each species are dependent on the mass of the PBH and are discussed in chapter seven. Elucidation of the details of the likely conjecture of an 8th particle species, spin-2 *G*, will probably need to await a more complete theory of quantum gravity.

It is a reasonable supposition that PBHs are a far-future evaporation state of stellar mass[4] and supermassive[5] black holes far beyond the end of the Stelliferous era[6].

1.3.2 White Holes (WHs)

Conjectured in 1964 by Novikov [44] as entirely hypothetical postulates, white holes are the consequences of the maximally extended Schwarzschild solution. White hole geometry is well-described using the Kruskal–Szekeres timelike coordinate $\left(T\right)$ and spacelike coordinate $\left(X\right)$. The transformation between Kruskal–Szekeres coordinates $\left(T, X\right)$ and Schwarzschild coordinates $\left(t, r, \theta, \phi\right)$ is given by

$$T = \left(\frac{r}{2GM} - 1\right)^{\frac{1}{2}} \exp\left(\frac{r}{4GM}\right) \sinh\left(\frac{t}{4GM}\right) \tag{1.16}$$

and

---

[4] The evaporation time for a stellar mass black hole is approximately 2×10^{67} years.

[5] The evaporation time for the TON 618 supermassive black hole ($\sim 6.6 \times 10^{10}\ M_{\oplus}$) is approximately 6×10^{99} years.

[6] This current era in Big Bang cosmology will end approximately 10^{14} years after the Big Bang.

$$X = \left(\frac{r}{2GM} - 1 \right)^{\frac{1}{2}} \exp\left(\frac{r}{4GM} \right) \cosh\left(\frac{t}{4GM} \right) \tag{1.17}$$

for the region exterior to the event horizon $(r > 2GM)$, and

$$T = \left(\frac{r}{2GM} - 1 \right)^{\frac{1}{2}} \exp\left(\frac{r}{4GM} \right) \cosh\left(\frac{t}{4GM} \right) \tag{1.18}$$

and

$$X = \left(\frac{r}{2GM} - 1 \right)^{\frac{1}{2}} \exp\left(\frac{r}{4GM} \right) \sinh\left(\frac{t}{4GM} \right) \tag{1.19}$$

for the region interior to the event horizon $(0 < r < 2GM)$.

In the maximally extended solution that arises from the transformation between Schwarzschild coordinates and Kruskal–Szekeres coordinates, there exist two singularities for $\pm T$ at $r = 0$. Diagrammatically, this is depicted in Figure 1.1 and Table 1.1.

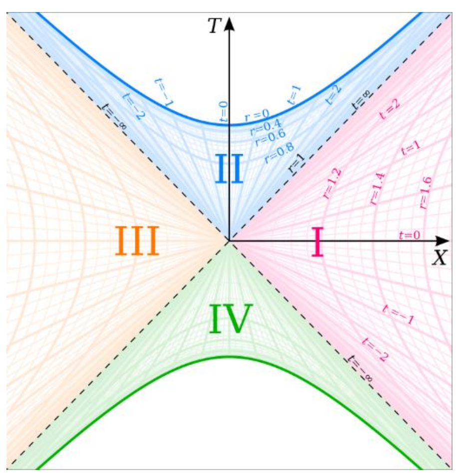

Figure 1.1: A Kruskal–Szekeres diagram for $2GM = 1$. The dotted lines represent the event horizons. The dark hyperbolas in regions II and IV are the singularities. The lighter hyperbolas represent the Schwarzschild *r*-coordinate contours, and the lighter solid straight lines through the origin represent the Schwarzschild *t*-coordinate contours [45].

Table 1.1: Region descriptions of the Kruskal–Szekeres diagram in Figure 1.1 in both Kruskal–Szekeres and Schwarzschild coordinates [45].

Region Number	Region Description	Kruskal–Szekeres Coordinates	Schwarzschild Coordinates
I	Exterior	$-X < T < +X$	$2GM < r$
II	Interior Black Hole	$\left\|X\right\| < T < \sqrt{1+X^2}$	$0 < r < 2GM$
III	Parallel Exterior	$+X < T < -X$	$2GM < r$
IV	Interior White Hole	$-\sqrt{1+X^2} < T < -\left\|X\right\|$	$0 < r < 2GM$

In contrast to black holes whose absorptivity has reached a limit of one and whose emissivity is zero, correspondingly, white holes have an absorptivity of zero and an emissivity of one. As such, no matter or energy is capable of entering a white hole. When a black hole is near its final stages of evaporation, its Schwarzschild radius decreases, and the Hawking radiation flux and particle energy increase resulting in a progressively opaquer and radially expanding particle shower. Any external particles on inward trajectories toward the eventually-quantum-scale black hole's (or quantum-scale PBH's) event horizon would interact with the emitted Hawking radiation, and consequently it would be prevented from entering the BH (or PBH).

Chapter seven discusses this particle interaction in detail and demonstrates that at the instant an evaporating PBH reaches the Planck scale, the probability of particle absorption by the PBH is zero, and for that last instant of the PBH's existence, in terms of its absorptivity and emissivity, it momentarily mimics a white hole.

CHAPTER TWO

Apparent Ultra-Relativistic Energy Density Inflation of Astrophysical Bodies into Apparent Black Stars

This chapter published as: J. S. Lee and G. B. Cleaver, "Apparent Ultra-Relativistic Energy Density Inflation of Astrophysical Bodies into Apparent Black Stars," *Journal of Applied Physical Science International*, vol. 9, no. 2, pp. 51-53, 2017.

2.1 Introduction

From SR, all objects of non-zero mass approaching or receding from an observer with a relative velocity of magnitude β will appear to the observer to have both a mass inflated by the Lorentz factor $\gamma = \frac{1}{\sqrt{1-\beta^2}}$, and a length contracted along the direction of relative motion by this same factor g. Although there has been historical contention in the literature about *length dilation* [46], [47], [48], and the *Principle of Photographability* [49], standard length contraction of receding objects, and not length dilation, is expected to occur. Therefore, $V = \frac{V_o}{\gamma}$, and receding and approaching objects are indistinguishable in terms of their densities.

Thus, an object that is spherical in its rest frame with radius R_o and is relativistically approaching toward, or receding from, an observer will appear as an oblate spheroid with motion along the polar axis and a volume given by $V = \frac{4\pi}{3}a^2b = \frac{4\pi}{3}\frac{R_0^3}{\gamma}$, where $a = R_o$ is the major axis, and $b = \frac{R_o}{\gamma}$ is the minor axis. Thus, in an inertial frame moving with regard to the rest frame, the observer in the rest frame would measure the volume of the oblate spheroid to be $V = \frac{V_o}{\gamma}$. Also, from SR, the relativistic mass becomes $M = \gamma M_o$. Therefore, the mass density ρ of an object in terms of its rest frame mass density ρ_o appears to the observer as:

$$\rho = \gamma^2 \rho_0 \tag{2.1}$$

The corresponding energy density of the moving object, ρ^{E}, appears to the observer as

$$\rho^{\mathrm{E}} = \gamma^2 c^2 \rho_0 \tag{2.2}$$

In order to avoid considering spacetime curvature, which would invalidate SR, black stars, rather than black holes, will be considered. Recall that the Schwarzschild radius of a black star in its rest frame is

$$R_S = \frac{2GM}{c^2}. \tag{2.3}$$

The rest frame mass density ρ_{BH} and the rest frame energy density $r^{\mathrm{E}}_{\mathrm{BH}} = r_{\mathrm{BH}} c^2$ of a Schwarzschild black star are thus given respectively by

$$\rho_{\mathrm{BH}} = \frac{M_o}{V_o} = \frac{3c^2}{8\pi G R_S^2} \tag{2.4}$$

and

$$\rho^{\mathrm{E}}_{\mathrm{BH}} = \frac{3c^4}{8\pi G R_S^2}, \tag{2.5}$$

where M_o is the rest frame mass of the object, V_o is the rest frame volume of the object, c is the speed of light, and G is Newton's gravitation constant.

2.2 *Apparent Black Star Perception*

If the Lorentz factor is sufficient, then an object's mass density, as measured by the inertial observer at rest, will appear to approach the density of a black star of mass M_o. From eq. (2.1), the critical velocity at which the relativistic mass density equals the Schwarzschild black star density is

$$\gamma_{\mathrm{BH}}^2 = \frac{\rho_{\mathrm{BH}}}{\rho_o}. \tag{2.6}$$

From eqs. (2.4) and (2.6),[1]

$$\gamma_{\mathrm{BH}} = \frac{c}{R_S}\sqrt{\frac{3}{8\pi G\rho_o}}. \tag{2.7}$$

For example, in the case of the 5.98×10^{24} kg, 6.38×10^{6} m radius Earth with a corresponding Schwarzschild radius of 8.86 mm, the minimum Lorentz factor at which it would "appear" to be a black star is $\sim1.93\times10^{13}$. This corresponds to a speed of $\beta = 1 - 1.34\times10^{-27}$. In terms of the rest mass and rest frame radius of the object, eq. (2.7) becomes

$$\gamma_{\mathrm{BH}} = c^3\left(\frac{R_o}{GM_o}\right)^{\frac{3}{2}}. \tag{2.8}$$

If the object is to appear to the observer to contract in length in the direction of motion to an arbitrary width $R_* < R_o$, then eq. (2.8) becomes

$$\gamma = \frac{c}{R_*}\sqrt{\frac{R_o^3}{2GM_o}}. \tag{2.9}$$

[1] As noted above, a moving spherical object would appear as an oblate spheroid as observed by an inertial observer. The increasing relativistic density in eq. (2.6) results from this increasing oblateness.

Also consider the Planck density, ρ_P, which is given by

$$\rho_P = \frac{c^5}{\hbar G^2}, \tag{2.10}$$

where $\hbar$ is the reduced Planck's constant. From quantum mechanics, this is likely the maximum rest frame density possible. In the case of $\gamma > \gamma_P$, the trans-Planckian problem emerges [50]. One proposed solution is a scenario whereby black holes are actually *black stars*, in which vibrations can result in the emission of a Hawking radiation spectrum. Also, the bosonic nature of photons does not require photon conservation in curved spacetime. In this case, the maximum mode frequencies never achieve trans-Planckian values, and the density never exceeds the Planck density, even for $\gamma > \gamma_P$.

The associated Lorentz factor γ_P, giving an object an apparent Planck density, results from combining eqs. (2.1) and (2.10), giving

$$\gamma_P = \frac{2}{G}\sqrt{\frac{\pi c^5 R_o^3}{3\hbar M_o}}. \tag{2.11}$$

When eq. (2.11) is applied to the Earth, $\gamma_P = 3.07 \times 10^{46}$ which corresponds to a speed of $\beta = 1 - 5.30 \times 10^{-94}$.

Note that a black star in its rest frame is an actual black star in every frame, although the Hawking spectra will differ. Furthermore, the extreme values of the Lorentz factor required for an inertial observer to perceive astrophysical bodies as apparent black stars ensure, at the observer's location in spacetime, a prodigious relativistic energy density, given by

$$\rho^{\mathrm{E}} = \frac{\gamma M c^2}{V} . \tag{2.12}$$

Interestingly, equating eqs. (2.5) and (2.12) gives the minimum Lorentz factor of

$$\gamma = \frac{3c^6 V}{32\pi G^3 M_o^3}, \tag{2.13}$$

for which an inertial object would be expected by the observer at rest to form a horizon and become self-trapped as a black star based on its *perceived* relativistic mass density interpreted instead as its rest mass density. In the literature on the relativistic collision of particles, and the possible formation of small black stars in accelerators, a different definition is often used. Specifically, the Schwarzschild radius belonging to the relativistic mass (not the rest mass) should exceed the transverse size of the body. See, for example, [51].

Defining $\rho_\gamma \equiv \dfrac{\gamma}{V}$, eq. (2.13) becomes:

$$\rho_\gamma = \frac{3c^6}{32\pi G^3 M_o^3} \tag{2.14}$$

2.3 Summary

Interestingly, it has been shown that at extremely high relativistic velocities close to *c*, with regard to an observer in an inertial frame, a massive object can *appear* to become a black star, based on its relativistic mass density. It is significant that the rest frame observer only *perceives* that such an object should *apparently* form a black star based on its relativistic mass density. In reality, the massive object does not form a black star. What determines if a distribution of mass is a black star or not is whether or not it creates an event horizon as predicted by the Einstein field equations. Whether or not it does, depends on the existence of an asymptotic region, and whether the gravity of the object would allow the light to escape to that region or not. However, it is independent of whatever inertial observer–even arbitrarily fast moving in the rest frame of the massive object–describes it. For example, the distribution of mass of the Earth does not create any horizon, no matter who describes it.

In other words, if an object's density exceeds that of a black star with the same mass, then that object would create a horizon, and would itself be a black star, as perceived by an external observer. However, this result is valid only when the quantities are taken in the *rest frame* of the object. Although the mass density may predict the existence of a horizon in other inertial frames, if not truly a black star in the rest frame, then not truly a black star in any frame.

CHAPTER THREE

1.

The Relativistic Blackbody Spectrum in Inertial and Non-Inertial Reference Frames

This chapter published as: J.S. Lee and G. B. Cleaver, "The Relativistic Blackbody Spectrum in Inertial and Non-Inertial Reference Frames", *New Astronomy*, Volume 52, 9 October 2016. arXiv:1507.06663

3.1 Introduction

The semi-empirical derivation and applications of the blackbody spectrum for exclusively stationary radiation sources have been well-established and are in many physics textbooks. However, significant progress in fully establishing the relativistic blackbody spectrum has been stymied, at least to some extent, by unresolved issues in relativistic thermodynamics.

This chapter makes use of the inverse temperature 4-vector to derive the Relativistic Planck's Law, the Relativistic Wien's Displacement Law, and the Relativistic Stefan-Boltzmann Law in inertial reference frames. In order to correctly describe the relativistic blackbody spectrum, *relativistic beaming* and *Doppler shifting*, in addition to *relativistic temperature transformation*, must be considered. Additionally, the non-inertial reference frame case is established with the azimuthally constant 4-acceleration and, when necessary, the proper time derivative of the spectral radiance, the wavelength of maximum irradiance, and the radiation irradiance. Also, non-trivial solutions are sought for equal spectral radiances, equal wavelengths of maximum irradiance, and equal irradiances of the relativistic and radiation frame blackbody spectra.

3.2 The Application of Inverse Temperature to the Blackbody Spectrum

Although attempts have been made to develop the Relativistic Blackbody Spectrum [52], [53], [54], these endeavors have been unsuccessful due, at least in part, to unresolved issues in relativistic thermodynamics [55], [15], [16], [56], [57], [58], [59]. Disputes have arisen supporting three published Lorentz group transformations: Temperature Deflation [15], [16], and Temperature Inflation [17], [18], [19] (which can be operationally quantified with a relativistic Carnot cycle [24], [25], [26]); and Temperature Invariance [20], [21], [22], [60].

Significant misperceptions have arisen concerning temperature in relativistic thermodynamics due in part to the confusion surrounding the respective differences between empirical and absolute temperatures. The *empirical temperature* is a Lorentz invariant, relativistic scalar that considers the radiation rest frame and the observer frame to be in thermal equilibrium [29]. This ensues from the Zeroth Law of Thermodynamics, and correlates directly to the absolute temperature in the radiation (source) frame. The Zeroth Law's validity is required without making use of any thermodynamic property (including entropy and energy) [30].

The *absolute temperature* of a thermodynamic system is a consequence of the Second Law of Thermodynamics. It is the product of the Lorentz factor and the absolute temperature in the radiation frame, and it contains no angular dependence. Even though the difference between empirical and absolute temperatures may be observable in non-relativistic thermodynamics, it becomes persuasively illuminated in relativistic thermodynamics.

The Planck distribution describes a solid angular photon number density, and it defines a *directional* (or *effective*) temperature. However, this results from solely mathematical manipulations, and its thermodynamic relevance is, at best, questionable. Alternatively, temperature transformations can be accomplished by treating *inverse temperature* as a van Kampen-Israel future-directed timelike 4-vector [53], [61]. Although Przanowski and Tosiek [27][2] have demonstrated temperature inflation without making use of inverse temperature, angular dependence is required for the relativistic blackbody spectrum.

3.3 Derivation of the Relativistic Spectral Radiance

The relativistic blackbody spectrum can be obtained by considering the blackbody spectrum of a stationary radiation source and including temperature inflation (in terms of inverse temperature), Doppler shifting, and relativistic beaming. The inertial and non-inertial frames cases are each examined. In the non-inertial case, the Unruh Effect is not considered because it is many orders of magnitude smaller than the effect presented here.

3.3.1 Inertial Frames

The radiation (source) frame photon energy density ε in frequency and wavelength spaces of a Planckian distribution are [62]:

$$\varepsilon_\nu d\nu = \frac{\left(\dfrac{8\pi h\nu^3}{c^3}\right)}{\exp\left(\dfrac{h\nu}{k_B T_o}\right)-1} d\nu \tag{3.1}$$

and

[2] By using a superfluidity gedanken experiment.

$$\varepsilon_\lambda d\lambda = \frac{\left(\frac{8\pi hc}{\lambda^5}\right)}{\exp\left(\frac{hc}{k_B \lambda T_o}\right) - 1} d\lambda \tag{3.2}$$

where h is Planck's constant, c is the speed of light, k_B is Boltzmann's constant, T_o is the rest frame absolute temperature, v is the frequency, and λ is the wavelength.

Relativistically, the reciprocal of absolute temperature is replaced by the inverse temperature 4-vector[3]:

$$|\beta| = \left|\frac{u}{T_o}\right| = |\beta_t - \beta_z \cos\theta|, \tag{3.3}$$

where T_o is the proper temperature (in the radiation frame), u_μ is the relative 4-velocity between the radiation and the observer, β_μ is the van Kampen-Israel inverse temperature 4-vector, and $V = \frac{u}{c}$ (fraction of light speed). | | denotes magnitude of the vector quantity. θ is the planar angle between the observer's motion and the source. If the observer if moving through a photonic gas, then θ is the planar angle between the observer's motion and the direction of observation.

The t and z components of the inverse temperature 4-vector can be determined from the number density of photons $n(\omega,\Omega)$ arriving through the solid angle Ω and with angular frequency ω which is given by [63], [64], [65]

[3] In this paper, the case of the azimuthally constant inverse temperature vector is chosen (hence, $\beta_x = \beta_y = 0$), and consequently, all motion is along the z-axis.

$$n(\omega,\Omega)\,d\omega d\Omega = \frac{\omega^2}{2\pi^2\left[\exp\left(\dfrac{\omega}{T_{\text{eff}}(\theta)}\right)-1\right]}\,d\omega d\Omega\,. \tag{3.4}$$

The directional (or effective) temperature is given by

$$T_{\text{eff}} = \frac{T_o\sqrt{1-V^2}}{1-V\cos\theta}\,. \tag{3.5}$$

The momentum of a photon within a photonic gas is determined from its four-dimensional wave number. If the observer is in motion along the *z*-axis at velocity *V*, the *x* and *y* components of the momentum must be zero. Therefore, the number of photons in the i^{th} wave mode is given by [53]

$$N_i = \frac{1}{\exp(\beta_t\omega_i - \beta_z k_{iz})-1}, \tag{3.6}$$

where k_{iz} and ω_i are the wave number and frequency, respectively, of the i^{th} mode.

By introducing polar coordinates (r,θ,ϕ), setting $\theta=0$ (the spatial wave vector's direction), assuming a continuous frequency distribution, and considering the photon dispersion relation $(\omega^2 = k_z^2)$, the number of photons is given by

$$n(\omega,\Omega)\,d\omega d\Omega = \frac{\omega^2}{2\pi^2\left[\exp\left[(\beta_t-\beta_z\cos\theta)\,\omega\right]-1\right]}\,d\omega d\Omega\,. \tag{3.7}$$

Comparing (3.4) and (3.7) yields [53]

$$\beta_t = \frac{1}{T_o\sqrt{1-V^2}} \tag{3.8}$$

and

$$\beta_z = \frac{V}{T_o\sqrt{1-V^2}}. \tag{3.9}$$

Although the azimuthally constant 4-vector β_μ is a function of the reciprocal of the effective temperature, given by eq. (3.5), it arises directly from thermodynamic considerations, whereas the effective temperature is obtained entirely from mathematical manipulation. Although T_{eff} is adequate to determine planetary and stellar motion with respect to the CMB [63], [64], [65], its thermodynamically non-physical origin leaves it unclear whether or not T_{eff} represents temperature. Additionally, relativistic beaming and Doppler shifting must be considered, and this is accomplished by introducing the Doppler factor $D = \sqrt{\frac{1+\beta}{1-\beta}}$.

Rewriting eqs. (3.1) and (3.2) in terms of inverse temperature yields[4]

$$\varepsilon_\nu^{'} d\nu d\Omega = \frac{\left(\frac{8\pi h \nu^3}{c^3}\right)}{\exp\left[\frac{h\nu}{k_B}\left(\beta_t - \beta_z\cos\theta\right)\right]-1} d\nu d\Omega \tag{3.10}$$

and

$$\varepsilon_\lambda^{'} d\lambda d\Omega = \frac{\left(\frac{8\pi hc}{\lambda^5}\right)}{\exp\left[\frac{hc}{k_B\lambda}\left(\beta_t - \beta_z\cos\theta\right)\right]-1} d\lambda d\Omega, \tag{3.11}$$

respectively.

[4] Primed quantities indicate the observer frame. Derivatives with respect to the proper time are denoted with dot notation.

From $B'_{\nu,\lambda} = \frac{c}{4\pi}\varepsilon'_{\nu,\lambda}$ and $\frac{B'_\lambda}{B_\lambda} = \left[\gamma(1 - V\cos\theta)\right]^{-3} = D^3$, eqs. (3.10) and (3.11)

become respectively

$$B'_\nu d\nu d\Omega = \frac{\left(\frac{2h\nu^3}{c^2}\right)}{\exp\left[\frac{h\nu}{k_B}(\beta_t - \beta_z\cos\theta)\right] - 1}\left[\gamma(1 - V\cos\theta)\right]^{-3} d\nu d\Omega \tag{3.12}$$

and

$$B'_\lambda d\lambda d\Omega = \frac{\left(\frac{2hc^2}{\lambda^5}\right)}{\exp\left[\frac{hc}{k_B\lambda}(\beta_t - \beta_z\cos\theta)\right] - 1}\left[\gamma(1 - V\cos\theta)\right]^{-3} d\lambda d\Omega\,, \tag{3.13}$$

where $\gamma = \frac{1}{\sqrt{1 - V^2}}$ is the Lorentz factor, D is the Doppler factor, B'_ν and B'_λ are

respectively the frequency and wavelength spectral radiances in the observer's frame.

Rewritten in terms of the temperature in the radiation frame, eqs. (3.12) and (3.13) become

$$B'_\nu d\nu d\Omega = \frac{\left(\frac{2h\nu^3}{c^2}\right)(1 - V^2)^{\frac{3}{2}}}{(1 - V\cos\theta)^3\left\{\exp\left[\left(\frac{h\nu}{k_B T_o}\right)\frac{(1 - V\cos\theta)}{(1 - V^2)^{\frac{1}{2}}}\right] - 1\right\}} d\nu d\Omega \tag{3.14}$$

and

$$B'_\lambda d\lambda d\Omega = \frac{\left(\frac{2hc^2}{\lambda^5}\right)(1 - V^2)^{\frac{3}{2}}}{(1 - V\cos\theta)^3\left\{\exp\left[\left(\frac{hc}{k_B \lambda T_o}\right)\frac{(1 - V\cos\theta)}{(1 - V^2)^{\frac{1}{2}}}\right] - 1\right\}} d\lambda d\Omega\,, \tag{3.15}$$

respectively. The dependency on wavelength of the spectral radiance in wavelength space is shown in Figure 3.1.

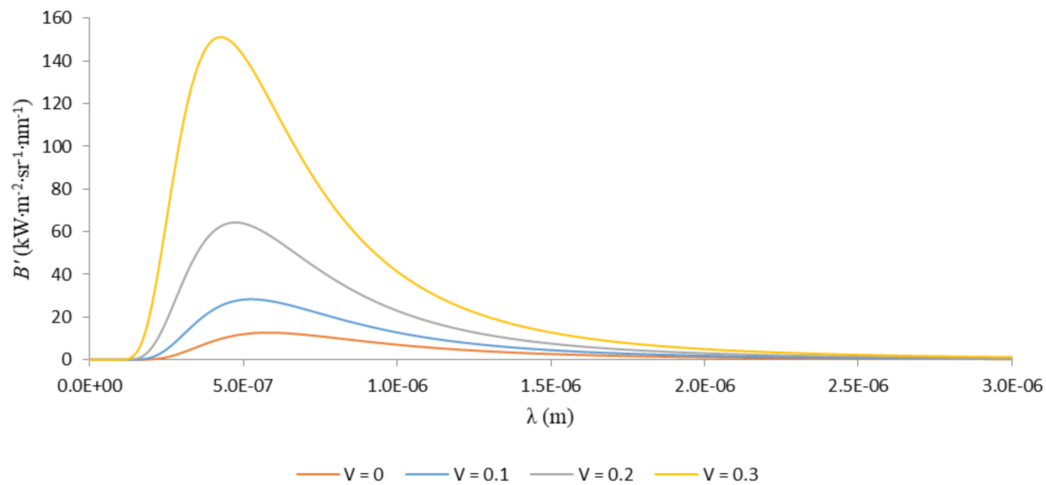

Figure 3.1: Spectral radiance versus wavelength for a 5000 K radiation source in four inertial reference frames. $\theta = 0$.

The dependency on speed of the spectral radiance in wavelength space is shown in Figure 3.2.

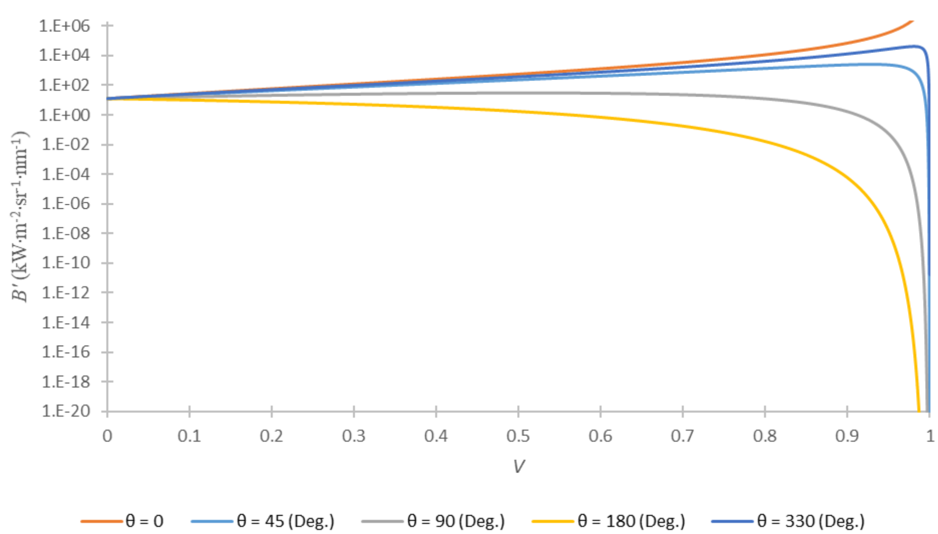

Figure 3.2: Spectral radiance versus speed at five angles for a 5000 K blackbody at the wavelength of maximum irradiance in the radiation frame (0.5796 μm). The B′-axis intercept is the spectral radiance in the radiation frame (12.7 kW·m^{-2}·sr^{-1}·nm^{-1}).

The contour lines on the V-θ contour plot (Figure 3.3) of eq. (3.15) reveal that B' increases with increasing V only for first and fourth quadrant angles ($\cos\theta > 0$), while it decreases for second and third quadrant angles ($\cos\theta < 0$). Expectedly, the inertial relativistic spectral radiance decreases most appreciably with increasing speed when θ = 180º. Thus, the 4-vector velocity behavior of relativistic spectral radiance does not trivially increase B' for increasing θ.

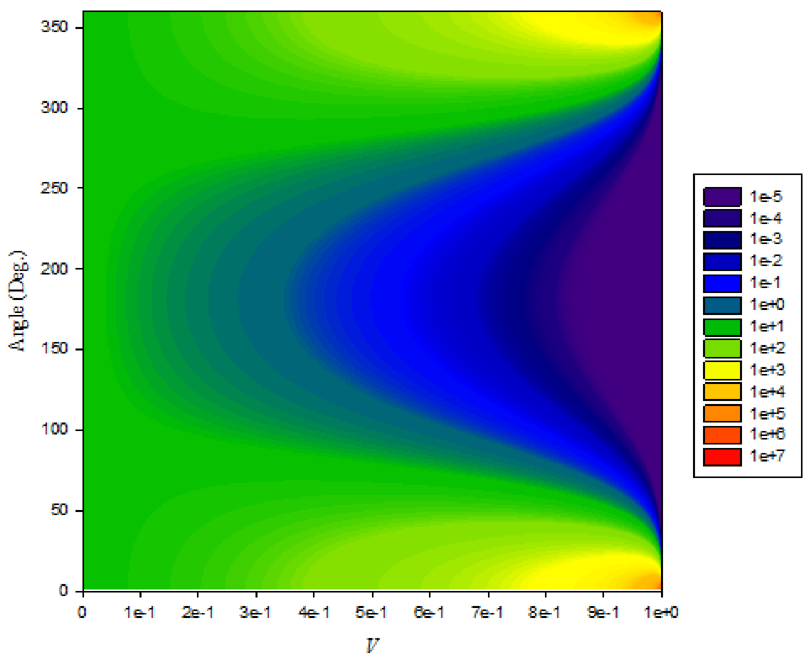

Figure 3.3: Contour plot of inertial relativistic spectral radiance as a function of speed and angle for a 5000 K blackbody at the wavelength of maximum irradiance in the rest frame (0.5796 μm). The color spectrum gives the approximate values of B' (kW·m^{-2}·sr^{-1}·nm^{-1}). The contour lines' intersections with the *Angle*-axis represent the spectral radiance in the rest frame, which is 12.7 kW·m^{-2}·sr^{-1}·nm^{-1}. The region of smallest spectral radiance is actually $B' \leq 10^{-5}$ kW·m^{-2}·sr^{-1}·nm^{-1}.

Several authors [53], [54], [31] have remarked that the Bose-Einstein distribution form of the blackbody spectrum of a stationary radiation source is not relativistically invariant. However, eqs. (3.14) and (3.15) clearly reveal that, in terms of the radiation frame temperature, the Bose-Einstein distribution for spectral radiance is retained in a relativistic inertial reference frame (as shown in Figure 3.1). Regardless, inverse temperature remains a valid thermodynamic quantity [53]. In the non-relativistic limit, eq. (3.15) becomes

$$B'_{\lambda} d\lambda d\Omega \sim \left\{ \frac{\left(\frac{2hc^2}{\lambda^5}\right)}{\exp\left(\frac{hc}{k_B \lambda T_o}\right)-1} + \left[\frac{\left(\frac{6hc^2}{\lambda^5}\right)}{\exp\left(\frac{hc}{k_B \lambda T_o}\right)-1} + \frac{\left(\frac{2h^2c^3}{\lambda^6}\right)\exp\left(\frac{hc}{k_B \lambda T_o}\right)\cos\theta}{\left[\exp\left(\frac{hc}{k_B \lambda T_o}\right)-1\right]^2} \right] V + O\left(V^2\right) \right\} d\lambda d\Omega \ . \tag{3.16}$$

From eq. (3.15), $V < 1$ clearly disallows any non-zero speed with respect to the radiation frame for which $B' = 0$, and also, since $\cos\theta \leq 1$, there is no subluminal speed for which B' is infinite. When $V = 0$, then $\beta_z = 0$, $\beta_t = 1/T_o$ (the zeroth component of inverse temperature in the radiation frame), and $\gamma = 1$. Therefore, as required, the stationary forms of eqs. (3.14) and (3.15) are recovered. This result is, of course, clear from eq. (3.16) as well from which the wavelength form (eq. (3.18)) emerges. The equivalent frequency form is given by eq. (3.17).

$$B_\nu = \frac{\left(\frac{2h\nu^3}{c^2}\right)}{\exp\left[\frac{h\nu}{k_B T_o}\right]-1} \tag{3.17}$$

and

$$B_\lambda = \frac{\left(\frac{2hc^2}{\lambda^5}\right)}{\exp\left[\frac{hc}{k_B \lambda T_o}\right]-1} \tag{3.18}$$

The inertial relativistic blackbody spectra for other spaces are summarized in Table 3.1.

Table 3.1: Inertial relativistic blackbody spectra in terms of six spectral variables.

Variable	Distribution
Frequency (ν)	$B'_{\nu} d\nu d\Omega = \dfrac{\left(\dfrac{2h\nu^3}{c^2}\right)\left(1-V^2\right)^{\frac{3}{2}}}{\left(1-V\cos\theta\right)^3\left\{\exp\left[\left(\dfrac{h\nu}{k_B T_o}\right)\dfrac{\left(1-V\cos\theta\right)}{\left(1-V^2\right)^{\frac{1}{2}}}\right]-1\right\}} d\nu d\Omega$
Wavelength (λ)	$B'_{\lambda} d\lambda d\Omega = \dfrac{\left(\dfrac{2hc^2}{\lambda^5}\right)\left(1-V^2\right)^{\frac{3}{2}}}{\left(1-V\cos\theta\right)^3\left\{\exp\left[\left(\dfrac{h\nu}{k_B T_o}\right)\dfrac{\left(1-V\cos\theta\right)}{\left(1-V^2\right)^{\frac{1}{2}}}\right]-1\right\}} d\lambda d\Omega$
Wavenumber $(\tilde{\nu})$	$B'_{\tilde{\nu}} d\tilde{\nu} d\Omega = \dfrac{2hc^2\tilde{\nu}^3}{\left(1-V^2\right)^{\frac{3}{2}}\left(1-V\cos\theta\right)^3\left\{\exp\left[\left(\dfrac{h\nu}{k_B T_o}\right)\dfrac{\left(1-V\cos\theta\right)}{\left(1-V^2\right)^{\frac{1}{2}}}\right]-1\right\}} d\tilde{\nu} d\Omega$
Angular Frequency (ω)	$B'_{\omega} d\omega d\Omega = \dfrac{\left(\dfrac{\hbar\omega^3}{4\pi^3 c^2}\right)\left(1-V^2\right)^{\frac{3}{2}}}{\left(1-V\cos\theta\right)^3\left\{\exp\left[\left(\dfrac{h\nu}{k_B T_o}\right)\dfrac{\left(1-V\cos\theta\right)}{\left(1-V^2\right)^{\frac{1}{2}}}\right]-1\right\}} d\omega d\Omega$
Angular Wavelength (y)	$B'_{y} d\lambda d\Omega = \dfrac{\left(\dfrac{\hbar c^2}{4\pi^3 y^5}\right)\left(1-V^2\right)^{\frac{3}{2}}}{\left(1-V\cos\theta\right)^3\left\{\exp\left[\left(\dfrac{h\nu}{k_B T_o}\right)\dfrac{\left(1-V\cos\theta\right)}{\left(1-V^2\right)^{\frac{1}{2}}}\right]-1\right\}} dy d\Omega$
Angular Wavenumber (k)	$B'_{k} d\omega d\Omega = \dfrac{\left(\dfrac{\hbar c^2 k^3}{4\pi^3}\right)\left(1-V^2\right)^{\frac{3}{2}}}{\left(1-V\cos\theta\right)^3\left\{\exp\left[\left(\dfrac{h\nu}{k_B T_o}\right)\dfrac{\left(1-V\cos\theta\right)}{\left(1-V^2\right)^{\frac{1}{2}}}\right]-1\right\}} dk d\Omega$

3.3.1.1. The Angular Periodicity of the Inertial Relativistic Spectral Radiance.

Due to $\cos\theta$ in eq. (3.15), the relativistic spectral radiance exhibits an angular periodicity with an angular wavelength of 360°. This result is independent of speed (Figure 3.4) and temperature when the radiation frame wavelength of maximum irradiance is considered (Figure 3.5); this is, of course, reasonable because the temperature dependence in the angular term of eq. (3.15) vanishes as a result of Wien's Displacement Law applied in the rest frame, as shown in eq. (3.19).

$$\exp\left[\left(\frac{hc}{k_B\lambda\cdot\left(T_0=\frac{b}{\lambda}\right)}\right)\frac{(1-V\cos\theta)}{(1-V^2)^{\frac{1}{2}}}\right]=\exp\left[\left(\frac{hc}{k_B b}\right)\frac{(1-V\cos\theta)}{(1-V^2)^{\frac{1}{2}}}\right], \tag{3.19}$$

where $b \sim 2.8977721\times10^6$ nm·K is Wien's displacement constant.

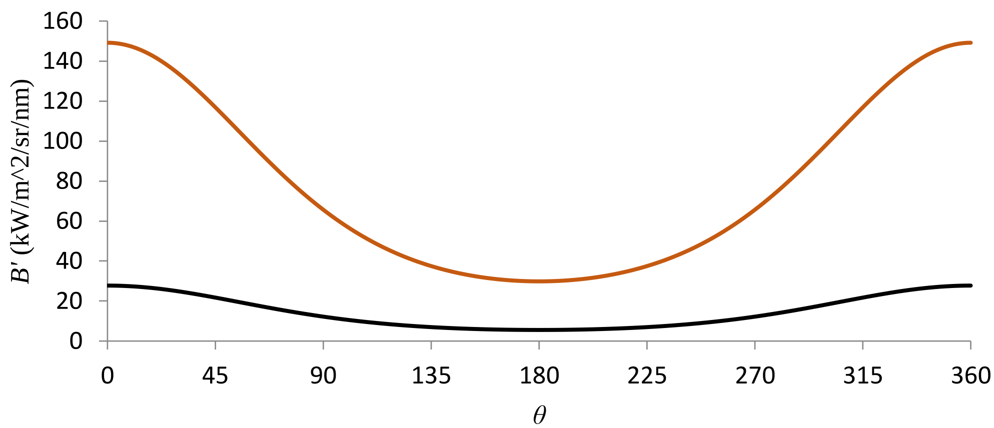

Figure 3.4: Inertial relativistic spectral radiance versus angle for a 5000 K blackbody at the wavelength of maximum irradiance in the rest frame (0.5796 μm). The black and orange lines represent V = 0.1 and V = 0.2, respectively.

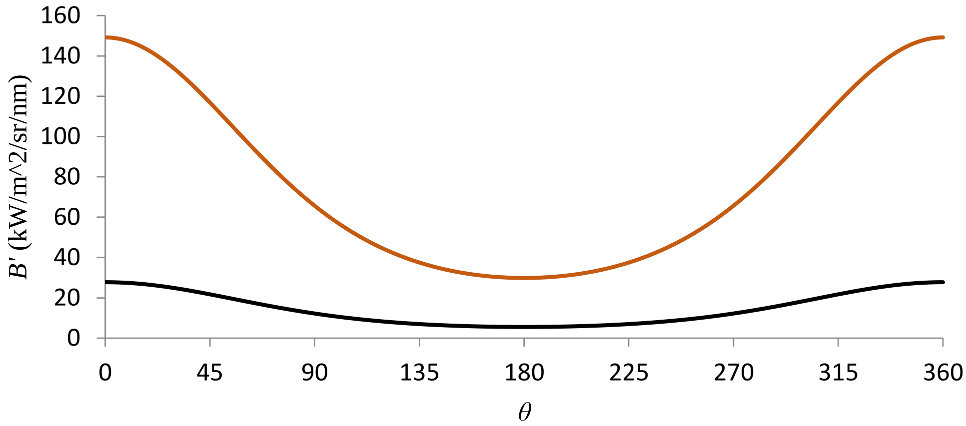

Figure 3.5: Relativistic spectral radiance versus angle for two blackbodies. The black and orange lines represent T_0 = 5000 K and T_0 = 7000 K, respectively. The wavelengths are for maximum irradiance in the rest frame (0.5796 μm for 5000 K and 0.4140 μm for 7000 K). V = 0.1.

The angles at which the maxima occur (0^o and 360^o) and minima occur (180^o) are not surprisingly independent of the speed and temperature.

3.3.2 Non-Inertial Frames

The relativistic spectral radiance in a non-inertial reference frame is determined with the 4-acceleration a_μ, which is the proper time (τ) derivative (denoted with dot notation) of the 4-velocity $\left(a_\mu = \dot{u}_\mu\right)$. Combining eq. (3.15) and

$$V = \tanh\left(A\tau\right), \tag{3.20}$$

where $A \equiv \frac{a}{c}$ (the zeroth term of the acceleration 4-vector), the relativistic spectral radiance in a non-inertial frame is given by

$$B_\lambda^{'} d\lambda d\Omega = \frac{\left(\frac{2hc^2}{\lambda^5}\right)\operatorname{sech}^3\left(A\tau\right)}{\left[1-\tanh\left(A\tau\right)\cos\theta\right]^3\left[\exp\left(\frac{hc}{k_B\lambda T_o}\left(\cosh\left(A\tau\right)-\sinh\left(A\tau\right)\cos\theta\right)\right)-1\right]} d\lambda d\Omega \cdot \tag{3.21}$$

As $A\tau \to \infty$, $B_\lambda^{'} \to 0$ when $\theta \neq 0$. Although this might not be intuitively obvious, it too, is sensible because for every $\theta \neq 0$ approach vector, the observer must eventually reach a closest point of approach to the source and begin receding from it indefinitely. Also, as $A\tau \to \infty$, $B_\lambda^{'} \to \infty$ when $\theta = 0$. This is reasonable because approaching the source directly will expectedly increase the spectral radiance. If the observer were to eventually reach the source, $\theta = 0 \to \theta = 180^o$, and the observer will, at that point, recede from the source indefinitely.

As required, when $A\tau = 0$, the stationary form of the spectral radiance, eq. (3.18), is recovered. A plot of eq. (3.21) is shown in Figure 3.6 and Figure 3.7.

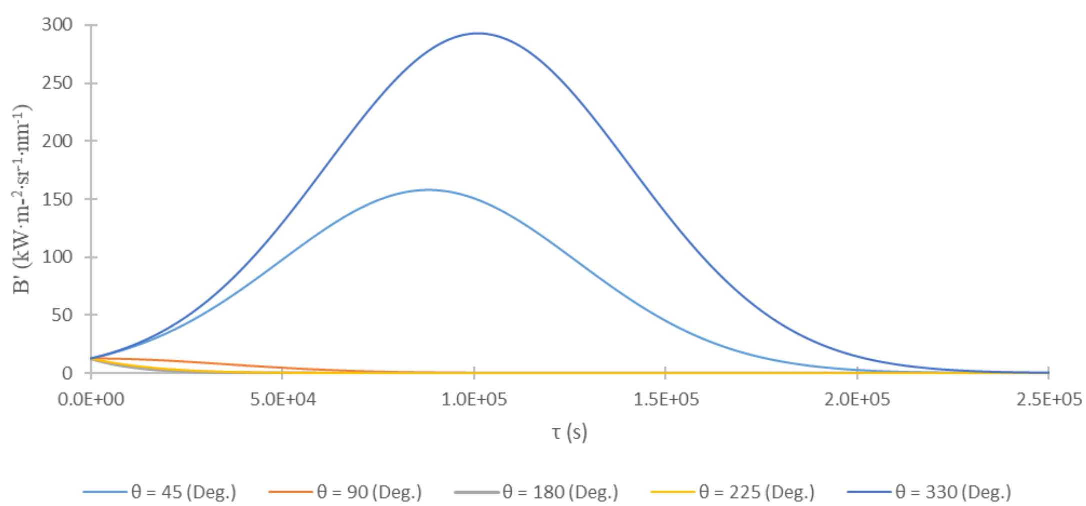

Figure 3.6: Non-inertial relativistic spectral radiance versus proper time for a 5000 K blackbody. $A = 10^{-5}$ $\left(a = 3\times10^3 \text{ m/s}^2\right)$. The lower left region is enlarged in Figure 3.7.

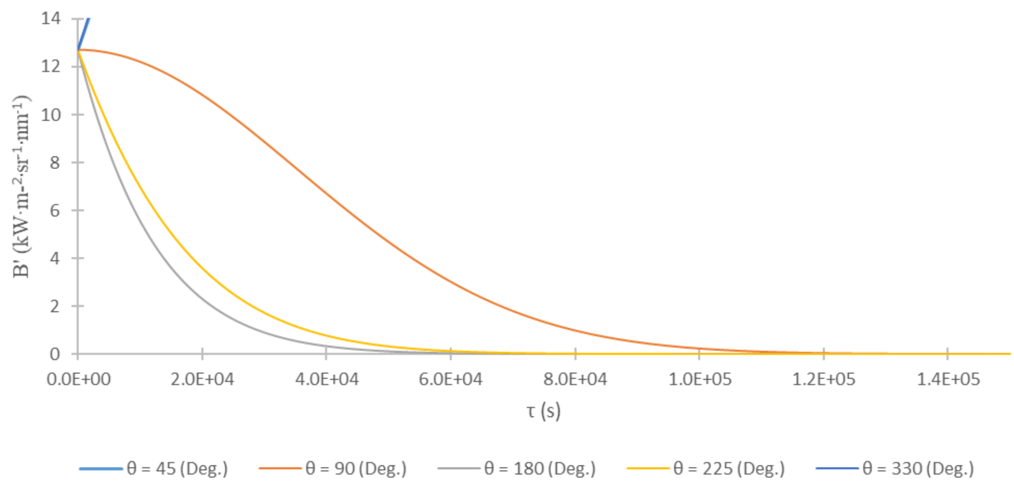

Figure 3.7: Non-inertial relativistic spectral radiance versus proper time for a 5000 K blackbody. $A = 10^{-5}$ $\left(a = 3\times10^{3}\ \text{m/s}^{2}\right)$.

For constant acceleration (in both magnitude and direction), the functional form of eq. (3.12) is unchanged. Hence, the angular dependence of the non-inertial spectral radiance is unchanged from the inertial case.

As $A\tau \to \infty$ for $0 \le \theta \le 90^{o}$ or $270^{o} \le \theta \le 360^{o}$ (approaching the radiation source), the non-inertial relativistic spectral radiance becomes infinite. However, for $90^{o} \le \theta \le 270^{o}$ (receding from the radiation source), $B' \to 0$. This angular dependence is the same for the inertial relativistic spectral radiance in eq. (3.12). Also, as required, when $A\tau = 0$, the stationary form of the non-inertial relativistic spectral radiance, eq. (3.15), is recovered. This behavior was discussed briefly in Section 3.3.1.

The time rate of change of the relativistic spectral radiance is its proper time derivative, $\dot{B}' \equiv \dfrac{dB'}{d\tau}$, and is non-trivially given by

$$\dot{B}_{\lambda}^{'} d\lambda d\Omega = \frac{2hc^2 \operatorname{sech}^2(A\tau)}{\lambda^6 k_B T_o \left(\exp\left(\frac{hc}{k_B \lambda T_o} (\cosh(A\tau) - \sinh(A\tau)\cos\theta) \right) - 1 \right)^2 (\tanh(A\tau)\cos\theta - 1)^4} \times$$
$$\left\{ \begin{array}{l} hc \exp\left(\frac{hc}{k_B \lambda T_o} (\cosh(A\tau) - \sinh(A\tau)\cos\theta) \right) (\tanh(A\tau)\cos\theta - 1) - 3k_B \lambda T_o \operatorname{sech}(A\tau) \times \\ \left(\exp\left(\frac{hc}{k_B \lambda T_o} (\cosh(A\tau) - \sinh(A\tau)\cos\theta) \right) - 1 \right) \end{array} \right\} \times \cdot$$
$$\left[\tanh(A\tau)\left(A + \dot{\theta}\sin\theta\right) - A\cos\theta \right] d\lambda d\Omega \tag{3.19}$$

For an observer in a photonic gas who is accelerating due to both a change in speed and a change in direction, θ becomes a time-dependent angle which, in general, is given by $\theta = \int d\tau \dot{\theta}$. As such, θ and τ are not independent quantities. The oscillatory behavior of the time rate of change of the spectral radiance is apparent in Figure 3.8 and Figure 3.9.

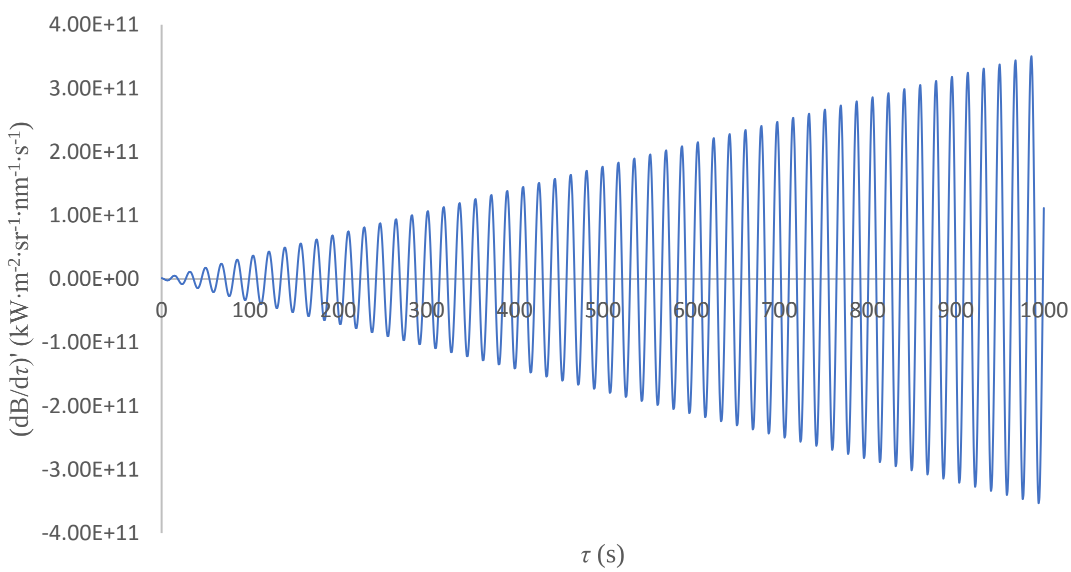

Figure 3.8: The rate of change of spectral radiance as a function of proper time for an observer with a proper acceleration of 10^{-5}, $\dot{\theta} = \frac{\pi}{9}\ \text{s}^{-1}$, and a rest frame temperature of 5,000 K.

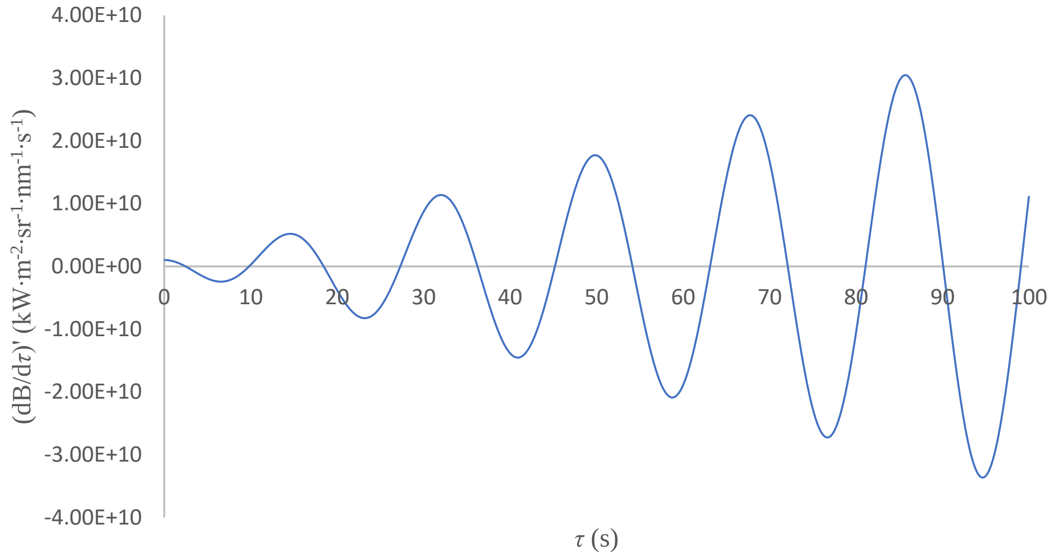

Figure 3.9: The rate of change of spectral radiance as a function of proper time for an observer with a proper acceleration of 10^{-5}, $\dot{\theta} = \frac{\pi}{9}\ \mathrm{s}^{-1}$, and a rest frame temperature of 5,000 K.

3.4 *The Relativistic Wien's Displacement Law*

The derivation of the Relativistic Wien's Displacement Law (RWDL) employs the same methodology as the stationary case for both the inertial and non-inertial reference frames and can be easily derived from the relativistic spectral radiance in wavelength space, eq. (3.13).

3.4.1 *RWDL in Inertial Reference Frames*

Letting $Q = \frac{hc}{k_B}\left(\beta_t - \beta_z \cos\theta\right)$ and setting the derivative (with respect to λ) of the relativistic spectral radiance in wavelength space, eq. (3.13), equal to zero yields

$$\frac{dB_\lambda^{'}}{d\lambda} = \frac{Q\exp\left(\frac{Q}{\lambda}\right)}{\exp\left(\frac{Q}{\lambda}\right)-1} - 5 = 0\,. \tag{3.23}$$

This is the familiar transcendental equation that arises in the Wien's Displacement Law derivation for stationary observers. Eq. (3.23) yields $b = \frac{Q}{\lambda'_{\max}} \approx 4.965224231\ldots$, and

$$\lambda'_{\max} = \frac{hc}{bk_B}\left(\beta_t - \beta_z \cos\theta\right). \tag{3.24}$$

Rewriting eq. (3.24) in terms of *V*:

$$\lambda'_{\max} = \frac{hc}{bk_B T_o \sqrt{1-V^2}}\left(1 - V\cos\theta\right) = D^{-1}\lambda_{\max}, \tag{3.25}$$

where $\lambda_{\max}$ is the wavelength of maximum irradiance in the radiation frame.

Eqs. (3.24) and (3.25) are the Relativistic Wien's Displacement Law. In the non-relativistic limit $(V << 1)$,

$$\lambda'_{\max} \sim \frac{hc}{bk_B T_o} - \frac{hc\cos\theta}{bk_B T_o} V + O\left(V^2\right), \tag{3.26}$$

where the first term in eq. (3.26) is $\lambda_{\max}$ (the radiation frame Stefan-Boltzmann Law).

Also, as $V \to 1$, $\lambda'_{\max} \to 0$ when $\theta = 0$, otherwise $\lambda'_{\max} \to \infty$. Consequently, when the velocity vector and the incident radiation vector are parallel (i.e. the observer is approaching the source directly), the frequency of radiation is completely blue shifted. Thus, the wavelength of maximum irradiance radiation in the observer frame approaches zero, and the frequency becomes infinite. However, for all off-axis observations of a moving radiation source, the wavelength becomes infinite and the frequency approaches zero because for increasing *θ*, the redshifted component of the velocity vector dominates for increasing *V*. Since the RWDL is independent of temperature inflation and depends exclusively on Doppler shifting, it obviously exhibits the same behavior as pure Doppler shifting. This result is shown in Figure 3.10.

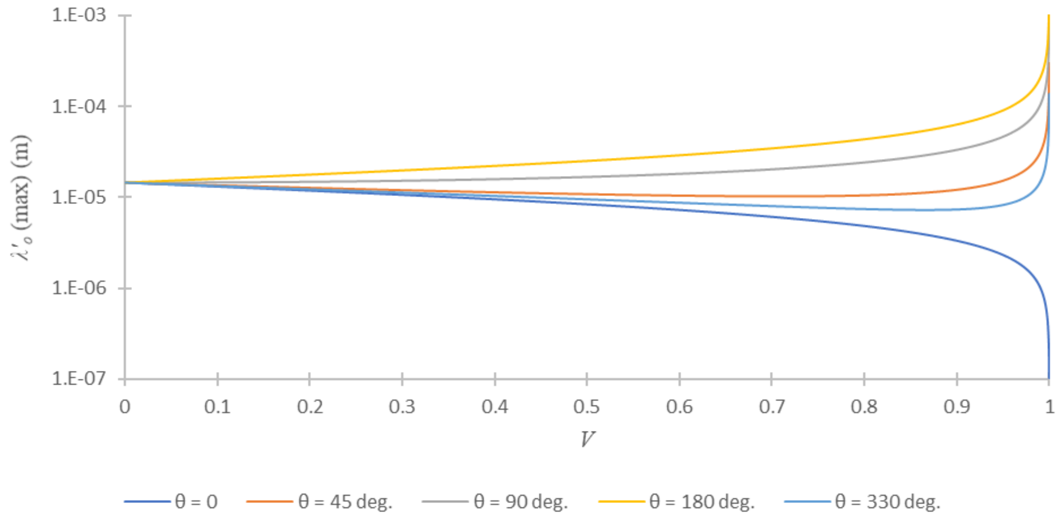

Figure 3.10: Wavelength of maximum irradiance versus speed for a radiation source with a proper temperature of 5000 K. The wavelength of maximum irradiance for the source when $V = 0$ is 0.5796 μm.

The angle which results in the maximum wavelength is expectedly the pure redshift case $(\theta = 180^o)$ and occurs from

$$\frac{d\lambda'_{\max}}{d\theta} = \frac{V\sin\theta}{\sqrt{1-V^2}} = 0\,, \tag{3.27}$$

and thus,

$$\lambda'_{\max}\left(\theta = 180^o\right) = \frac{hc}{bk_B T_o}\sqrt{\frac{1+V}{1-V}}\,, \tag{3.28}$$

as required.

3.4.2 *RWDL in Non-Inertial Reference Frames*

When the Relativistic Wien's Displacement Law is considered in a non-inertial reference frame, eqs. (3.20) and (3.25) are combined to give

$$\lambda'_{\max} = \frac{hc}{bk_B T_o}\cosh(A\tau)\left(1-\tanh(A\tau)\cos\theta\right) = \cosh(A\tau)\left(1-\tanh(A\tau)\cos\theta\right)\lambda_{\max}\,. \quad (3.29)$$

The angular dependence of the non-inertial, but constant-direction, RWDL is a simple cosine function, and its dependence on constant-direction acceleration and proper time is ultimately the same as the velocity dependence in eq. (3.25).

The time rate of change of the wavelength of maximum irradiance with a constant acceleration magnitude and a constant time rate of change of direction is

$$\dot{\lambda}'_{\max} \equiv \frac{d\lambda'_{\max}}{d\tau} = \frac{hc}{bk_B T_o}\left[A\sinh(A\tau)\left(1-\tanh(A\tau)\cos(\dot{\theta}\tau)\right) + A\cosh(A\tau)\cos(\dot{\theta}\tau) + \dot{\theta}\sinh(A\tau)\sin(\dot{\theta}\tau)\right]\cdot \quad (3.30)$$

Clearly, if both the speed and direction components of the acceleration 4-vector are zero, then $\dot{\lambda}'_{\max} = 0$. Plots of eq. (3.30) are shown in Figure 3.11, Figure 3.12, and Figure 3.13.

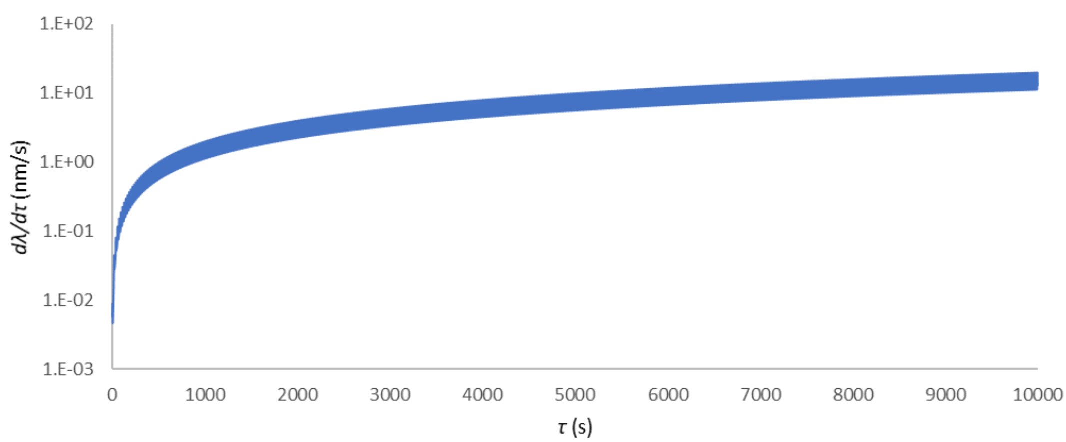

Figure 3.11: Time rate of change of wavelength of maximum irradiance versus proper time using an iterative scheme of 10,000 timesteps ($d\tau$ = 1s). T_o = 5000 K, $A = 10^{-5}$, $\dot{\theta} = \frac{\pi}{9}\cdot s^{-1}$.

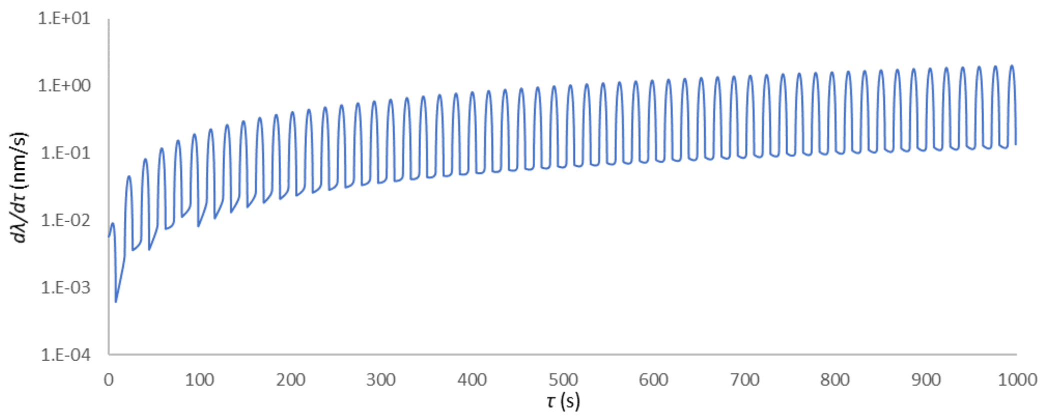

Figure 3.12: Time rate of change of wavelength of maximum irradiance versus proper time using an iterative scheme of 10,000 timesteps ($d\tau$ = 0.1s). T_o = 5000 K, $A = 10^{-5}$, $\dot{\theta} = \frac{\pi}{9} \cdot s^{-1}$. (See the discussion regarding the apparent jaggedness for τ.)

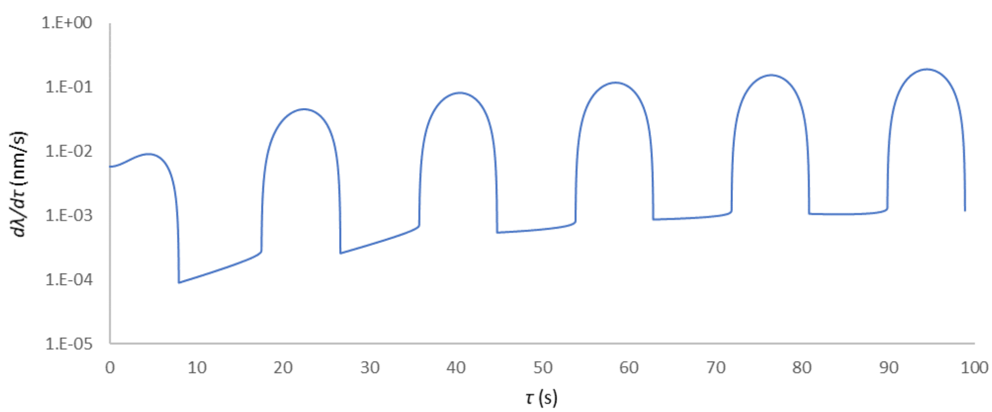

Figure 3.13: Time rate of change of wavelength of maximum irradiance versus proper time using an iterative scheme of 10,000 time steps ($d\tau$ = 0.01s). T_o = 5000 K, $A = 10^{-5}$, $\dot{\theta} = \frac{\pi}{9} \cdot s^{-1}$.

The non-trivial periodicity of $\dot{\lambda}'_{max}$ produces a function with an average period, in the above-mentioned example, of 0.06 s. The numeric noise, which is evident at a resolution of 0.1 s, is largely smoothed out at a resolution of 0.01 s.

3.5 The Relativistic Stefan-Boltzmann Law

Attempts to derive the Relativistic Stefan-Boltzmann Law have not relied on inverse temperature. Veitsman [54] did not rely on the invocation of the inverse temperature 4-vector and asserts the necessity of accounting for the tensor character of temperature. However, his specific solution for $\theta = 0$ and his general solution for all θ do not agree, and numeric differences due to renormalization from using different coordinate systems is not, in contrast to his claim, a viable explanation for this discrepancy.

3.5.1 *Inertial Reference Frames*

The derivation of the Relativistic Stefan-Boltzmann Law can be accomplished by considering the power (P'), the area (A'), and the irradiance (S') in frequency space, in a matter analogous to the derivation of the stationary Stefan-Boltzmann Law.

$$S' = \frac{P'}{A'} = \int_0^\infty \int B_\nu' d\Omega' d\nu' \tag{3.31}$$

From eqs. (3.12) and (3.31)[5],

$$S' = \int_0^\infty \int_0^{\frac{\pi}{2}} \frac{\frac{2h\nu^3}{c^2}}{\exp\left[\frac{h\nu}{k_B}(\beta_t - \beta_z \cos\theta)\right] - 1} \left[\gamma(1 - V\cos\theta)\right]^{-3} \cos\theta \sin\theta d\theta d\nu \int_0^{2\pi} d\phi\,. \tag{3.32}$$

[5] The integral over ϕ is independent of V because the motion is azimuthally constant. The $\cos\theta\sin\theta$ product arises from Lambert's Cosine Law ($\cos\theta$) and the solid angle integration ($\sin\theta$).

By setting $\alpha = \frac{2h}{c^2}\left[\gamma(1-V\cos\theta)\right]^{-3}\cos\theta\sin\theta\int_0^{2\pi}d\phi = \frac{4\pi h}{c^2}\left[\gamma(1-V\cos\theta)\right]^{-3}\cos\theta\sin\theta$,

letting $R=\beta_t-\beta_z\cos\theta$, and setting $x=\frac{h}{k_B}R\nu$, eq. (3.32) becomes

$$S^{'} = \int_0^{\infty}\int_0^{\frac{\pi}{2}}\frac{\alpha\,\nu^3}{e^x-1}d\theta d\nu, \tag{3.33}$$

$$S^{'} = \frac{k_B^4}{h^4}\int_0^{\infty}\int_0^{\frac{\pi}{2}}\frac{\alpha x^3}{R^4\left(e^x-1\right)}d\theta dx. \tag{3.34}$$

The integral over x yields $\zeta(4)=\frac{\pi^4}{15}$, where ζ is the Riemann zeta function.

Thus,

$$S^{'} = \frac{\pi^4 k_B^4}{15h^4}\int_0^{\frac{\pi}{2}}\frac{\alpha}{R^4}d\theta, \tag{3.35}$$

which becomes

$$S^{'} = \frac{4\pi^5 k_B^4}{15c^2h^3}\int_0^{\frac{\pi}{2}}\frac{\left[\gamma(1-V\cos\theta)\right]^{-3}\cos\theta\sin\theta}{\left(\beta_t-\beta_z\cos\theta\right)^4}d\theta. \tag{3.36}$$

From eqs. (3.12) and (3.35), and expanding eq. (3.36),

$$S^{'} = \frac{2\pi^5 k_B^4}{225\,c^2h^3}\left[\frac{(1+V)^2\left(1-V^2\right)^{\frac{3}{2}}\left(V^4-6V^3+15V^2-20V+15\right)}{(1-V)^4}\right]T_o^4. \tag{3.37}$$

Eq. (3.37) is the inertial Relativistic Stefan-Boltzmann Law, which can also be rewritten in terms of the rest frame irradiance, S.

$$S' = \frac{S}{15}\left[\frac{(1+V)^2(1-V^2)^{\frac{3}{2}}(V^4-6V^3+15V^2-20V+15)}{(1-V)^4}\right] \tag{3.38}$$

In the non-relativistic limit,

$$S' \sim \frac{2\pi^5 k_B^4 T_o^4}{15c^2h^3} + \frac{28\pi^5 k_B^4 T_o^4}{45c^2h^3}V + O(V^2), \tag{3.39}$$

where the first term in eq. (3.39) is expectedly the radiation-frame Stefan-Boltzmann Law. Also, in eq. (3.37), when $V \to 1$, relativistic beaming and temperature inflation cause $S' \to \infty$, also as expected. Illustrated in Figure 3.14 is the irradiance of an inertial relativistic radiation source.

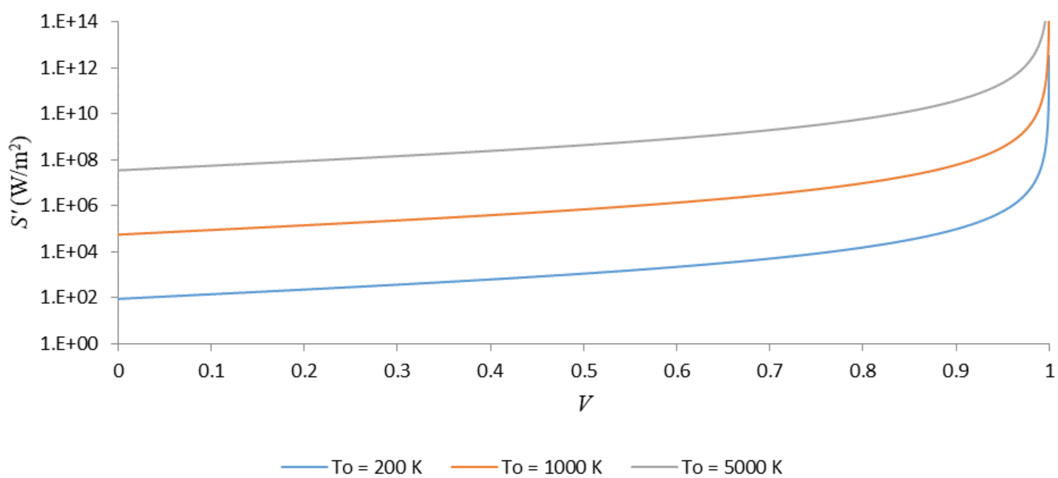

Figure 3.14: The inertial Relativistic Stefan-Boltzmann Law showing irradiance versus speed for a relativistic radiation source at three different temperatures. The S'-axis intercepts represent the irradiances in the radiation frame (90.3 W/m^2 for 200 K, 5.64×10^5 W/m^2 for 1000 K, 3.53×10^7 W/m^2 for 5000 K).

3.5.2 *Non-Inertial Reference Frames*

When the proper acceleration (with constant direction) is considered, eq. (3.40) results from eqs. (3.20) and (3.37), and it is plotted in Figure 3.15.

$$S' = \frac{2\pi^5 k_B^4}{225 c^2 h^3}\left[\frac{\begin{pmatrix}\tanh^6(A\tau) - 4\tanh^5(A\tau) + 4\tanh^4(A\tau) + 4\tanh^3(A\tau) \\ -10\tanh^2(A\tau) + 10\tanh(A\tau) + 15\end{pmatrix}(1+\tanh(A\tau))}{\cosh(A\tau)(1-\tanh(A\tau))^3}\right]T_o^4 \quad (3.40)$$

As expected, when $A\tau = 0$, $S' = S$, and when $A\tau \to \infty$, $S' \to \infty$.

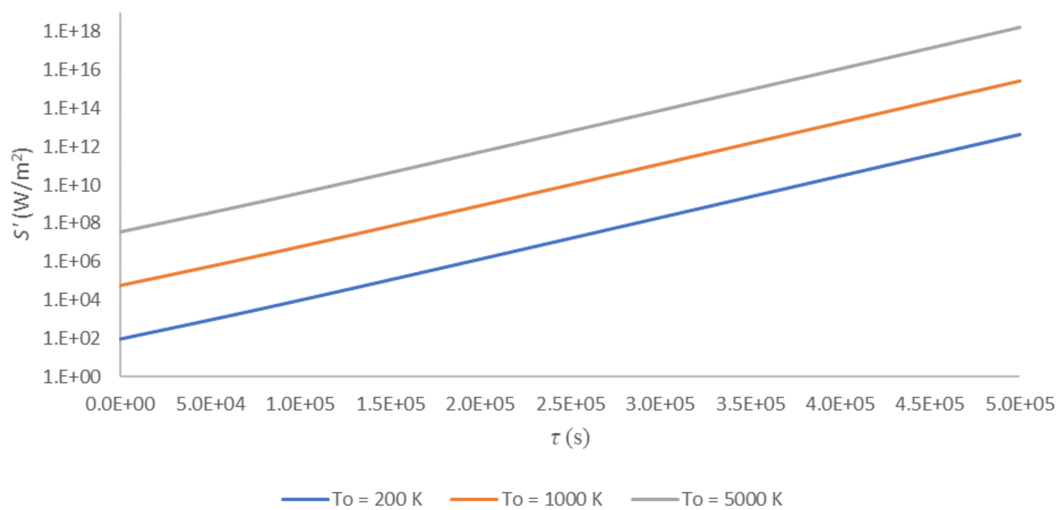

Figure 3.15: The inertial Relativistic Stefan-Boltzmann Law showing irradiance versus time for a non-inertial relativistic radiation source at three different temperatures. The S'-axis intercepts represent the irradiances in the radiation frame. $A = 10^{-5}$.

The time rate of change of the Relativistic Stefan-Boltzmann Law requires the proper time derivative of eq. (3.40) $\left(\dot{S}' \equiv \frac{dS'}{d\tau}\right)$, which produces the cumbersome result:

$$\dot{S}' = \frac{2\pi^5 k_B^4 T_o^4 A\left(\tanh\left(A\tau\right)+1\right)}{225c^2h^3\cosh\left(A\tau\right)\left(\tanh\left(A\tau\right)-1\right)^3}\times \begin{bmatrix} 5\tanh^7\left(A\tau\right)-20\tanh^6\left(A\tau\right)+22\tanh^5\left(A\tau\right)+12\tanh^4\left(A\tau\right) \\ -42\tanh^3\left(A\tau\right)+28\tanh^2\left(A\tau\right)-35\tanh\left(A\tau\right)-70 \end{bmatrix}. \tag{3.41}$$

When $A = 0$, the irradiance is constant. However, in the non-relativistic limit when $A \neq 0$ and $\tau \sim 0$,

$$\dot{S}' \sim \frac{28\pi^5 k_B^4 T_o^4}{45c^2h^3} A. \tag{3.42}$$

Perhaps unexpectedly, it is reasonable that both S' and $\dot{S}'$ lack angular dependence, even though the 4-acceleration is, in general, directionally dependent. This arises because the strict definition of $\dot{S}' \equiv \frac{dS'}{d\tau}$ requires the proper time differentiation of a function from which all angular dependence has been removed by the prior $d\Omega$ integration. Defining $\dot{S}' \equiv \int_0^\infty \int \dot{B}_\nu' d\Omega d\nu$ does not adhere to the required proper time derivative definition of $\dot{S}'$, in part because the order of the differentiation and integration must be preserved. Figure 3.16 illustrates the proper time rate of change of the irradiance.

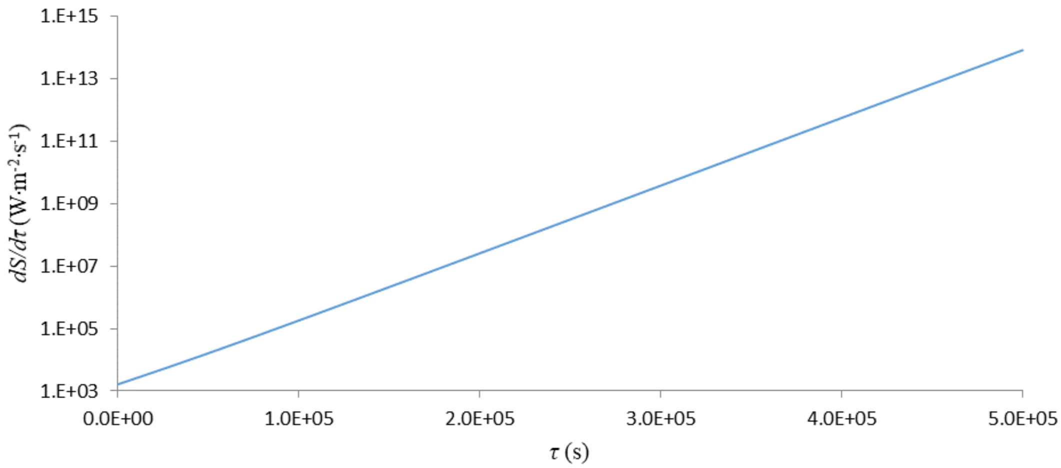

Figure 3.16: Proper time rate of change of irradiance of a relativistic blackbody. To = 5000 K, $A = 10^{-5}$.

3.6 *Observer and Radiation Frame Equivalences*

The relativistic Planckian spectrum poses numerous questions of interest. Among them is whether there are non-trivial solutions for which the observer frame and radiation frame spectral radiances, wavelengths of maximum irradiance, and irradiances are equal.

3.6.1 *Relativistic and Radiation Frame Spectral Radiances*

The case of equal relativistic and radiation frame spectral radiances comes from equating eqs. (3.15) and (3.18)[6]. Eq. (3.43) is the ratio of eqs. (3.15) and (3.18) set equal to 1.

$$\frac{\left[\exp\left(\frac{hc}{k_B \lambda T_o}\right)-1\right]\left(1-V^2\right)^{\frac{3}{2}}}{\left(1-V\cos\theta\right)^3\left\{\exp\left[\left(\frac{hc}{k_B \lambda T_o}\right)\frac{\left(1-V\cos\theta\right)}{\left(1-V^2\right)^{\frac{1}{2}}}\right]-1\right\}}=1 \tag{3.43}$$

[6] This is in wavelength space. The case for frequency space is analogous.

Obviously, neither V nor θ can be isolated as a closed-form function. However, a contour plot of eq. (3.43) is shown in Figure 3.17, and it is clear (as it was in Figure 3.2 and Figure 3.3) that there are non-zero speeds, as well as angles, for which B' is equal to B, or even less than B.

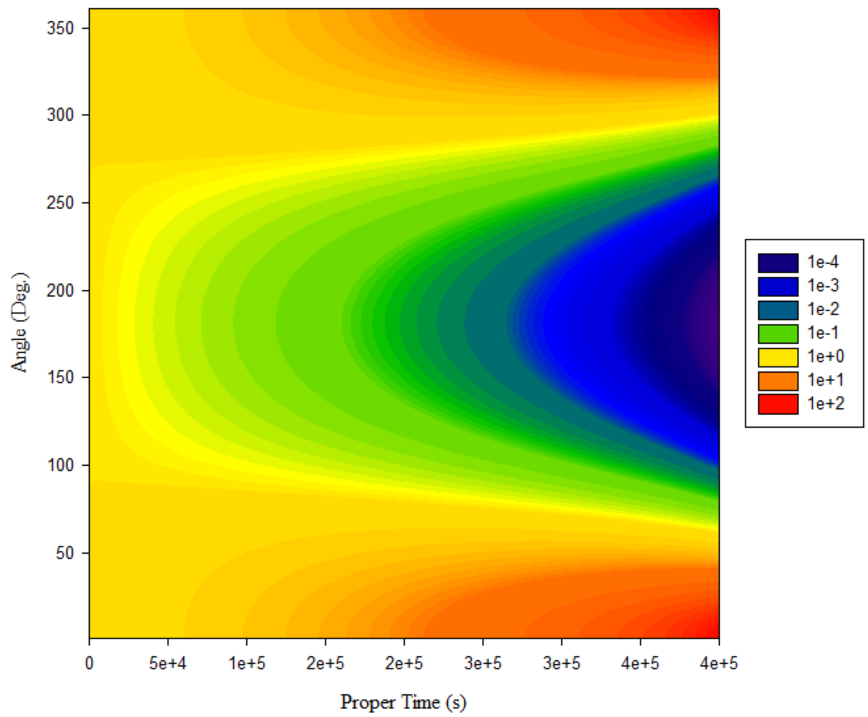

Figure 3.17: Contour plot of the ratio of inertial relativistic and radiation frame spectral radiances for a 5000 K blackbody observed at its wavelength of maximum irradiance (0.5796 μm). The yellow region indicates the V and θ values at which the inertial relativistic spectral radiance is equal to the radiation frame spectral radiance. The green and blue regions represent the V and θ values for which B' is less than B. The region of smallest spectral radiance is actually $B'/B \leq 10^{-4}$.

3.6.2 *Wavelengths of Maximum Irradiance*

Far simpler is determining V and θ for which the wavelength of maximum irradiance in the observer frame is equal to the wavelength of maximum irradiance in the radiation frame. From eq. (3.25),

$$\cos\theta = \sqrt{\frac{1+V}{1-V}}\,, \tag{3.44}$$

which has no subluminal solution. When eq. (3.25) is solved for *V*,

$$V = \frac{\cos^2\theta - 1}{\cos^2\theta + 1}. \tag{3.45}$$

However, since $0 \le V < 1$, $V = 0$ is the only physical solution to eq. (3.45). Therefore, as expected, there is no frame which is not comoving with the radiation frame in which $\lambda'_{\max} = \lambda_{\max}$.

3.6.3 *Irradiances*

The solution for the irradiance from the Relativistic Stefan-Boltzmann Law comes from eq. (3.38). The only real solution to eq. (3.46) (plotted in Figure 3.18) is $V = 0$. Expectedly, there is no frame which is not comoving with the radiation frame in which the irradiance equals the irradiance in the radiation frame.

$$S' = \frac{S}{15}\left[\frac{(1+V)^2(1-V^2)^{\frac{3}{2}}(V^4 - 6V^3 + 15V^2 - 20V + 15)}{(1-V)^4}\right] = S \tag{3.46}$$

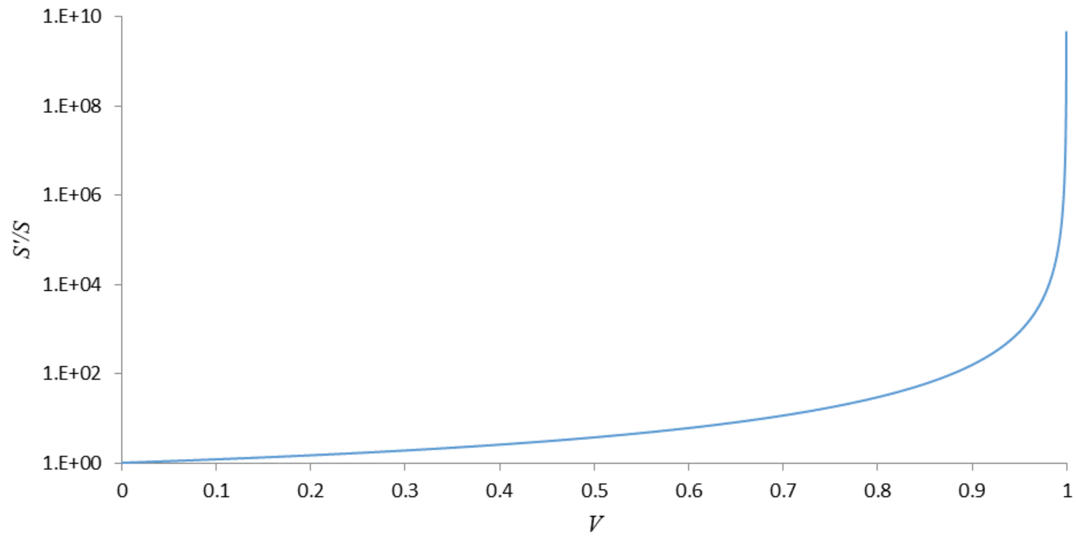

Figure 3.18: Ratio of irradiances in the observer and radiation frames as a function of speed for a blackbody. Clearly, only for V >> 0 does the departure from unity of S′/S become significant.

3.7 Summary

The Relativistic Planck's Law, the Relativistic Wien's Displacement Law, and the Relativistic Stefan-Boltzmann Law have been established in inertial and non-inertial reference frames by invoking the inverse temperature 4-vector, 4-acceleration, relativistic beaming, Doppler shifting, and, when required, the appropriate proper time derivatives. In the low velocity limit of the relativistic blackbody spectrum, the corresponding and well-established stationary blackbody spectrum has been shown to emerge for each of the aforementioned relativistic laws. The Relativistic Wien's Displacement Law was shown to be independent of temperature inflation and entirely dependent on Doppler shifting. In each case, the high velocity limit of the relativistic blackbody spectrum produced the expected zero or infinite outcome.

The angular periodicity of the Relativistic Planck's Law was determined, and further work needs to be done to elucidate the emergent picture. The relativistic versions of Planck's Law, Wien's Displacement Law, and the Stefan-Boltzmann Law were compared to the stationary versions, and it was determined that only in the case of spectral radiance are there non-trivial solutions by which the descriptions produce equal results.

CHAPTER FOUR

Black Sun: Ocular Invisibility of Relativistic Luminous Astrophysical Bodies

This chapter published as: J.S. Lee, and G.B. Cleaver, "Black Sun: Ocular Invisibility of Relativistic Luminous Astrophysical Bodies", *Journal of High Energy Physics, Gravitation and Cosmology*, 2, pp. 562-570, 12 September 2016. http://dx.doi.org/10.4236/jhepgc.2016.24048.

4.1 Introduction

The relativistic blackbody spectrum suggests the intriguing possibility that a luminous astrophysical body can be rendered optically invisible to the human eye by relativistic Doppler shifting the wavelengths of maximum intensity from the visible frequency range to above or below the frequency thresholds of human vision.[1] This chapter examines, as a gedanken experiment, the specific conditions under which this effect would occur.[2]

Furthermore, relativistic blackbody radiators will emit spectral radiances which are increased (in the case of approaching) or decreased (in the case of receding), due to temperature inflation and relativistic beaming. By considering in the gedanken experiment the relativistic blackbody spectrum, the proper distances can be determined at

[1] For this effect, CCD detectors could be considered in place of human eyes, but the nature of the phenomenon wouldn't change. Of course, the numbers would strongly change, due to the strong differences between the spectral response function of human eye and CCD cameras: for instance, a relativistic Doppler shift could make the object even more detectable by an IR sensitive CCD.

[2] Whether the physical situations could exist for this effect to be realized is VERY uncertain. As an example, relativistic speeds might be obtainable in the expulsion of a low-mass star from the region of the Galactic Center as a consequence of a fly-by with the central massive black hole. Nevertheless, such a star might already appear invisible from earth because of its distance, rather than as a result the relativistic Doppler Effect and would be strongly decelerated (or even completely destroyed) by the relativistic drag of the dense interstellar matter of the Galactic Center region. The possible astrophysical application of this gedanken experiment is thus unlikely.

which the apparent magnitude of a blackbody radiator is greater (i.e., dimmer) than approximately 6.5 (the threshold of vision for the typical unaided human eye).

Additionally, laboratory tests of the sensitivity of the unassisted human eye are described, and this paper asserts that the Judd & Voss CIE 1978 photopic luminous efficiency function would not be applicable to the situation of LABs due to the much greater luminosity than in the laboratory tests.

4.2 The Apparent Magnitude of Blackbody Radiators in the Rest Frame

The relationship between absolute magnitude, apparent magnitude, and distance to an arbitrary stationary blackbody radiation source has been well established and is given by

$$M = m + 5 - 5\log z \, . \tag{4.1}$$

where M is the absolute magnitude of any blackbody radiator, m is its apparent magnitude, and z is the distance to the observer in parsecs. Also, in terms of luminosity,

$$M = M_o - 2.5\log\left(\frac{L}{L_o}\right). \tag{4.2}$$

where M_o is the absolute magnitude of a reference star (e.g., the sun), L is the luminosity of the radiation source at an arbitrary distance z, and L_o is the absolute luminosity of that source[3].

[3] The luminosity of the source at the absolute magnitude distance (i.e., 10 parsecs).

Equating eqs. (4.1) and (4.2) yields

$$z = 10^{\frac{m+5-M_o}{5}} \sqrt{\frac{L}{L_o}} \,. \tag{4.3}$$

Thus, for the sun, M_o = 4.83, $L = L_o$ = 1, and for it to be invisible to the naked eye in the [nearly] total blackness of interstellar space, m = 6.5 [66] (discussed in Section 4.4). Therefore, the sun is visible to the unaided eye at distances up to 21.58 pc (70.39 LY).

4.3 The Apparent Magnitude of Relativistic Blackbody Radiators

Sufficiently high-speed relativistic motion of blackbody radiators would clearly Doppler shift the wavelengths of maximum luminosity to beyond the human visual range. Therefore, the lower luminosity wavelengths are Doppler shifted into the visible range, and the overall visible luminosity is reduced.

However, in the case of an approaching blackbody, the radiation is relativistically beamed, and the blackbody temperature is "inflated". Both of these effects serve to increase the luminosity. For a receding blackbody, relativistic beaming ("expanding") and temperature "deflation" will have the reverse effect. Therefore, eq. (4.3) becomes

$$z = 10^{\frac{m+5-M_o}{5}} \sqrt{\frac{L'}{L_o}} \,. \tag{4.4}$$

where L' and L_0 are the luminosities in the relativistic and rest frames respectively[4]. Luminosity is obtained by integrating the spectral radiance over frequency and solid angle:

[4] Primed quantities indicate the relativistic frame.

$$\frac{L'}{L_o} = \frac{\int_{\nu_1}^{\nu_2}\int B' d\Omega' d\nu'}{\int_{\nu_1}^{\nu_2}\int B_o d\Omega d\nu} \tag{4.5}$$

where ν_1 and ν_2 are the mean lower and upper frequencies of ocular visibility. B' and B_o are the spectral radiances in the relativistic and rest frames respectively, which must be integrated over the appropriate solid angle Ω.

The relativistic spectral radiance in frequency space, accounting for Doppler shifting, relativistic beaming, and temperature inflation, was determined in Chapter 3.3 and is given eq. (3.12) (restated as eqs. (4.6), (4.7) and (4.8)), by:

$$B_\nu' d\nu d\Omega = \frac{\left(\frac{2h\nu^3}{c^2}\right)}{\exp\left[\frac{h\nu}{k_B}\left(\beta_t - \beta_z \cos\theta\right)\right] - 1}\left[\gamma\left(1 - V\cos\theta\right)\right]^{-3} d\nu d\Omega \tag{4.6}$$

where [67],

$$\beta_t = \frac{1}{T_o\sqrt{1-V^2}} \tag{4.7}$$

$$\beta_z = \frac{V}{T_o\sqrt{1-V^2}}, \tag{4.8}$$

T_o is the proper absolute temperature, u_μ is the relative 4-velocity between the radiation and the observer, $\left[\beta_t, \beta_x, \beta_y, \beta_z\right]$ is the van Kampen-Israel inverse temperature 4-vector, θ is the angle between u_μ and β_μ, and $V = \frac{u}{c}$ (fraction of light speed).

The integration of the spectral radiance over all frequencies is straightforward because, with the limits of 0 and ∞, the result is simply $\pi^4/15$. However, the in-band luminosity requires integration over a finite frequency range. Here, the method of Widger and Woodall is followed [68].

$$B_\nu^{'} d\Omega = \int_{\nu_1}^{\nu_2} \frac{\left(\frac{2h\nu^3}{c^2}\right)}{\exp\left[\frac{h\nu}{k_B}\left(\beta_t - \beta_z \cos\theta\right)\right] - 1} \left[\gamma(1 - V\cos\theta)\right]^{-3} d\nu d\Omega \tag{4.9}$$

Let

$$Q' = \frac{\left(\frac{2h}{c^2}\right)\left(1 - V^2\right)^{\frac{3}{2}}}{\left(1 - V\cos\theta\right)^3} \tag{4.10}$$

and

$$R' = \frac{h(1 - V\cos\theta)}{k_B T_o \sqrt{1 - V^2}} . \tag{4.11}$$

Also, letting $x' = R'\nu$, and from eqs. (4.7) and (4.8), eq. (4.9) becomes

$$B_\nu^{'} d\Omega = \frac{Q'}{R'^4} \int_{\nu'_1}^{\nu'_2} \frac{x'^3}{e^{x'} - 1} dx' d\Omega \tag{4.12}$$

Expanding eq. (4.12) as a difference of integrals:

$$B_\nu^{'} d\Omega = \frac{Q'}{R'^4} \left[\int_{\frac{x'_1}{R}}^{\infty} \frac{x'^3}{e^{x'} - 1} - \int_{\frac{x'_2}{R}}^{\infty} \frac{x'^3}{e^{x'} - 1} \right] dx' d\Omega . \tag{4.13}$$

Evaluating eq. (4.13) and re-substituting $x' = R'\nu$:

$$B_{\nu}^{'} d\Omega = \frac{Q'}{R'^4} \left[\begin{array}{l} \sum_{n=1}^{\infty} \left(\frac{R'^3 \nu_1^3}{n} + \frac{3R'^2 \nu_1^2}{n^2} + \frac{6R'\nu_1}{n^3} + \frac{6}{n^4} \right) e^{-nR'\nu_1} \\ -\sum_{n=1}^{\infty} \left(\frac{R'^3 \nu_2^3}{n} + \frac{3R'^2 \nu_2^2}{n^2} + \frac{6R'\nu_2}{n^3} + \frac{6}{n^4} \right) e^{-nR'\nu_2} \end{array} \right] d\Omega \, . \qquad (4.14)$$

Expanding the solid angle integration, combining sums, and making use of

$L_{\nu}^{'} = \int_{\nu_1}^{\nu_2} \int B' d\Omega' d\nu'$ from eq. (4.5), the relativistic luminosity in frequency space (eq.

(4.14)) becomes[5]

$$L_{\nu}' = \frac{Q'}{R'^4} \int \int \sum_{n=1}^{\infty} \left[\begin{array}{l} \left(\frac{R'^3 \nu_1^3}{n} + \frac{3R'^2 \nu_1^2}{n^2} + \frac{6R'\nu_1}{n^3} + \frac{6}{n^4} \right) e^{-nR'\nu_1} \\ -\left(\frac{R'^3 \nu_2^3}{n} + \frac{3R'^2 \nu_2^2}{n^2} + \frac{6R'\nu_2}{n^3} + \frac{6}{n^4} \right) e^{-nR'\nu_2} \end{array} \right] \cos\theta \sin\theta d\theta d\varphi \, . \qquad (4.15)$$

In the case of approaching the LAB [approximately] directly, a simplification of eq. (4.15), which cannot be resolved as a closed form function, can be made. Since θ is very small, $\sin\theta \sim \theta$ and $\cos\theta \sim 1$. This removes the angular dependence from eq. (4.11), which reduces to

$$R = \frac{h}{k_B T_o} \sqrt{\frac{1-V}{1+V}} \, . \qquad (4.16)$$

[5] The cosθ term accounts for the Lambertian radiator, and the sinθ term arises from the solid angle integration.

Frequently, when evaluating the $d\Omega$ integration, the solid angle over which the integration is performed is the solid angle through which the blackbody radiates. However, that is not the case here. The solid angle is that which is subtended by the blackbody from the vantage point of the observer.

Therefore, when $z >> D$, $\theta \sim D/z$ (*z* is the observer proper distance, and *D* is the diameter of the blackbody). For a blackbody with a circular *x*-*y* cross-section, $\varphi \sim D/z$. Therefore,

$$L_\nu^{'} \approx \frac{Q'}{R'^4} \sum_{n=1}^{\infty} \begin{bmatrix} \left(\frac{R'^3 \nu_1^3}{n} + \frac{3R'^2 \nu_1^2}{n^2} + \frac{6R'\nu_1}{n^3} + \frac{6}{n^4} \right) e^{-nR'\nu_1} \\ -\left(\frac{R'^3 \nu_2^3}{n} + \frac{3R'^2 \nu_2^2}{n^2} + \frac{6R'\nu_2}{n^3} + \frac{6}{n^4} \right) e^{-nR'\nu_2} \end{bmatrix} \int_0^{\frac{D}{z}} \theta d\theta \int_0^{\frac{D}{z}} d\varphi . \tag{4.17}$$

Thus,

$$L_\nu^{'} \approx \frac{2k_B^4 T_o^4}{c^2 h^3} \sum_{n=1}^{\infty} \begin{bmatrix} \left(\frac{R'^3 \nu_1^3}{n} + \frac{3R'^2 \nu_1^2}{n^2} + \frac{6R'\nu_1}{n^3} + \frac{6}{n^4} \right) e^{-nR'\nu_1} \\ -\left(\frac{R'^3 \nu_2^3}{n} + \frac{3R'^2 \nu_2^2}{n^2} + \frac{6R'\nu_2}{n^3} + \frac{6}{n^4} \right) e^{-nR'\nu_2} \end{bmatrix} \left(\frac{D}{z} \right)^3 \left(\frac{1-V}{1+V} \right)^{\frac{7}{2}} . \tag{4.18}$$

Similarly,

$$L_o \approx \frac{2k_B^4 T_o^4}{c^2 h^3} \sum_{n=1}^{\infty} \begin{bmatrix} \left(\frac{R^3 \nu_1^3}{n} + \frac{3R^2 \nu_1^2}{n^2} + \frac{6R\nu_1}{n^3} + \frac{6}{n^4} \right) e^{-nR\nu_1} \\ -\left(\frac{R^3 \nu_2^3}{n} + \frac{3R^2 \nu_2^2}{n^2} + \frac{6R\nu_2}{n^3} + \frac{6}{n^4} \right) e^{-nR\nu_2} \end{bmatrix} \left(\frac{D}{z} \right)^3 . \tag{4.19}$$

Combining eq. (4.3), in terms of relativistic luminosity, with eqs. (4.18) and (4.19) yields

$$z = 10^{\frac{m+5-M_o}{5}} \left[\frac{\sum_{n=1}^{\infty}\left[\left(\frac{R'^3\nu_1^3}{n}+\frac{3R'^2\nu_1^2}{n^2}+\frac{6R'\nu_1}{n^3}+\frac{6}{n^4}\right)e^{-nR'\nu_1}-\left(\frac{R'^3\nu_2^3}{n}+\frac{3R'^2\nu_2^2}{n^2}+\frac{6R'\nu_2}{n^3}+\frac{6}{n^4}\right)e^{-nR'\nu_2}\right]}{\sum_{n=1}^{\infty}\left[\left(\frac{R^3\nu_1^3}{n}+\frac{3R^2\nu_1^2}{n^2}+\frac{6R\nu_1}{n^3}+\frac{6}{n^4}\right)e^{-nR\nu_1}-\left(\frac{R^3\nu_2^3}{n}+\frac{3R^2\nu_2^2}{n^2}+\frac{6R\nu_2}{n^3}+\frac{6}{n^4}\right)e^{-nR\nu_2}\right]} \right]^{\frac{1}{2}} \left(\frac{1-V}{1+V}\right)^{\frac{7}{4}} \cdot \quad (4.20)$$

Evaluation of the infinite sums is greatly simplified due, in large part, to the rapid convergence of the series as a result of the $e^{-nR\nu}$ terms. The smallest value of R (requiring the largest number of summation terms) occurs when $V = 0$, and from eq. (4.11), is $\frac{h}{k_B T_o}$. The smallest useful value of $R\nu = 0.400$ would result from an O-class star with a surface temperature of ~50,000 K and at the lowest frequency of human visibility.

Table 4.1 gives the number of summation terms (n) (in eq. (4.20)) that would be required to produce at least 10 significant figure convergence for $0.1 \le R\nu \le 25$.

Table 4.1: Number of summation terms required for series convergence of eq. (3.22) to at least 10 significant figures [68].

Rv	Number of Summation Terms (*n*)
0.1	101
0.2	65
0.3	50
0.4	50
0.5	35
0.6	30
0.7	25
0.8	22
0.9–1.4	20
1.5–1.9	15
2.0–2.9	10
3.0–3.9	8
4.0–4.9	6
5.0–9.9	4
10.0–24.9	3
≥ 25.0	1

4.4 The Ocular Invisibility of Relativistic Radiators

The visibility to the naked eye of astronomical objects has been discussed extensively in the literature [69], [70], [71], [72], [73]. The "sky" of interstellar space is considered to be absolutely black, and a viewing port is taken to be, at optical wavelengths, a perfectly transparent aperture that subtends a solid angle of at least the human field of vision and with a magnification of 1.

The efficiency by which photons are used by the retina was accounted for by correcting for the Stiles-Crawford effect of the first (SCE I) and second (SCE II) kind[6],

[6] The Stiles-Crawford effect of the first kind is the phenomenon by which light entering the edge of the pupil elicits a smaller response from the cone photoreceptors than light entering the center of the pupil. The Stiles-Crawford effect of the second kind states that the perceived hue from a monochromatic light source is dependent on its obliquity with respect to the retina.

photon absorption by the optical media, photopigment absorption of photons, and the photon isomerization efficiency of the photopigment.

For a 22´ (diameter), 10 ms, 507 nm monochromatic source, in which, of the ~100 quanta incident upon the retina, 10 to 15 were absorbed by the ~1600 illuminated rods [74]. From this experiment, Packer and Williams determined the rod actinometric, radiometric, and photometric[7] absolute thresholds to be 0.35 γ/s, 4.35×10^{-6} $W\cdot m^{-2}\cdot sr^{-1}$, and 1.33×10^{-3} $cd\cdot m^{-2}$, respectively [75]. However, also examined was the case of a stimulus which exceeded the visual system's spatial summation area and temporal integration time, in which the rod actinometric, radiometric, and photometric absolute thresholds are 2.00×10^{-4} γ/s, 2.47×10^{-9} $W\cdot m^{-2}\cdot sr^{-1}$, and 7.5×10^{-7} $cd\cdot m^{-2}$, respectively.

However, even accounting for the standard observer's spectral sensitivity by applying the Judd & Voss CIE 1978 photopic luminous efficiency function, these results are difficult to apply to the scenario presented here because of the enormous disparity between the spectral irradiances of the Hallett test sources [74] and stars.

The frequency range of human vision is slightly variable. However, 4.17×10^{14} Hz and 7.89×10^{14} Hz, which correspond to wavelengths of 720 nm and 380 nm respectively, are acceptable approximations of the limits of human vision, and are in keeping with the wavelengths of 700 nm and 390 nm published by Starr [76]. The limiting magnitude of the unassisted human eye is taken to be 6.5 [66]. This figure applies to all visible wavelengths and accounts for eye sensitivity. Consequently, inclusion of the Judd & Voss CIE 1978 photopic luminous efficiency function would not be appropriate.

[7] Assuming a 6 mm in diameter pupil.

4.4.1 $\theta = 0$ *Ocular Invisibility*

In the case of approaching the sun directly ($\theta = 0$), the distance at which the apparent magnitude is 6.5 can be determined from eq. (4.20), and is shown in Figure 4.1.

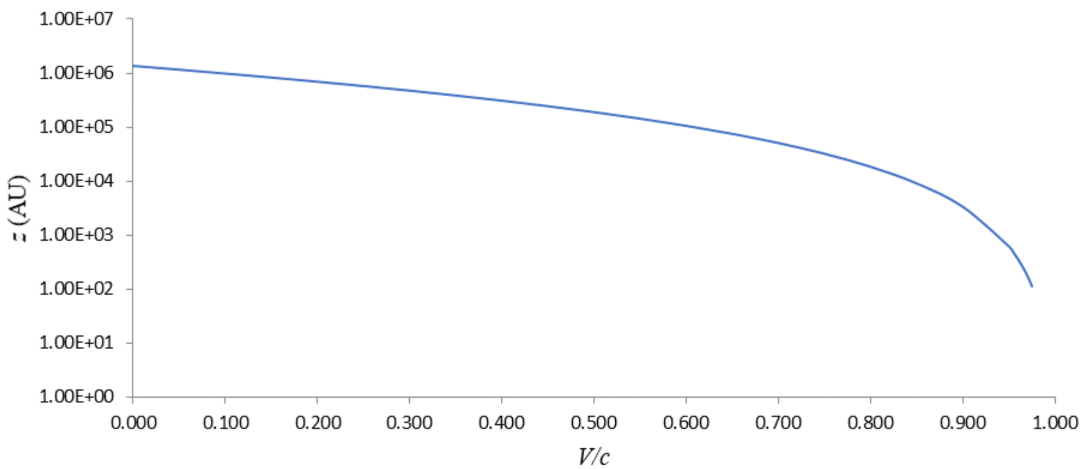

Figure 4.1: Distance versus speed for limiting magnitude (m = 6.5) of the sun. The wavelengths of vision are taken to be between 380 nm and 720 nm, and the temperature is 5780 K. The region below the curve represents the distance at which the sun is visible to the typical unaided eye of an observer in the frame of the sun.

4.4.2 *Ocular Invisibility for Arbitrary* θ

In order to determine the ocular invisibility curve for an arbitrary velocity vector, the solid angle integration in eq. (4.15), and correspondingly for the stationary case, must be performed. However, since the solid angle over which the integration must be taken does not significantly exceed ~10 mrad[8] (and is considered primarily for angles much smaller), z can be approximated as being constant at each value of θ in the 315-time step iterative scheme, which was used to evaluate the solid angle integral. When eq. (4.20) is evaluated for the sun, Figure 4.2 results.

---

[8] The angle subtended by the sun at approximately 1 AU.

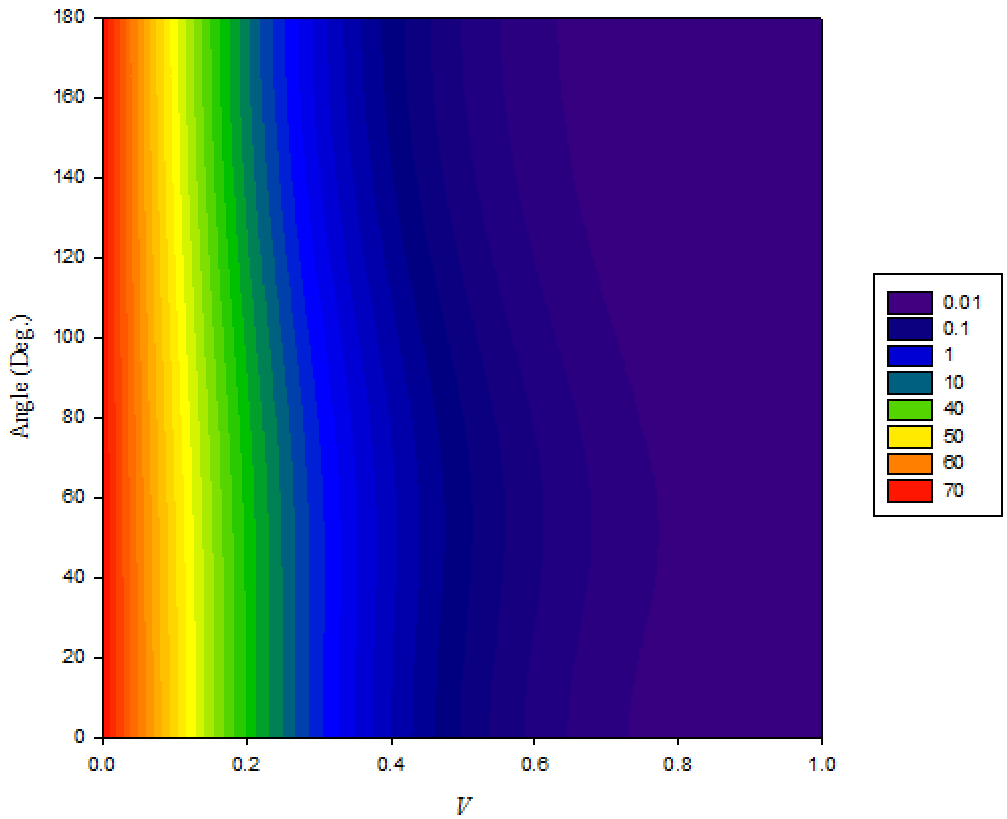

Figure 4.2: Proper distance of limiting magnitude as a function of V and θ for the sun. The wavelengths of vision are taken to be 380 nm to 720 nm, and the temperature is 5780 K. The numbers in the legend represent the proper distances in light years at which the apparent magnitude is 6.5. The purple region of 0.01 LY represents proper distances which are $\leq$ 0.01 LY. The intersection of the contours with the *Angle*-axis is expectedly 70.39 LY (as determined in Section 4.2).

As expected and shown in Figure 4.2, ultra-relativistic velocities permit exceptionally close approaches to luminous astrophysical bodies, while maintaining an apparent magnitude which is less than the limiting magnitude of the unaided human eye.

4.5 Summary

By making use in this gedanken experiment of the relativistic blackbody spectrum, the velocity profile for the apparent magnitude of a LAB has been determined. Optical invisibility to the unaided eye arises due to the Doppler shifting of the wavelengths of maximum radiance to beyond the limits of human visual sensitivity. Temperature inflation and relativistic beaming can either increase this incident radiance (for an approaching source) or decrease it (for a receding source). By considering the wavelength limits of human vision to be 380 nm and 720 nm, and the limiting magnitude of the unaided human eye to be 6.5, the proper distance versus velocity function for ocular invisibility of relativistic luminous astrophysical bodies has been determined; this profile was determined for the sun.

Whether the physical situations could exist for this effect to be realized is uncertain. As an example, relativistic speeds might be obtainable in the expulsion of a low-mass star from the region of the galactic center as a consequence of a fly-by with the central massive blackhole. Nevertheless, such a star might already appear invisible from earth because of its distance, rather than as a result the relativistic Doppler Effect. The possible realization of this gedanken experiment is an open question.

CHAPTER FIVE

Relativistic Drag and Emission Radiation Pressures in an Isotropic Photonic Gas

This chapter published as: J.S. Lee and G. B. Cleaver, "Relativistic Drag and Emission Radiation Pressures in an Isotropic Photonic Gas", *Modern Physics Letters A,* Volume 31, Issue 19, 21 June 2016. arXiv:1508.00534

5.1 Introduction

This chapter challenges the results of Balasanyan and Mkrtchian [77], in which the blackbody radiation drag on a relativistically moving mirror is calculated. To determine the relativistic photon drag, temperature inflation, Doppler shifting, and relativistic beaming of radiation in the direction of motion must all be considered.

Here, a *z*-axis-directed relativistic planar surface with an arbitrary absorptivity/emissivity, which is in thermal equilibrium with an isotropic thermalized photonic gas, is examined. Relativistic temperature transformations are accomplished by means of *inverse temperature*, a van Kampen-Israel future-directed timelike 4-vector. The body experiences radiation drag due to the momentum transfer from Doppler shifted and relativistically beamed photons incident upon its forward-directed planar surface.

With increasing speed, the radiation field becomes progressively more anisotropic in the inertial frame, thus, creating a rising temperature difference between the forward- and rearward-directed thermally isolated surfaces of the body; this results in an emission radiation pressure gradient. If thermal sequestration of the forward- and rearward-directed surfaces is removed, the resulting temperature gradient across the body induces a short-lived Carnot cycle with a speed-dependent efficiency.

Additionally, the non-inertial reference frame case for drag and emission radiation pressures is established by making use of the proper time derivative of the inertial frame relativistic radiation pressures. For surfaces which are not thermally isolated, a positive forward-to-rearward temperature gradient induces an ongoing Carnot cycle, as the surface temperatures never equalize. If the forward-to-rearward temperature gradient is negative (i.e., the body's speed is reducing), the Carnot cycle ceases upon thermal equilibrium of the surfaces. Also, the drag radiation pressure acting upon a body with an arbitrary frontal surface geometry is determined.

5.2 The Drag Radiation Pressure

There are significant unresolved issues in the literature regarding temperature in relativistic thermodynamics [55], [15], [16], [56], [57], [58]. Throughout the twentieth century, three published Lorentz group transformations have emerged: Temperature Deflation [15], [16] and Temperature Inflation [17], [18], [19] (which can be operationally quantified with a relativistic Carnot cycle [24], [25], [26]), and Temperature Invariance [20], [21], [22], [23].

The *empirical temperature* (a Lorentz invariant), which follows from the Zeroth Law of Thermodynamics, is a relativistic scalar that reflects the radiation rest frame and the observer frame as being in thermal equilibrium [29]. The validity of the Zeroth Law is necessarily independent of any reference of any thermodynamic property (including energy and entropy) [30].

The Second Law of Thermodynamics gives rise to the *absolute temperature*, which contains no angular dependence, and is the product of the radiation rest frame absolute temperature and the Lorentz factor.

Temperature transformations can be successfully realized by treating *inverse temperature* as a van Kampen-Israel future-directed timelike 4-vector. Although Przanowski and Tosiek [27][1] have demonstrated temperature inflation without making use of inverse temperature, a relativistic blackbody spectrum necessitates a consideration of angular dependence.

Balasanyan and Mkrtchian [77] calculate the drag pressure from blackbody radiation on a relativistic mirror. However, temperature, rather than the thermodynamically relevant inverse temperature, is transformed as a scalar. Also, relativistic beaming and Doppler shifting of incident radiation, which are essential to describing the relativistic spectral radiance and energy density of a blackbody, are not considered.

5.2.1 *Inertial Frames*

The total radiation pressure on an opaque object in an inertial frame with a frequency-independent absorption/emission coefficient ε, is the sum of the radiation pressures due to absorption and reflection:

$$P_{\mathrm{TOT}} = \varepsilon P_{\mathrm{INC}} + 2(1-\varepsilon) P_{\mathrm{INC}} = (2-\varepsilon) P_{\mathrm{INC}}, \tag{5.1}$$

where P_{INC} is the incident radiation pressure[2].

Also,

$$P_{\mathrm{TOT}} = \frac{2-\varepsilon}{c} \int_0^\infty \int_{2\pi} B_\nu \cos^2 \theta d\Omega d\nu, \tag{5.2}$$

[1] With a superfluidity gedanken experiment.

[2] This is the total radiation pressure experienced by a body with an absorptivity coefficient of 1.

where c is the speed of light, θ is the angle of incoming radiation with respect to the direction vector of the object's motion, ν is the frequency of incoming photons, and B_ν is the spectral radiance in frequency space.

The solid angle integration is performed over 2π sr $\left(0 \le \phi \le \pi\right)$ because the photon drag occurs only on the forward-directed side of the object. Relativistically, eq. (5.2) transforms to

$$P_{\mathrm{TOT}}^{'} = \frac{2-\varepsilon}{c}\int_{0}^{\infty}\int_{2\pi} B_{\nu}^{'} \cos^{2}\theta' d\Omega' d\nu' . \tag{5.3}$$

The relativistic spectral radiance in frequency space was discussed in chapters 2 and 3, and is given by the frequency- and solid angle-integrated form of eq. (3.12), which is eq. (5.4).

$$B_{\nu}^{'} = \frac{\left(\frac{2h\nu^{3}}{c^{2}}\right)}{\exp\left[\frac{h\nu}{k_{B}}\left(\beta_{t} - \beta_{z}\cos\theta\right)\right] - 1}\left[\gamma\left(1 - V\cos\theta\right)\right]^{-3} \tag{5.4}$$

where the time-axis and z-axis velocity vector components were given by eqs. (3.8) and (3.9) respectively and are restated as eqs. (5.5) and (5.6) respectively.

$$\beta_{t} = \frac{1}{T_{o}\sqrt{1-V^{2}}} \tag{5.5}$$

$$\beta_{z} = \frac{V}{T_{o}\sqrt{1-V^{2}}} \tag{5.6}$$

where T_o is the proper temperature. $\left[\beta_t, \beta_x, \beta_y, \beta_z\right]$ is the van Kampen-Israel inverse temperature 4-vector. u_μ is the relative 4-velocity between the radiation and the observer. $\gamma = \left(1 - V^2\right)^{-\frac{1}{2}}$ is the Lorentz factor. $V = \frac{u}{c}$ (fraction of light speed). h and k_B are Planck's and Boltzmann's constants, respectively.

Combining eqs. (5.3) and (5.4) yields:

$$P_{\mathrm{TOT}}^{'} = \frac{2-\varepsilon}{c}\int_0^{\infty}\int_0^{\frac{\pi}{2}} \frac{\left(\frac{2h\nu^3}{c^2}\right)}{\exp\left[\frac{h\nu}{k_B}\left(\beta_t - \beta_z\cos\theta\right)\right]-1}\left[\gamma\left(1 - V\cos\theta\right)\right]^{-3}\cos^2\theta\sin\theta\int_0^{\pi} d\phi d\nu \qquad (5.7)$$

Since motion is along the z-axis, and the radiation is [azimuthally] isotropic, the relativistic spectral radiance can be separated from the azimuthal integral (i.e., $\beta_x - \beta_y = 0$). By setting:

$$\alpha = \frac{2h\left(2-\varepsilon\right)}{c^3}\left[\gamma\left(1 - V\cos\theta\right)\right]^{-3}\cos^2\theta\sin\theta\int_0^{\pi} d\phi = \frac{2\pi h\left(2-\varepsilon\right)}{c^3}\left[\gamma\left(1 - V\cos\theta\right)\right]^{-3}\cos^2\theta\sin\theta,$$

letting $R = \beta_t - \beta_z\cos\theta$, and setting $x = \frac{h}{k_B}R\nu$, $P_{\mathrm{TOT}}^{'}$ becomes

$$P_{\mathrm{TOT}}^{'} = \int_0^{\infty}\int_0^{\frac{\pi}{2}} \frac{\alpha\nu^3}{e^x - 1} d\theta d\nu \,. \qquad (5.8)$$

The integral over frequency yields $\frac{\pi^4}{15}$.

Thus,

$$P_{\mathrm{TOT}}^{'} = \frac{\pi^4 k_B^4}{15h^4}\int_0^{\frac{\pi}{2}} \frac{\alpha}{R^4} d\theta \,. \qquad (5.9)$$

From eqs. (3.8), (3.9), and evaluating eq. (5.9),

$$P'_{\mathrm{TOT}} = \frac{\pi^5(2-\varepsilon)k_B^4}{450\,c^3h^3}\left[\left(V^3 - 6V^2 + 15V - 20\right)\sqrt{1-V^2}\left(\frac{V+1}{V-1}\right)^3\right]T_o^4 . \qquad (5.10)$$

Eq. (5.10) is the total radiation pressure experienced by a relativistic body with arbitrary absorptivity. Expectedly, when $V \to 1$, relativistic beaming and temperature inflation cause $P' \to \infty$. Also, as expected, when $V = 0$:

$$P = \frac{2\pi^5(2-\varepsilon)k_B^4T_o^4}{45c^3h^3} = (2-\varepsilon)\frac{\sigma T_o^4}{3c} = (2-\varepsilon)\frac{S}{3c} = (2-\varepsilon)\frac{U}{3} \qquad (5.11)$$

where *S* is the radiation frame intensity, $\sigma = \dfrac{2\pi^5 k_B^4}{15h^3c^2}$ is the Stefan-Boltzmann constant, and *U* is the energy density. In the cases of a perfect blackbody $(\varepsilon = 1)$ and a perfect reflector $(\varepsilon = 0)$, $P' = \dfrac{U}{3}$ and $P' = \dfrac{2U}{3}$ respectively, as required.

Balasanyan and Mkrtchian [77] contend that the drag force (and drag pressure) are zero when an object is at rest in the photon field. However, this is not correct, as there will always exist a radiation pressure on all objects, regardless of whether they are in the same frame as the radiation source. Of course, an observer can be at rest in the frame of the radiation *source*, but is never at rest in the frame of the *photons*. In an isotropic radiation field, the *net* drag radiation pressure will be zero when an axially symmetric object is stationary. However, this requires angular dependent Doppler shifting of the incident photons, which was not considered in [77]. This is shown in Figure 5.1.

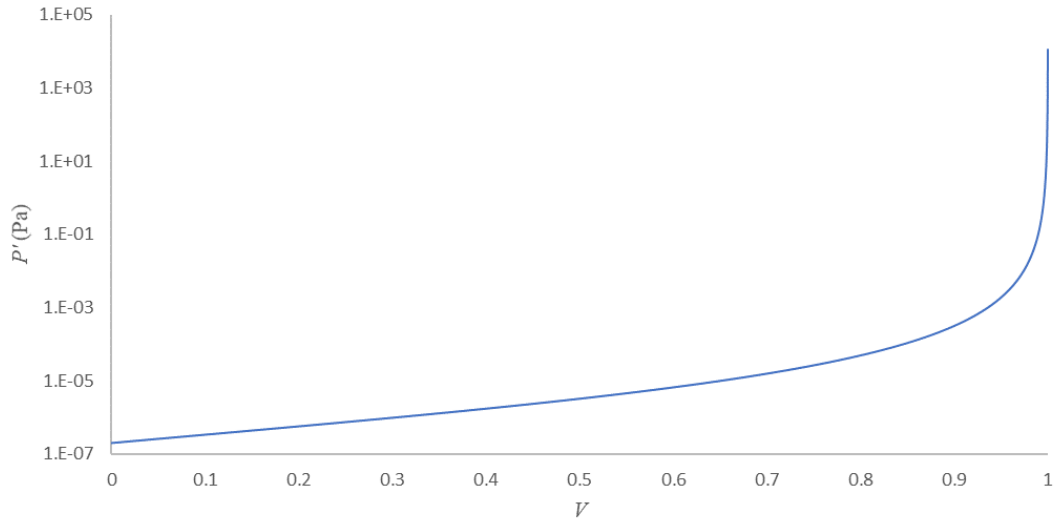

Figure 5.1: Drag radiation pressure versus speed for a perfectly absorbent blackbody (ε = 1) at 200 K. The P'-axis intercept represents the radiation pressure in the radiation frame and is 0.2006 μPa.

5.2.2 *Non-Inertial Frames*

The radiation pressure in a non-inertial reference frame is determined with the 4-acceleration a_μ, which is the proper time (τ) derivative (denoted with dot notation) of the 4-velocity $\left(a_\mu = \dot{\beta}_\mu\right)$. Combining eqs. (5.12) and (5.10), and defining $A = \frac{a}{c}$ (the zeroth term of the acceleration 4-vector), the relativistic spectral radiance in a non-inertial frame is given by eq. (5.13).

$$V = \tanh(A\tau) \tag{5.12}$$

$$P'_{\mathrm{TOT}} = \frac{\pi^5 (2-\varepsilon) k_B^4}{450 c^3 h^3} \left[\frac{\left(\tanh^3(A\tau) - 6\tanh^2(A\tau) + 15\tanh(A\tau) - 20\right)}{\cosh(A\tau)} \left(\frac{\tanh(A\tau)+1}{\tanh(A\tau)-1} \right)^3 \right] T_o^4 \tag{5.13}$$

As $A\tau \to \infty$, $P'_{\mathrm{TOT}} \to \infty$, and when $A\tau = 0$, the rest frame radiation pressure, given by eq. (5.11), is recovered. A plot of eq. (5.13) is shown in Figure 5.2.

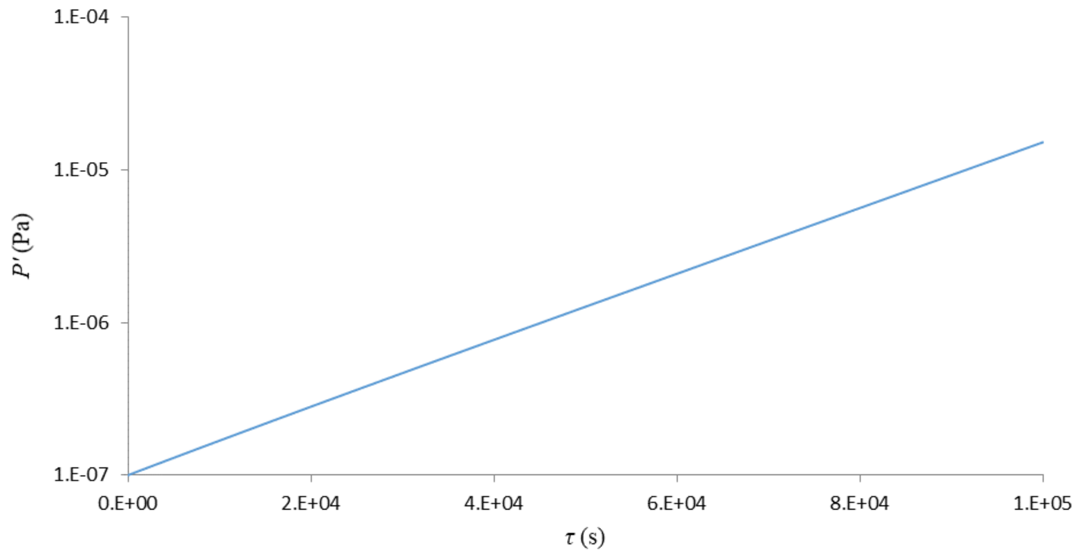

Figure 5.2: Radiation pressure as a function of proper time for a 200 K blackbody (ε = 1). $A = 10^{-5}$. The P'-axis intercept represents the radiation pressure in the radiation frame and is 0.2006 μPa.

In general, V and θ will be time-dependent functions, and the time rate of change of radiation pressure is described by the proper time (τ) derivative (denoted with dot notation) of the relativistic radiation pressure. Thus, $\dot{P} \equiv \frac{dP}{d\tau}$.

When eq. (5.13) is differentiated, the result is eq. (5.14), which is plotted in Figure 5.3.

$$\dot{P}'_{\mathrm{TOT}} = \frac{\pi^5(2-\varepsilon)k_B^4}{450c^3h^3} A\left[\frac{(\tanh(A\tau)+1)^2\left(4\tanh^5(A\tau)-20\tanh^4(A\tau)+39\tanh^3(A\tau)-35\tanh^2(A\tau)+7\tanh(A\tau)+105\right)}{\cosh(A\tau)(1-\tanh(A\tau))^3}\right]T_o^4 \quad (5.14)$$

Although perhaps unexpected, it is reasonable that $\dot{P}'_{\mathrm{TOT}}$ does not have angular dependence, even though V and θ are time-dependent functions, because the strict definition of $\dot{P} \equiv \frac{dP}{d\tau}$ requires the proper time differentiation of a function from which all angular dependence has been removed by the $d\Omega$ integration.

Defining $\dot{P}_{\mathrm{TOT}}^{'} = \frac{2-\varepsilon}{c}\int_{0}^{\infty}\int_{2\pi}\dot{B}_{\nu}^{'}\cos^2\theta' d\Omega' d\nu'$ does not adhere to the required proper time derivative definition of $\dot{P}_{\mathrm{TOT}}^{'}$, in part because the order of the differentiation and integration cannot be inverted.

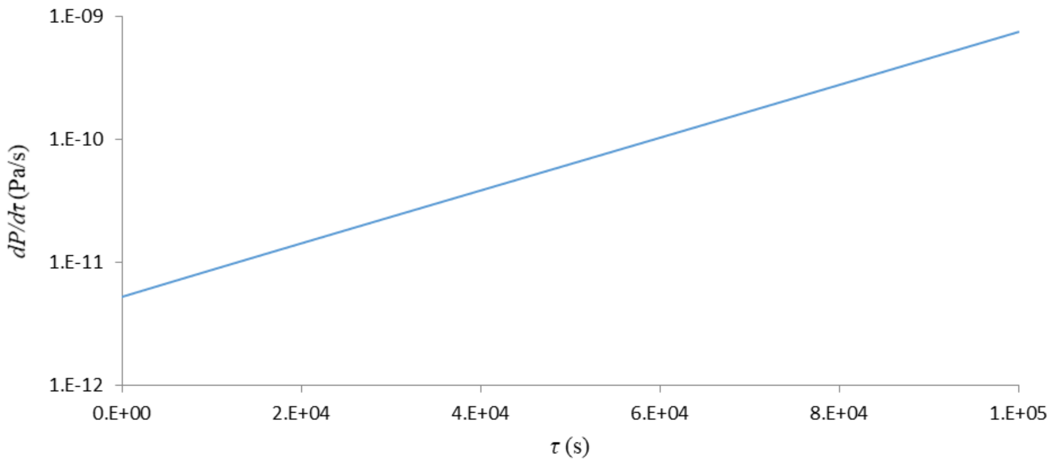

Figure 5.3: Time rate of change of radiation pressure as a function of proper time for a 200 K blackbody (ε = 1). $A = 10^{-5}$. $dP/d\tau'$-axis intercept is the initial instantaneous rate of change of the radiation pressure (5.27 pPa/s).

Also,

$$\dot{P}_{\mathrm{TOT}}^{'}(\tau = 0) = \frac{7\pi^5(2-\varepsilon)k_B^4}{30c^3h^3}AT_o^4 = \frac{7\sigma}{4c}T_o^4 A = \frac{7}{4}UA\,. \tag{5.15}$$

Expectedly, when $A = 0$, $\dot{P}_{\mathrm{TOT}}^{'} = 0$.

5.3 Emission Radiation Pressure in Inertial Reference Frames

For a relativistic body in thermal equilibrium with an incident blackbody spectrum, the radiation pressure due to emission can be calculated. Since temperature is not a Lorentz invariant, the temperature at which the body equilibrates with the surrounding radiation is relativistically transformed. For bodies with forward- and rearward-directed surfaces which are in thermal isolation, the temperature gradient through the body is maintained, and there is a net forward-directed radiation pressure. If the surfaces are not thermally isolated, the temperatures equalize by means of internal heat conduction, and the net emitted radiation pressure approaches zero. The emitted radiation pressure experienced by the body in its frame is:

$$P_{\text{emission}} = \frac{S}{c} = \frac{\varepsilon\sigma}{cT_o^{-4}} \tag{5.16}$$

5.3.1 *Radiation Pressure due to Forward Emitted Radiation*

The pressure due to radiation emitted in the direction of motion $(\theta = 0)$ $P_{\text{emission}}^{\rightarrow}$, can be determined from eqs. (5.5), (5.6), and by replacing T_o^{-1} with the inverse temperature 4-vector $\beta_\mu = \frac{u_\mu}{T_o} = \beta_t - \beta_z \cos\theta$.

$$P_{\text{emission}}^{\rightarrow} = \frac{\varepsilon\sigma}{c}\left(\frac{1+V}{1-V}\right)^2 T_o^4 \tag{5.17}$$

Clearly, when $V = 0$, the rest frame Stefan-Boltzmann Law (divided by *c*) is recovered. As $V \rightarrow 1$, the emission radiation pressure becomes infinite.

For $V \sim 0$, a series expansion of eq. (5.17) yields

$$P_{\text{emission}}^{\rightarrow} \sim \frac{\varepsilon\sigma}{c}\left(1 + 4V + 8V^2 + O\left(V^3\right)\right)T_o^4 \,. \tag{5.18}$$

The emissivity which produces equal drag and forward-directed emission radiation pressures is independent of temperature, can easily be calculated by equating eqs. (5.10) and (5.17), and is given by

$$\varepsilon = \frac{2\left(V^3 - 6V^2 + 15V - 20\right)}{\left(\frac{-60}{\sqrt{1-V^2}}\right) + V^3 - 6V^2 + 15V - 20}. \tag{5.19}$$

A plot of eq. (5.19) is shown in Figure 5.4.

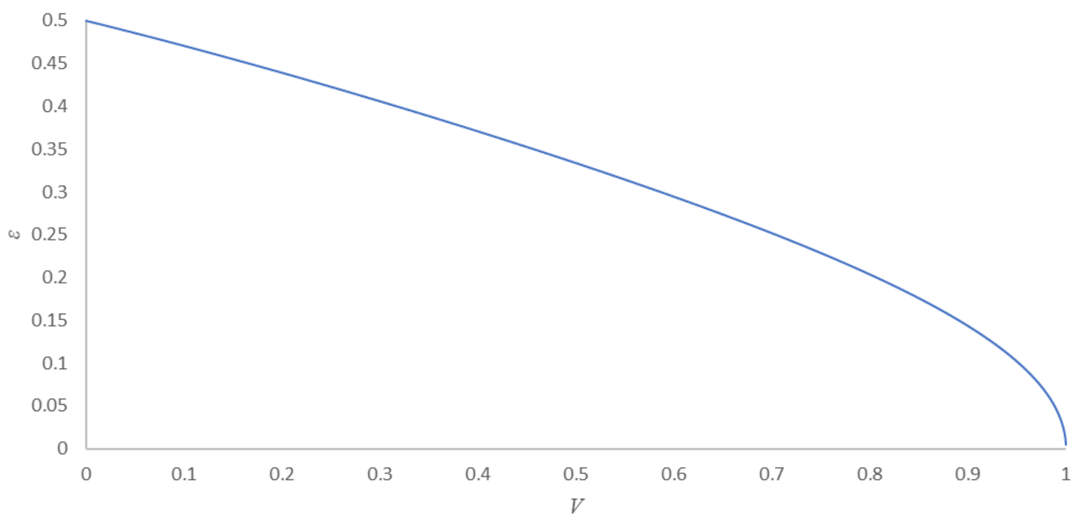

Figure 5.4: Emissivity versus speed for equal drag and forwarded-directed emission radiation pressures.

The emissivities which produce equal radiation pressures when $V = 0$ and $V \to 1$ are not surprising 0.5 and 0 respectively.

The speed which produces equal drag and emission radiation pressures for a given emissivity is also independent of temperature, and is given by the non-trivial solution to

$$\left(V^3 - 6V^2 + 15V - 20\right)\sqrt{1-V^2} = \frac{60\varepsilon}{\varepsilon - 2}. \tag{5.20}$$

5.3.2 *Radiation Pressure due to Rearward Emitted Radiation*

The pressure due to radiation emitted in the direction opposite of motion $\left(\theta = 180^{o}\right)$ $P^{\leftarrow}_{\text{emission}}$, can be determined again from eqs. (5.5), (5.6), and by replacing T_o^{-1} with the inverse temperature 4-vector $\beta_\mu = \frac{u_\mu}{T_o} = \beta_t - \beta_z \cos\theta$:

$$P^{\leftarrow}_{\text{emission}} = \frac{\varepsilon\sigma}{c}\left(\frac{1-V}{1+V}\right)^2 T_o^4 \tag{5.21}$$

As is the case with eq. (5.17), when $V = 0$, the rest frame Stefan-Boltzmann Law is recovered. As $V \rightarrow 1$, the emission radiation pressure becomes zero.

For $V \sim 0$, a series expansion of eq. (5.21) gives:

$$P^{\leftarrow}_{\text{emission}} \sim \frac{\varepsilon\sigma}{c}\left(1 - 4V + 8V^2 + O\left(V^3\right)\right)T_o^4 \tag{5.22}$$

A comparison of drag radiation pressure and emission radiation pressures is shown in Figure 5.5.

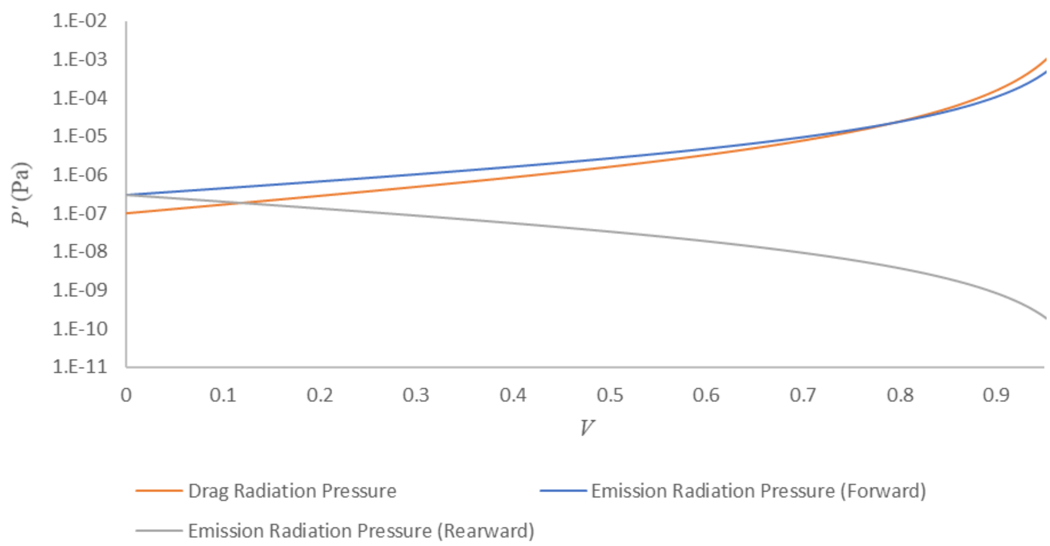

Figure 5.5: Drag, forward-directed, and rearward-directed emission radiation pressures for a 200 K blackbody ($\varepsilon = 1$). The drag and forward-directed radiation pressures are equal for a speed of ~0.7927*c*. The drag and rearward-directed radiation pressures are equal for a speed of ~0.1189*c*. Clearly, the forward-directed and rearward-directed radiation pressures are equal only when the object is stationary.

This result is in contradiction to the calculation of Balasanyan and Mkrtchian [77], in which a speed of ~0.1*c* results in equal drag and emission radiation pressures. However, they show that as $V \rightarrow 1$, the drag radiation pressure vastly exceeds the emission radiation pressure, with which Figure 5.5 is in agreement.

Although the forward-directed emission radiation pressure is markedly greater than the drag radiation pressure for the expected speeds of a solar sail spacecraft $\left(V \sim 10^{-4} - 10^{-3}\right)$, the flux anisotropy of incident radiation results in a greater rearward-directed thrust from both the forward-directed emission radiation pressure and the rearward-directed drag radiation pressure.

The emissivity which produces equal forward drag radiation pressure and rearward emission radiation pressure is also independent of temperature, can easily be calculated by equating eqs. (5.10) and (5.21), and is given by

$$\varepsilon = \frac{2\left(V^3 - 6V^2 + 15V - 20\right)\sqrt{1-V^2}\left(\frac{V+1}{V-1}\right)^5}{60 + \left(V^3 - 6V^2 + 15V - 20\right)\sqrt{1-V^2}\left(\frac{V+1}{V-1}\right)^5}. \tag{5.23}$$

A plot of eq. (5.23) is shown in Figure 5.6.

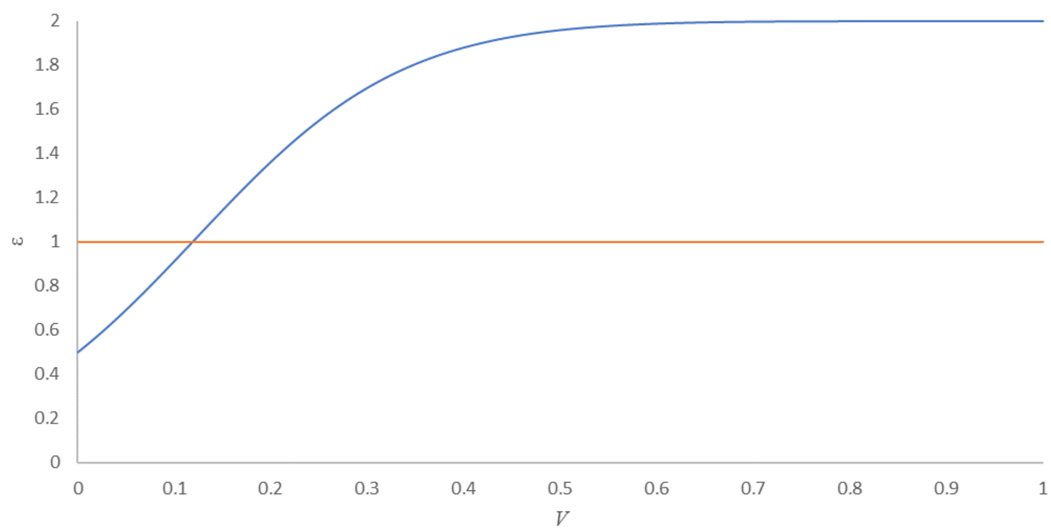

Figure 5.6: Emissivity versus speed for equal drag and rearward-directed emission radiation pressures. The region of the graph above the orange line represents non-physical emissivities, and thus speeds for which it is not possible for these radiation pressures to be equal. As expected from Figure 5.5, the cutoff speed at which the radiation pressures are equal is ~0.1189*c*. The emissivity which produces equal radiation pressures when $V = 0$ is, not surprisingly, 0.5.

5.3.3 *Emitted Radiation Pressure in Non-Inertial Frames*

The forward- and rearward-directed emission radiation pressures in a non-inertial frame can be determined by combining eq. (5.12) with eqs. (5.17) and (5.21) respectively.

Therefore,

$$P_{\text{emission}}^{\substack{\rightarrow \\ \leftarrow}} = \frac{\varepsilon\sigma}{c}\left(\frac{1 \pm \tanh(A\tau)}{1 \mp \tanh(A\tau)}\right)^2 T_o^4 \,. \tag{5.24}$$

A plot of eq. (5.24) is shown in Figure 5.1.

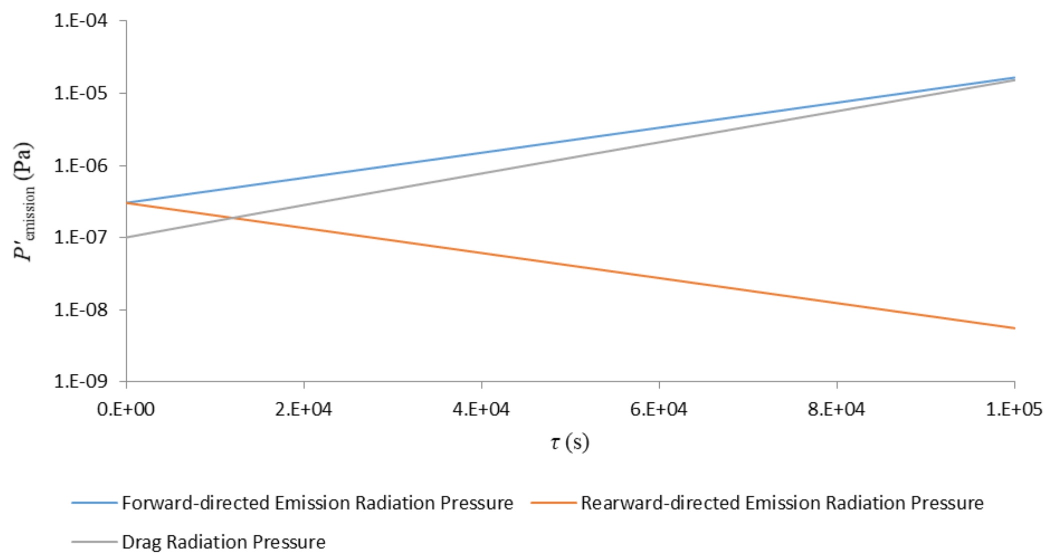

Figure 5.7: Drag, forward-directed, and rearward-directed emission radiation pressures for a 200 K blackbody (ε = 1). $A = 10^{-5}$. The drag and forward-directed radiation pressures are equal at a proper time of ~1.0835×10^5 s. The drag and rearward-directed radiation pressures are equal for a speed of ~1.2001×10^4 s. Clearly, the forward-directed and rearward-directed radiation pressures are equal only when the object is stationary.

The time rate of change of the forward- and rearward-directed emission radiation pressures can be easily determined.

$$\dot{P}_{\text{emission}} \equiv \frac{dP_{\text{emission}}}{d\tau} \tag{5.25}$$

Therefore, from eq. (5.24):

$$\dot{P}_{\text{emission}}^{\substack{\rightarrow \\ \leftarrow}} = \pm\frac{4\varepsilon\sigma}{c} A\left(\frac{1 \pm \tanh(A\tau)}{1 \mp \tanh(A\tau)}\right)^2 T_o^4 = \pm 4AP_{\text{emission}}^{\substack{\rightarrow \\ \leftarrow}} \tag{5.26}$$

Clearly, when $A\tau = 0$, $\dot{P}^{\overrightarrow{\leftarrow}}_{\text{emission}} = \pm \frac{4\varepsilon\sigma}{c} A$, and when $A\tau \to \infty$, $\dot{P}^{\rightarrow}_{\text{emission}} \to \infty$ and $\dot{P}^{\leftarrow}_{\text{emission}} \to 0$.

5.3.4 *Temperature Gradient-Induced Carnot Cycle*

Since the forward surface of the body experiences temperature inflation and the rearward surface experiences temperature deflation, then if the surfaces of the body are not thermally isolated, heat will flow from the forward to the rearward surface, and a Carnot cycle results. The efficiency η of a Carnot cycle in the inertial frame of the body is

$$\eta = 1 - \frac{T_C}{T_H}, \tag{5.27}$$

where T_C and T_H are the cold and hot reservoir temperatures respectively.

From eqs. (5.5), (5.6), and by replacing T_o^{-1} with the inverse temperature 4-vector $\beta_\mu = \frac{u_\mu}{T_o} = \beta_t - \beta_z \cos\theta$, T_C $\left(\theta = 180^o\right)$, T_H $\left(\theta = 0\right)$, η in terms of V can easily be determined.

$$\eta = \frac{2V}{1+V} \tag{5.28}$$

Expectedly, when $V = 0$, the efficiency is zero, and the Carnot cycle does not exist due to the zero-temperature gradient. As $V \to 1$, $\eta \to 1$.

However, without thermal isolation in an inertial frame (or a non-inertial frame with negative acceleration, see below), the surface temperatures eventually equilibrate, and the Carnot cycle shuts down in a proper time which is dependent on the thermal diffusivity of the body.

In a non-inertial frame, the Carnot efficiency is obtained by combining eqs. (5.12) and (5.28), is given by eq. (5.29)[3], and is plotted in Figure 5.8.

$$\eta = \frac{2\tanh\left(|A|\tau\right)}{1+\tanh\left(|A|\tau\right)} \tag{5.29}$$

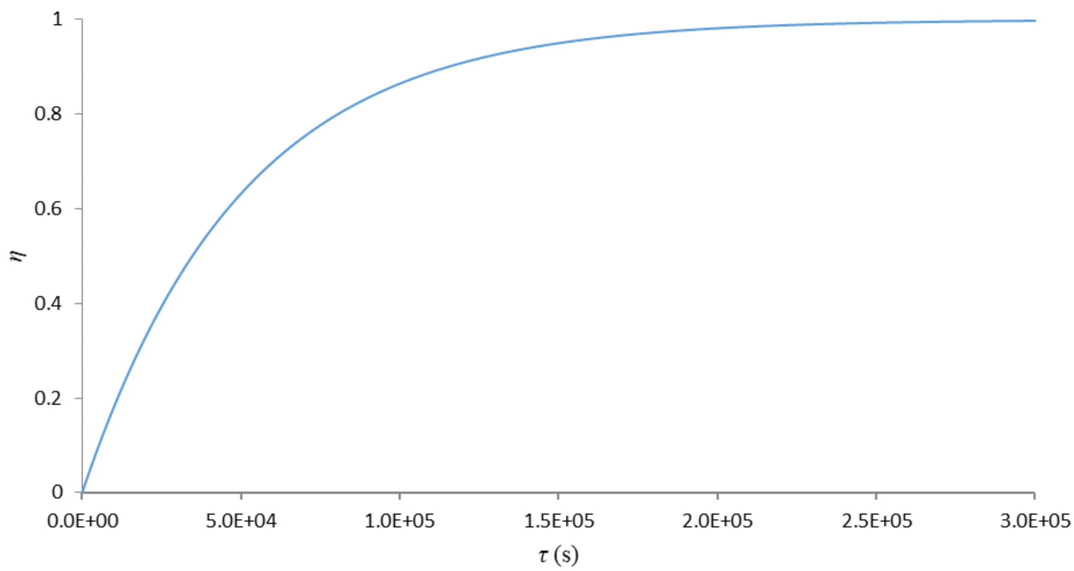

Figure 5.8: Efficiency of a Carnot cycle as a function of proper time for an accelerating blackbody with a radiation frame temperature of 200 K. $A = 10^{-5}$.

In the frame of the body, the time rate of change of the Carnot cycle efficiency is the proper time derivative of eq. (5.24), and is given by eq. (5.30) and is plotted in Figure 5.9 for positive acceleration and Figure 5.10 for negative acceleration.

[3] $|A|$ is required because $V = A\tau \geq 0$.

$$\dot{\eta} = 2A\left(\frac{1-\tanh(A\tau)}{1+\tanh(A\tau)}\right) \tag{5.30}$$

With positive acceleration and consequently increasing speed, the Carnot cycle continues indefinitely because the constantly rising temperature of the forward surface and the finite time required for heat to flow through the body collectively prevent the forward and rearward surfaces from ever achieving thermal equilibrium, as $\eta \to 1$ and $\dot{\eta} \to 0$. However, in the case of negative acceleration, the Carnot efficiency is decreasing in time, as $\eta \to 0$ and $\dot{\eta} \to -\infty$. Therefore, the surfaces do approach thermal equilibrium, and the Carnot cycle eventually shuts down.

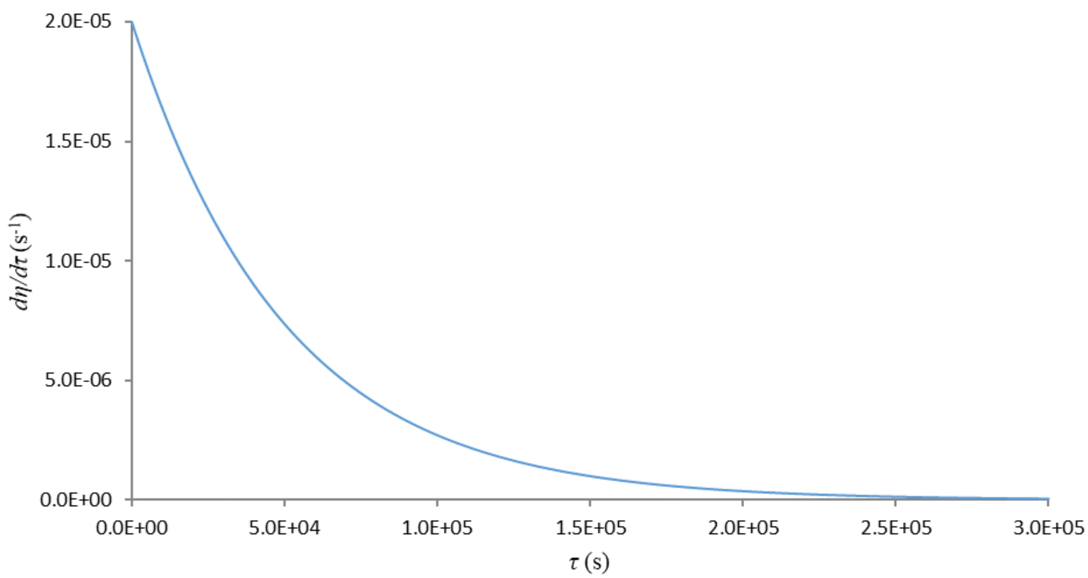

Figure 5.9: Logarithmic plot of the time rate of change of the Carnot efficiency as a function of proper time for a 200 K blackbody. $A = 10^{-5}$.

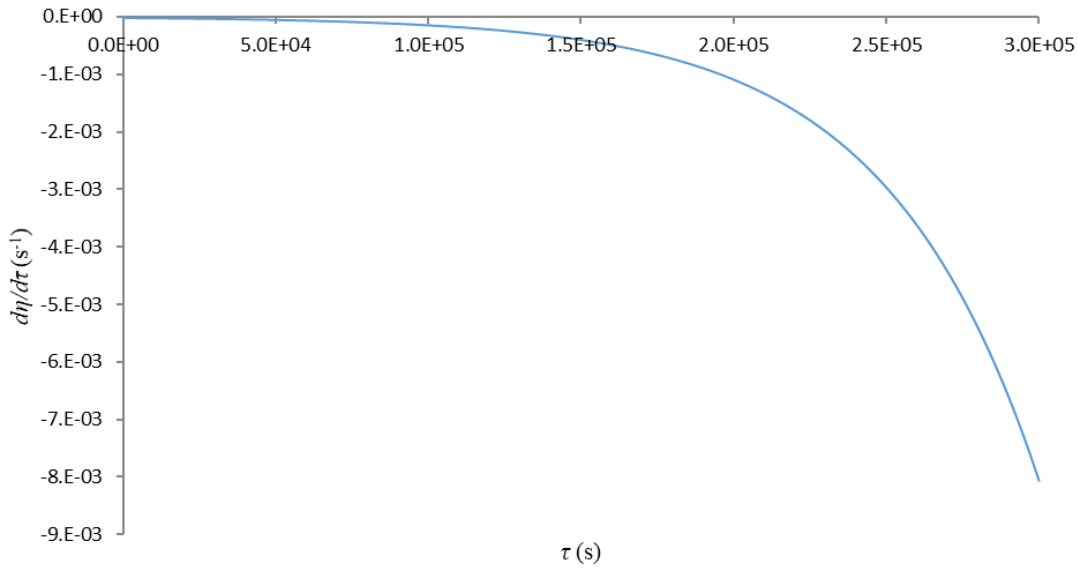

Figure 5.10: Logarithmic plot of the time rate of change of the Carnot efficiency as a function of proper time for a 200 K blackbody. $A = 10^{-5}$.

5.4 *Drag Radiation Pressure on a Surface of Arbitrary Geometry*

For an object with an arbitrary frontal surface geometry moving relativistically in an inertial reference frame and in thermal equilibrium with an isotropic radiation field, the drag radiation pressure can be calculated. If the surface is described by the function $F(x, y, z) = 0$, then the normal $\hat{n}$ to the surface is clearly

$$\hat{n} = \frac{\nabla F}{|\nabla F|}. \tag{5.31}$$

The total drag radiation pressure P'_{TOT} is merely the scalar product of the total drag radiation pressure vector $\vec{P}'_{\mathrm{TOT}}$ and the surface normal vector.

$$P'_{\mathrm{TOT}} = \vec{P}'_{\mathrm{TOT}} \cdot \hat{n} \tag{5.32}$$

Since motion occurs only along the z-axis,

$$P'_{\mathrm{TOT}} = \frac{\left|\vec{P}'_{\mathrm{TOT}}\right| \hat{z} \cdot \nabla F}{\left|\nabla F\right|}. \tag{5.33}$$

If the frontal surface geometry is a plane parallel to the x-y plane, then $\nabla F = \hat{z}$, and P'_{TOT} is given by eq. (5.33). If the reference frame in non-inertial, then the time rate of change of the drag radiation pressure is

$$\dot{P}'_{\mathrm{TOT}} = \frac{d}{d\tau}\left[\frac{\left|\vec{P}'_{\mathrm{TOT}}\right| \hat{z} \cdot \nabla F}{\left|\nabla F\right|}\right], \tag{5.34}$$

which yields,

$$\dot{P}'_{\mathrm{TOT}} = \frac{\left|\dot{\vec{P}}'_{\mathrm{TOT}}\right| \hat{z} \cdot \nabla F}{\left|\nabla F\right|} + \left|\vec{P}'_{\mathrm{TOT}}\right| \hat{z} \cdot \left[\frac{\nabla \dot{F}}{\left|\nabla F\right|} - \frac{\nabla F}{\left|\nabla F\right|^3}\left(F_x \dot{F}_x + F_y \dot{F}_y + F_z \dot{F}_z\right)\right], \tag{5.35}$$

where F_i are the partial derivatives of F, and $\left|\dot{\vec{P}}'_{\mathrm{TOT}}\right|$ is given by

$$\left|\dot{\vec{P}}'_{\mathrm{TOT}}\right| = \left| \frac{\pi^5 (2-\varepsilon) k_B^4 A}{450 c^3 h^3} \times \left[\frac{\left(\tanh(A\tau)+1\right)^2 \left(4\tanh^5(A\tau) - 20\tanh^4(A\tau) + 39\tanh^3(A\tau) - 35\tanh^2(A\tau) + 7\tanh(A\tau) + 105\right)}{\cosh(A\tau)\left(1-\tanh(A\tau)\right)^3}\right] T_o^4 \right|, \tag{5.36}$$

which is just the magnitude of eq. (5.14). If the frontal surface geometry is a plane parallel to the x-y plane, then $\nabla F = \hat{z}$, and $\dot{P}'_{\mathrm{TOT}}$ is given by eq. (5.14).

5.5 Summary

The relativistic radiation pressure due to drag, experienced by a thermally equilibrated planar surface moving through an isotropic radiation field in both inertial and non-inertial reference frames, has been determined. These have been compared to the forward- and rearward-directed emission radiation pressures caused by the thermally isolated surfaces of the body. Also, the speeds at which the emission and drag radiation pressures are equal were determined and shown to be dependent on the emissivity, and independent of the temperature of the photonic gas.

An inertial body (or a non-inertial body with a negative acceleration), through which thermal conduction can occur, will experience a Carnot cycle between its forward- and rearward surfaces which will continue until the surface temperatures equalize in a time which is dependent on the body’s thermal diffusivity. However, for such a body in a non-inertial frame with a positive acceleration, there will be a continuous Carnot cycle with a steadily increasing acceleration-dependent efficiency.

CHAPTER SIX

Ultra-relativistic Thermodynamics and Aberrations of the Cosmic Microwave Background Radiation

This chapter published as: J.S. Lee and G. B. Cleaver, "Ultra-relativistic Thermodynamics and Aberrations of the Cosmic Microwave Background Radiation", *Modern Physics Letters A*, Volume 30, Issue 09, 21 March 2015.

6.1 Introduction

The pervasiveness and extreme isotropy of the Cosmic Microwave Background radiation result in every ultra-relativistic reference frame with an arbitrary velocity vector encountering an extremely Lorentz transformed CMB. This chapter extends the work of Przanowski and Tosiek [27] by demonstrating that the occupation number (also a Lorentz invariant) can be used to revise the thermodynamic stress-energy tensor and that Temperature Inflation by the Lorentz factor $\left(\gamma = \left(1-\beta^2\right)^{-\frac{1}{2}}\right)$ of an isotropic radiation field (CMB) and not only a relativistic perfect fluid, as set forth by Ott [17], Arzelies [18], and Møller [19], is ultimately supported. Additionally, ultra-relativistic motion would induce a significant intensification of the CMB in the non-laboratory frame due to "Doppler Boosting".

In this chapter, Planck units (i.e., $c = h = k = 1$) are used, where h and k are Planck's and Boltzmann's constants respectively.

6.2 Directional Temperature and Inverse Temperature Approaches to the Lorentz Transformation of Temperature

Alternatively, the transformations can be undertaken by treating *inverse* temperature as a van Kampen-Israel future-directed timelike 4-vector. However, this method does not provide a unique determination of the correct transformation.

6.2.1 *Directional Temperature*

By taking the CMB to be blackbody radiation, it can be described by the Planck distribution given by eq. (6.1):

$$\rho_n(\omega) = \frac{\omega^2}{2\pi^2\left[\exp\left(\frac{\omega}{T}\right) - 1\right]}, \tag{6.1}$$

where ρ_n is the number density of photons with frequency ω, and T is the temperature.

For an object moving with respect to the CMB frame, the photon number density, which is incident through solid angle Ω, can be determined.

$$\rho_n(\omega) = \int \frac{\omega^2}{2\pi^2\left[\exp\left(\frac{\omega}{T_{\text{eff}}(\theta)}\right) - 1\right]} d\omega d\Omega \tag{6.2}$$

where $T_{\text{eff}}(\theta)$ is the so-called *effective* or *directional* temperature, and is defined as

$$T_{\text{eff}}(\theta) = \frac{T_o\sqrt{1-\beta^2}}{1-\beta\cos\theta}, \tag{6.3}$$

where θ is the angle between the velocity vector and a reference point in the CMB, and $\beta = \frac{v}{c}$.

However, effective temperature comes about solely from mathematical manipulation, and does not require any thermodynamic consideration. Although sufficient for the determination of planetary and stellar motion with respect to the CMB [63], [64], [65], the lack of any direct thermodynamic connection renders it unclear whether or not $T_{\text{eff}}(\theta)$ represents temperature.

For instance, the direction of heat flow is indeterminable for an object with a proper temperature $T_{\text{eff}}(0) < T < T_{\text{eff}}\left(\frac{\pi}{2}\right)$. Consequently, the cases of temperature inflation and temperature deflation become indistinguishable.

6.2.2 *Inverse Temperature as a 4-vector*

Although Landsberg and Matsas [32], [33] have argued that the relativistic transformation of temperature is impossible, Wu [78] has asserted that such a transformation can be accomplished because inverse temperature, as a van Kampen-Israel future-directed timelike 4-vector, can be applied to a superfluidity gedanken experiment. However, the supposition that the inverse temperature 4-vector β_μ takes the form

$\beta_\mu = \frac{u_\mu}{T_o}$ (where u_μ is the 4-velocity, and T_o is the temperature in the laboratory frame)

is, in and of itself, unsuccessful at resolving the transformation dilemma.

If the zeroth component of the inverse temperature is T^{-1}, then β_μ has components $(T_o^{-1},0,0,0)$ in the co-moving frame, and temperature deflation is supported. If the zeroth component of the inverse temperature is T, then β_μ has components $(T_o,0,0,0)$ in the co-moving frame, and temperature inflation results. If the temperature is a scalar, then the outcome is temperature invariance. Wu [78] argues for the existence of a frame in which β_μ has the form $\left(T_o^{-1},0,0,0\right)$, although this frame may not be the co-moving frame. However, this chapter supports the work of Przanowski and Tosiek [27], in which a Lorentz transformation of temperature can be determined without the use of inverse temperature as a 4-vector.

6.3 *Justification for Temperature Inflation of the CMB using Occupation Number*

The CMB is a highly isotropic radiation field and constitutes a continuous medium in thermodynamic equilibrium with particles in the moving frames. A domain of spacetime with a unit volume $\left(V_o = 1\right)$ is chosen to move at constant velocity $\vec{v}$ with respect to the rest frame of the universe. To avoid the complexities associated with finiteness, a periodic boundary condition is imposed. The spatial axes in the CMB and moving frames are assumed to be mutually parallel. The spacetime metric is given by:

$$\eta_{ij} = \eta^{ij} = \mathrm{diag}(-,-,-,+) \tag{6.4}$$

By making use of the Lorentz transformation $x^j = \Lambda^j_k x^k_o$, the coefficients of which are given by

$$\Lambda^\mu_\nu = \delta^\mu_\nu - \frac{\mathrm{v}^\mu \mathrm{v}^\nu}{\mathrm{v}^2}(1-\gamma), \quad \Lambda^4_\mu = \mathrm{v}^\mu \gamma, \quad \Lambda^\mu_4 = \mathrm{v}^\mu \gamma, \quad \Lambda^4_4 = \gamma\,. \tag{6.5}$$

The energy-momentum tensor T_{jk} is [79], [80], [81], [82]:

$$T_{jk} = \varepsilon_o u_j u_k + \tau_{jk} = T_{kj}\,, \tag{6.6}$$

where ε_o is the energy density in the CMB frame, $u^j = \left(\mathrm{v}^\mu \gamma, \gamma\right)$ is the 4-velocity, and

$\tau^{jk} = \Lambda^j_\mu \Lambda^k_\nu \tau_o^{\mu\nu}$ ($\tau_o^{\mu\nu}$ is the stress tensor).

$\tau_o^{4j} = \tau_o^{j4} = 0$ because in the rest frame, $\tau_o^{4\mu} = 0$. Additionally, $T^{44} = \varepsilon_o$ and $\tau_o^{44} = 0$. From eq. (6.5), $\tau^{jk} = \Lambda^j_\mu \Lambda^k_\nu \tau_o^{\mu\nu}$, and eq. (6.6), the total energy can be calculated. It is merely the volumetric integral of T^{44}.

$$E = \gamma\left(E_o + \mathrm{v}^\nu \mathrm{v}^\rho \bar{\tau}_{o_{\nu\rho}}\right). \tag{6.7}$$

where E_o is the energy in the CMB frame.

The 4-momentum can be similarly calculated:

$$P^\mu = \int_V T^{\mu 4} dx^1 dx^2 dx^3 = \mathrm{v}^\mu \gamma E_o + \frac{\mathrm{v}^\nu}{c^2}\left[\left(\gamma - 1\right)\frac{\mathrm{v}^\nu \mathrm{v}^\rho}{\mathrm{v}^2} - \eta^{\mu\rho}\right]\bar{\tau}_{o_{\nu\rho}} \tag{6.8}$$

where $\bar{\tau}_{o_{\nu\rho}} := \int_{V_o} \tau_{o_{\nu\rho}} dx_o^1 dx_o^2 dx_o^3$.

Application of the generalized conservation law $\frac{\partial T^{jk}}{\partial x^k} = 0$ to objects in thermodynamic equilibrium with the CMB results in

$$\frac{\partial \tau_o^{\mu\nu}}{\partial x^\nu} = 0\,. \tag{6.9}$$

Eq. (6.10) follows from eq. (6.9) [80], [81].

$$\bar{\tau}_o^{\mu\nu} = \int_{V_o} \tau_o^{\mu\nu} dx_o^1 dx_o^2 dx_o^3 = -\oint_{\partial V_o} \tau_{o\rho}{}^{\mu} x_o^\nu l_o^\rho d\sigma_o\,, \tag{6.10}$$

where l_o^ρ is the ρ component of the outward unit vector which is normal to the boundary ∂V_o of V_o. $d\sigma_o$ is the surface element of ∂V_o. From the symmetry of eq. (6.10):

$$\bar{\tau}_{o\mu\nu} = -\frac{1}{2}\oint_{\partial V_o}\left(\tau_{o\mu\rho}x_{o\nu} + \tau_{o\nu\rho}x_{o\mu}\right)l_o^\rho d\sigma_o \tag{6.11}$$

Although the stress-energy tensor is often rewritten by considering the relativistic motion of an ideal fluid, such an invocation would not be apropos for the CMB. The obvious appeal of an ideal fluid is the Lorentz invariance of pressure. Since occupation number (also defined as the number density of photons with a given momentum and polarization) is directly relevant to the CMB, and is a Lorentz invariant, it is used to rewrite T_{jk}. The following results:

$$\begin{aligned} T_{jk} &= \left(n_{\alpha\vec{p}} + \varepsilon_o\right)u_j u_k - n_{\alpha\vec{p}}\eta_{jk} \\ \tau_{o_{\mu\nu}} &= -n_{\alpha\vec{p}}\eta_{\mu\nu} \\ \bar{\tau}_{o_{\mu\nu}} &= -n_{\alpha\vec{p}}\eta_{\mu\nu} \end{aligned} \tag{6.12}$$

where $n_{\alpha\vec{p}}$ is the occupation number, and α & $\vec{\mathrm{p}}$ designate the polarization and momentum, respectively.

Due to the Lorentz invariance of occupation number, and since $V = \frac{1}{\gamma}$, the energy and momentum differentials can be calculated:

$$dE + \sum_{\alpha=1}^{2} n_{\alpha\vec{p}} h\nu^3 \cos\theta\, dA\, dt\, d\nu\, d\Omega = \gamma\left(dE_o + \sum_{\alpha=1}^{2} n_{\alpha\vec{p}} h\nu_o^3 \cos\theta_o\, dA_o\, dt_o\, d\nu_o\, d\Omega_o\right) \tag{6.13}$$

$$dP^{\mu} = \gamma\left[dE_o + \sum_{\alpha=1}^{2} n_{\alpha\vec{p}} h\nu^3 \cos\theta \, dA \, dt \, d\nu \, d\Omega \right] \mathrm{v}^{\mu} \tag{6.14}$$

The $\sum_{\alpha=1}^{2} n_{\alpha\vec{p}}$ term accounts for both polarization states. From eqs. (6.5), (6.13), and (6.14), it is clear that the 4-momentum is $\left(P^1, P^2, P^3, E + E_{n_{\alpha\vec{p}}}\right)$ [57], [19], [83], [84], [85]. The quantity $h\nu_o^3$ is the specific intensity I_{ν}. It is noteworthy that $\frac{I_{\nu}}{\nu_o^3} = h$ must also be a Lorentz invariant, and could have been used instead to rewrite the stress-energy tensor.

The first law of thermodynamics is constrained to have its covariant form:

$$dE_o = \delta Q_o + \delta L_o \, , \tag{6.15}$$

where δQ_o is the heat entering the moving frame from the CMB, and δL_o is the thermodynamic work done on an object in the moving frame. It is assumed that the thermodynamic process is reversible, and therefore,

$$\begin{aligned} \delta L_o &= n_{\alpha\bar{p}} \int_{\partial V_o} \eta_{\mu\nu} l_o^{\nu} dx_o^{\mu} d\sigma_o = -n_{\alpha\bar{p}} dV_o \\ \delta Q_o &= T_o dS_o \end{aligned} \quad , \tag{6.16}$$

where T_o is the CMB frame temperature, and S_o is the system's entropy.

From eqs. (6.7), (6.8), and (6.15), the first law of thermodynamics in the moving frame is:

$$dE = \gamma\left(dQ_o + \delta L_o + \mathrm{v}^{\nu}\mathrm{v}^{\rho} d\bar{\tau}_{o_{\mu\rho}}\right) \tag{6.17}$$

$$P^{\mu} = \gamma \mathrm{v}^{\mu}\left[\delta Q_o + \delta L_o\right] + \mathrm{v}^{\nu}\left[(\gamma - 1)\frac{\mathrm{v}^{\mu}\mathrm{v}^{\rho}}{\mathrm{v}^2} - \eta^{\mu\rho}\right] d\bar{\tau}_{o_{\nu\rho}} \tag{6.18}$$

Since any adiabatic reversible process needs to be frame independent, $\delta Q = 0$. Thus, eq. (6.15) becomes

$$dE = \delta Q + \delta L\,. \tag{6.19}$$

Eq. (6.20) specifies the direction of heat flow. Thus, the forward-directed heat in the moving frame must always be greater than or equal to (in the case of $\gamma = 1$) the heat in the CMB frame.

$$\delta Q = \gamma \delta Q_o\,. \tag{6.20}$$

To determine a relativistic dependence for absolute temperature, the Clausius inequality for cyclic reversible processes, eq. (6.21), in addition to the stipulations in eq. (6.22) for a smooth continuous function for temperature, are needed.

$$\oint \frac{\delta Q_o}{T_o} = 0 \tag{6.21}$$

$$T = T(T_o, \mathrm{v}) \qquad , \qquad \lim_{\mathrm{v}\to 0} T(T_o, \mathrm{v}) = T_o \tag{6.22}$$

This yields the Ott [17], Arzelies [18] and Møller [19] result of relativistic temperature inflation:

$$T = \gamma T_o \tag{6.23}$$

From Figure 6.1, it is clear that in the Earth frame $\left(\beta \sim 10^{-4}\right)$, the directional and absolute temperatures of the CMB are effectively indistinguishable. However, at ultra-relativistic velocities, the difference becomes considerable.

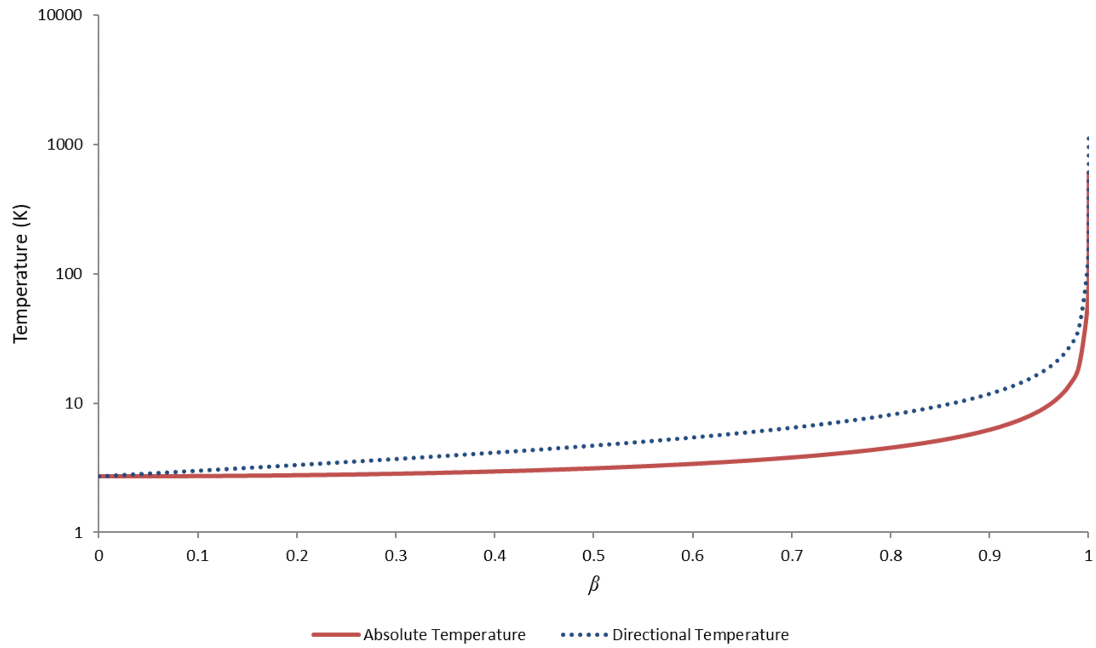

Figure 6.1: Absolute Temperature and Directional Temperature ($\theta = 0$) of the CMB versus Speed.

6.4 Relativistic Aberration of the CMB

The CMB will also be relativistically aberrated. Doppler Boosting (the increase of the CMB intensity) is confidently expected. For an object moving at proper speed β, the CMB intensity in the moving frame I_ν, in terms of the CMB intensity in the CMB frame I_{ν_o}, is given by

$$\frac{I_\nu(\theta)}{I_{\nu_o}(\theta)} = [\gamma(1-\beta\cos\theta)]^{-3}. \qquad (6.24)$$

where $\gamma(1-\beta\cos\theta)$ is the Doppler Factor D, and θ is the angle between the proper velocity and the direction of observation.

Therefore, the ratio of the total intensities can be calculated by determining the surface integral through the forward-directed solid angle (2π).

$$\frac{I_\nu}{I_{\nu_o}} = \int_S \left[\gamma(1-\beta\cos\theta)\right]^{-3} d\Omega \tag{6.25}$$

This results in

$$\frac{I_\nu}{I_{\nu_o}} = \frac{1}{2}\frac{(1+\beta)\sqrt{1-\beta^2}(2-\beta)}{1-\beta}. \tag{6.26}$$

Treating the CMB as an isotropic blackbody, the flux density F_{ν_o} through a spherical Gaussian surface is πI_{ν_o}. This cancels with the π factor that emerges from the azimuthal component of the solid angle integration. Expectedly, $\lim_{\beta\to 1}\frac{I_\nu}{I_{\nu_o}} = \infty$ and $\lim_{\beta\to 0}\frac{I_\nu}{I_{\nu_o}} = 1$. A plot of eq. (6.26) is shown in Figure 6.2.

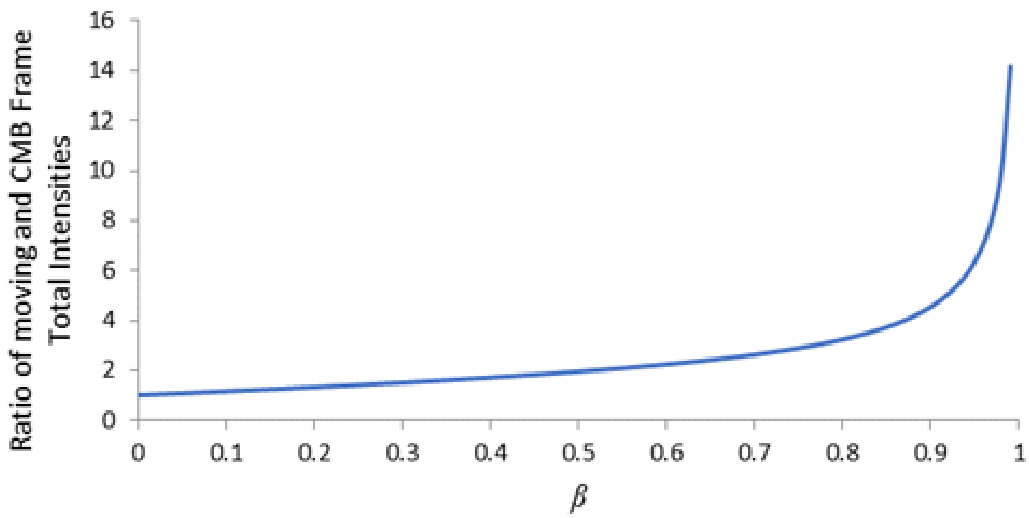

Figure 6.2: Plot of I_ν/I_{ν_o} for the CMB versus speed.

6.5 Summary

Since the relativistic motion of an ideal fluid is not directly relevant to the CMB, the stress-energy tensor has been rewritten by means of the occupation number. The inflation of heat and temperature from their rest frame values by the Lorentz factor is supported. Additionally, Doppler boosting at ultra-relativistic speeds is significant. Consequently, the CMB is manifested as a relativistically aberrated, velocity-dependent heat bath in the direction motion.

CHAPTER SEVEN

White Holes as the Asymptotic Limit of Evaporating PBHs

This chapter published as: J.S. Lee and G. B. Cleaver, "White holes as the asymptotic limit of evaporating PBHs", *International Journal of Modern Physics A*, Volume 31, Number 30, 24 October 2016.

7.1 Introduction

The Hawking radiation spectrum of a PBH with a Schwarzschild radius in the attometer (10^{-18} m) range is awash with p, $\bar{p}$, $e^{\pm}$, γ, ν, and $\bar{\nu}$. Particles of a surrounding radiation field, incident upon the PBH, will interact with the expelled Hawking radiation and form an accretion cloud of high opacity.

This chapter provides an overview of the Hawking spectrum of a PBH and the interactions between incident fermions and each of the emitted particle species. Significant analyses of the interactions have been done and are described in the literature.

Although the Hawking radiation is not self-interactive and does not itself form an accretion cloud, the scattering and particle annihilation that occurs from incident fermions does result in a highly opaque accretion cloud through which particles with energies comparable to the PBH's mass energy cannot retain sufficient energy to have a high absorption probability. It is shown that when extrapolated to Planck-sized PBHs, the absorption probability, although extremely negligible, is non-zero. Consequently, Planck-sized PBHs can approximately mimic white holes' zero-absorption characteristic, but they do not achieve it. Thus, in terms of absorptivity, white holes are the asymptotic limit of evaporating PBHs.

7.2 Evaporation Times of a PBH

The classical evaporation time t_{ev}, of a Schwarzschild black hole with initial Schwarzschild radius R_{s_o} and initial mass M_o, obtained from solving $P = -c^2 \frac{dM}{dt}$ (using classical Hawking power) and expressed in MKS units, is

$$t_{ev} = \frac{5120\,\pi G_N^2 M_0^3}{\hbar c^4}\,. \tag{7.1}$$

Since,

$$R_{S_o} = \frac{2G_N M_0}{c^2}\,, \tag{7.2}$$

therefore,

$$t_{ev} = \frac{640\pi c^2 R_{S_0}^3}{\hbar G_N}\,, \tag{7.3}$$

where G_N is the Newtonian Gravitation Constant (6.6738×10^{-11} m^3·kg^{-1}·s^{-2}).

However, significantly shorter evaporation times are calculated when particle production is considered. Crane and Westmoreland [86] have calculated the approximate range of evaporation times to be

$$\frac{c^4}{75G_N^2 a}\left(R_{s_0}^3 - R_{s_Y}^3\right) \le t_{ev} - t_0 \le \frac{c^4}{6G_N^2 af\left(T_{H_0}\right)}\left(R_{s_0}^3 - R_{s_Y}^3\right), \tag{7.4}$$

where R_{s_Y} is the Schwarzschild radius of a reference PBH (taken to be 0.6 am) with an evaporation time of t_o (calculated to be one year), a is the radiated power constant (1.06×10^{-20} W·m^2), and $f\left(T_{H_0}\right)$ is a numerical function accounting for particle production [43]. In supersymmetric, and beyond the standard model (BSM) in general, it has been postulated that $f\left(T_{H_0}\right) \lessapprox 100$.

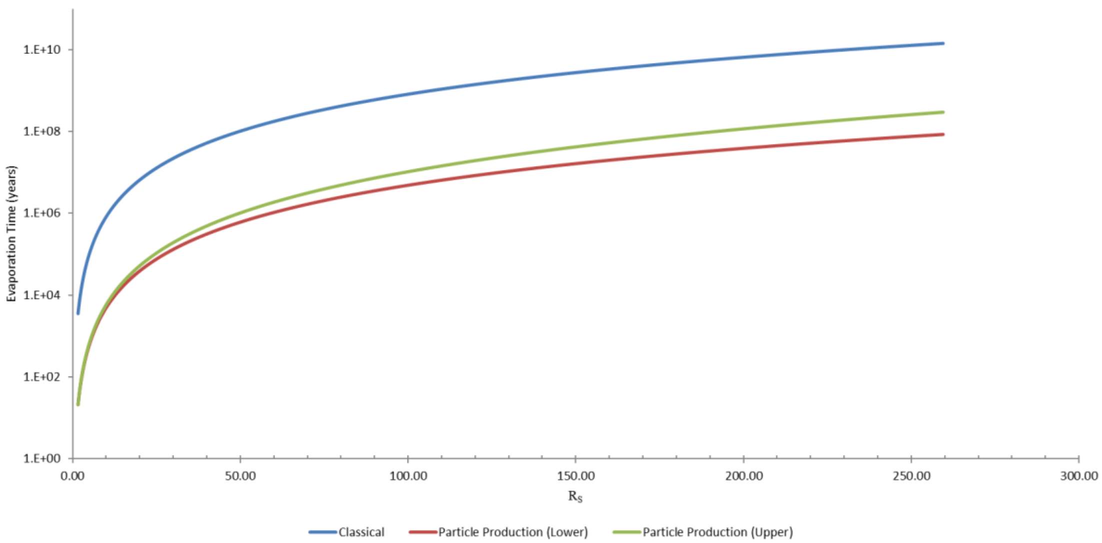

Figure 7.1: Life expectancy vs. initial Schwarzschild radius for a PBH showing the classical and particle production life expectancies.

Therefore, the classical evaporation time calculation exaggerates a PBH's life expectancy by 2-3 orders of magnitude. The relevant data is shown in Table 7.1, Figure 7.1, Table 7.2, Table 7.3, and Table 7.4.

Table 7.1. Schwarzschild radius in attometers, mass in megatons, temperature in gigaelectron-volts, power (petawatts), evaporation rate (kg/s), evaporation time (years), power per unit mass (petawatts per megaton) for PBHs. The results shown here are in accord with Crane and Westmoreland [86].

R_S (am)	M (MT)	$k_B T$ (GeV)	P (PW)	P/c^2 (kg/sec)	L (years)	P/M (PW/MT)
0.16	0.108	98.1	5519	61.4	0.04	51101.85185
0.3	0.202	52.3	1527	17	0.12	7559.405941
1	0.673	15.7	129	1.43	5	191.679049
1.5	1.01	10.5	56.2	0.626	16-17	55.64356436
2	1.35	7.85	31.3	0.348	39-40	23.18518519
2.5	1.68	6.28	19.8	0.221	75-80	11.78571429
3	2.02	5.23	13.7	0.152	131-140	6.782178218
6	4.04	2.62	3.26	0.0362	1042-1177	0.806930693
7	4.71	2.24	2.36	0.0262	1661-1903	0.501061571
10	6.73	1.57	1.11	0.0123	4843-5783	0.164933135

MacGibbon [43] has calculated the fractions of total flux, total power, and kinetic energy transported by each particle species.

Table 7.2. Fractions of total power transported by the emitted species, including statistical errors [43].

T (GeV)	Total Power	$p\bar{p}$	$e^{\pm}$	γ	$\nu\bar{\nu}$
0.3	$P_{TOT} = 2.17 \pm 0.05 \times 10^{23}$ s^{-1}	10.23%	20.65%	23.09%	46.03%
	(% of P_{TOT})	(±0.31%)	(±0.47%)	(±0.51%)	(±0.99%)
	Jet Products	10.23%	11.18%	21.37%	30.35%
	(% of P_{TOT})	(±0.31%)	(±0.94%)	(±0.64%)	(±1.34%)
1	$P_{TOT} = 3.03 \pm 0.05 \times 10^{24}$ s^{-1}	8.79%	20.19%	24.14%	46.89%
	(% of P_{TOT})	(±0.19%)	(±0.30%)	(±0.35%)	(±0.66%)
	Jet Products	8.79%	12.14%	22.20%	32.15%
	(% of P_{TOT})	(±0.19%)	(±0.46%)	(±0.42%)	(±0.69%)
10	$P_{TOT} = 3.56 \pm 0.09 \times 10^{26}$ s^{-1}	11.22%	18.71%	24.73%	45.33%
	(% of P_{TOT})	(±0.20%)	(±0.23%)	(±0.25%)	(±0.43%)
	Jet Products	11.22%	12.13%	23.12%	32.86%
	(% of P_{TOT})	(±0.20%)	(±0.59%)	(±0.34%)	(±0.71%)
50	$P_{TOT} = 9.79 \pm 0.28 \times 10^{27}$ s^{-1}	11.36%	18.79%	24.77%	45.08%
	(% of P_{TOT})	(±0.21%)	(±0.30%)	(±0.41%)	(±0.92%)
	Jet Products	11.36%	12.37%	23.26%	33.75%
	(% of P_{TOT})	(±0.21%)	(±0.53%)	(±0.50%)	(±1.22%)
100	$P_{TOT} = 3.91 \pm 0.12 \times 10^{28}$ s^{-1}	11.10%	18.93%	24.70%	45.27%
	(% of P_{TOT})	(±0.17%)	(±0.19%)	(±0.25%)	(±0.52%)
	Jet Products	11.10%	12.37%	23.22%	24.52%
	(% of P_{TOT})	(±0.17%)	(±0.44%)	(±0.36%)	(±0.84%)

Table 7.3. Fractions of total flux transported by the emitted species, including statistical errors [43].

T (GeV)	Flux	$p\bar{p}$	$e^{\pm}$	γ	$\nu\bar{\nu}$
0.3	$\dot{N}_{TOT} = 1.13 \pm 0.02 \times 10^{24}$ GeV^{-1}·s^{-1} (% of $\dot{N}_{TOT}$)	1.75% (±0.04%)	20.62% (±0.23%)	20.33% (±0.23%)	57.30% (±0.49%)
	Jet Products (% of $\dot{N}_{TOT}$)	1.75% (±0.04%)	18.24% (±0.27%)	19.89% (±0.25%)	52.69% (±0.55%)
1	$\dot{N}_{TOT} = 1.05 \pm 0.01 \times 10^{25}$ GeV^{-1}·s^{-1} (% of $\dot{N}_{TOT}$)	1.75% (±0.03%)	20.15% (±0.14%)	20.89% (±0.15%)	58.20% (±0.31%)
	Jet Products (% of $\dot{N}_{TOT}$)	1.75% (±0.03%)	18.89% (±0.16%)	20.35% (±0.16%)	54.13% (±0.37%)
10	$\dot{N}_{TOT} = 3.89 \pm 0.08 \times 10^{26}$ GeV^{-1}·s^{-1} (% of $\dot{N}_{TOT}$)	2.18% (±0.03%)	19.62% (±0.13%)	22.19% (±0.14%)	56.01% (±0.28%)
	Jet Products (% of $\dot{N}_{TOT}$)	2.18% (±0.03%)	19.25% (±0.13%)	22.00% (±0.20%)	44.06% (±0.29%)
50	$\dot{N}_{TOT} = 4.28 \pm 0.09 \times 10^{27}$ GeV^{-1}·s^{-1} (% of $\dot{N}_{TOT}$)	2.30% (±0.02%)	19.64% (±0.09%)	22.09% (±0.09%)	55.97% (±0.19%)
	Jet Products (% of $\dot{N}_{TOT}$)	2.30% (±0.02%)	19.49% (±0.09%)	22.02% (±0.10%)	55.59% (±0.19%)
100	$\dot{N}_{TOT} = 1.12 \pm 0.03 \times 10^{28}$ GeV^{-1}·s^{-1} (% of $\dot{N}_{TOT}$)	2.37% (±0.02%)	19.63% (±0.09%)	23.13% (±0.10%)	55.88% (±0.21%)
	Jet Products (% of $\dot{N}_{TOT}$)	2.37% (±0.02%)	19.50% (±0.44%)	22.07% (±0.11%)	55.59% (±0.21%)

Table 7.4. Average kinetic energies in GeV of the emitted species, including statistical errors [43].

T (GeV)	$p\bar{p}$	$e^{\pm}$	γ	$\nu\bar{\nu}$
0.3	0.190 (±0.001)	0.192 (±0.001)	0.219 (±0.001)	0.155 (±0.001)
1	0.515 (±0.001)	0.289 (±0.001)	0.335 (±0.001)	0.238 (±0.001)
10	3.781 (±0.001)	0.872 (±0.002)	1.021 (±0.001)	0.741 (±0.001)
50	10.340 (±0.023)	2.187 (±0.009)	2.565 (±0.013)	1.843 (±0.018)
100	15.450 (±0.040)	3.367 (±0.006)	3.899 (±0.005)	2.829 (±0.012)

A convincingly comprehensive discussion of the thermal nature of the Hawking flux has been offered by Visser [87].

7.3 PBH Absorption of Incident Radiation

Neglecting any interaction with Hawking radiation, the de Broglie wavelength of an incoming particle needs to be comparable to the Schwarzschild radius, in order to have a significant probability of being absorbed by a PBH. For a wavelength of, for instance, 1 am, this corresponds to an energy of 1.24 TeV.

Absorption probabilities are being considered in the rest frame of the PBH near (and specifically outside of) the event horizon. This follows from the WKB approximation approach used (and discussed) by R. Sini and V. Kuriakose in [88] and by R. Sini, N. Varghese, and V. Kuriakose in [89]. The discussion here is based on this approach also. The non-relativistic Planckian spectrum is given by

$$B_\lambda(T) = \frac{2hc^2}{\lambda^5}\left(\frac{1}{\exp\left(\frac{hc}{\lambda k_B T}\right) - 1}\right), \tag{7.5}$$

where k_B is the Boltzmann Constant.

For the G-type star and a 1 am PBH, $\log\left(B_{10^{-18}\,\mathrm{m}}\left(T \approx 5778\,\mathrm{K}\right)\right) \approx -10^{12}$. Of the approximately 10^{62} photons emitted to date by the sun, confidently, none have had sufficiently short wavelengths to be absorbed by a PBH. From Wien's Law, the temperature required to emit radiation dominated by 10^{-18} m photons is approximately 10^{15} K; the CMB was at this temperature during the Quark Epoch of the Radiation Era (10^{-10} s after the Big Bang).

Since the electric charge of an attometer-sized PBH would be radiated away in a time that is much shorter than the evaporation time [90], the Schwarzschild metric is apropos. Additionally, if fermions are considered as the particles incident upon the horizon of a PBH, the relativistic particle shower in which the PBH would be engulfed, would constitute a high intensity Dirac field.

7.3.1 *The Dirac Field in Schwarzschild Spacetime*

For convenience and clarity, $\hbar = c = k_B = 1$. The Schwarzschild metric, in spherical coordinates, is given by

$$ds^2 = \left(1 - \frac{1}{r}\right)dt^2 - \frac{dr^2}{\left(1 - \frac{1}{r}\right)} - r^2 d\theta^2 - r^2 \sin^2\theta d\phi^2. \tag{7.6}$$

The Schwarzschild horizon is located at $r = 1$ (the location of the singularity). For incident particles, the relevant region for absorption is $r \to 1$. In curved spacetime, the Dirac equation is

$$\left(i\gamma^a e_a^\mu \left(D_\mu + \Gamma_\mu\right) + m\right)\psi = 0, \tag{7.7}$$

where $D_\mu = \partial_\mu - \frac{i}{4}\omega_\mu^{ab}\sigma_{ab}$ is the covariant derivative for fermion fields, e_a^μ is the vierbein given by eq. (7.8), $\sigma_{ab} = \frac{i}{2}[\gamma_a, \gamma_b]$ is the commutator of the Dirac matrices, and ω_μ^{ab} are the spin correction components.

$$e_a^\mu = \begin{pmatrix} f^{-\frac{1}{2}} & 0 & 0 & 0 \\ 0 & f^{\frac{1}{2}}\sin\theta\cos\phi & r^{-1}\cos\theta\cos\phi & -r^{-1}\csc\theta\sin\phi \\ 0 & f^{\frac{1}{2}}\sin\theta\sin\phi & r^{-1}\cos\theta\sin\phi & -r^{-1}\csc\theta\cos\phi \\ 0 & f^{\frac{1}{2}}\cos\theta & -r^{-1}\sin\theta & 0 \end{pmatrix} \tag{7.8}$$

Eq. (7.9) specifies the spin.

$$\Gamma_\mu = \frac{1}{2}\left[\gamma^a, \gamma^b\right] e_a^\nu e_{b\nu;\mu}, \tag{7.9}$$

where γ_a are the Dirac matrices, $e_{b\nu;\mu} = \partial_\mu e_{b\nu} - \Gamma_{\nu\mu}^\kappa e_{b\kappa}$ is the covariant derivative of $e_{b\nu}$, and $\Gamma_{\nu\mu}^\kappa$ are the Christoffel symbols.

It can be shown that the Dirac radial equation for a spherically symmetric solution of a stationary spacetime metric is

$$\frac{d^2G}{dx^2}+\left[\frac{d}{dx}\left(\frac{f^{\frac{1}{2}}}{1+\lambda f^{\frac{1}{2}}}\frac{k}{r}\right)-\frac{f}{\left(1+\lambda f^{\frac{1}{2}}\right)^2}\left(\frac{k}{r}\right)^2+\varepsilon^2\left(\frac{1-\lambda f^{\frac{1}{2}}}{1+\lambda f^{\frac{1}{2}}}\right)\right]G=0, \tag{7.10}$$

where G is the fermion field function. From $f=\rho^2$:

$$\frac{d^2G}{dx^2}+\left[\frac{d}{dx}\left(\frac{\rho}{1+\lambda\rho}\frac{k}{r}\right)-\frac{\rho^2}{(1+\lambda\rho)^2}\left(\frac{k}{r}\right)^2+\varepsilon^2\left(\frac{1-\lambda\rho}{1+\lambda\rho}\right)\right]G=0 \tag{7.11}$$

Using the convenient substitution $dx=\frac{1+\lambda\rho}{\rho^2}dr$ and the relationship $\lambda=\frac{\mu}{\varepsilon}$, the inverse of the vierbein e_a^μ is [88]

$$\begin{aligned}&\frac{d^2G}{dx^2}+\frac{1}{\rho^2}\frac{d\rho^2}{dr}\frac{dG}{dr}+(1+\lambda\rho)\frac{d}{dr}\left((1+\lambda\rho)^{-1}\right)\frac{dG}{dr}+\\&\left[\frac{1}{\rho^2}\frac{k}{r}\frac{d\rho}{dr}+\left(\frac{1+\lambda\rho}{\rho}\frac{k}{r}\right)\frac{d}{dr}\left(\frac{1+\lambda\rho}{\rho}\right)+\frac{1}{\rho}\frac{d}{dr}\left(\frac{k}{r}\right)-\left(\frac{k}{r}\right)^2\left(\frac{1}{\rho}\right)+\frac{\varepsilon^2}{\rho^4}-\left(\frac{\mu}{\rho}\right)^2\right]G=0\end{aligned}. \tag{7.12}$$

$\Im(G)$ (the radial wave function), obtained through the WKB approximation, contains wave functions for both the incident and reflected waves. For $r\sim1$ (i.e., in the purlieu of the horizon), the interference between incident (the first term in eq. (7.13)) and reflected (the second term in eq. (7.13)) waves is:

$$\Im(G(r))\approx\exp(-i\varepsilon\ln(r-1))+|R|\exp(i\varepsilon\ln(r-1)) \tag{7.13}$$

After completion of a 2π rotation in the complex z-plane, $\Im(G)$ attains the value $\Im(G(r,2\pi))\neq\Im(G)$ on its Riemannian surface.

$$G(r,2\pi) \sim \varsigma \exp(-i\varepsilon \ln(r-1)) + \frac{|R|}{\varsigma} \exp(i\varepsilon \ln(r-1)) \tag{7.14}$$

where $|R|$ is the reflection coefficient, and $\varsigma = \exp(-2\pi\varepsilon) < 1$. Thus, $|R| = \varsigma = \exp(-2\pi\varepsilon)$. Since the wave will either be reflected or absorbed, therefore, $P_{\text{ref}} + P_{\text{abs}} = 1$ and $P_{\text{ref}} = |R|^2$, and thus, $P_{\text{abs}} = 1 - \exp(-4\pi\varepsilon)$. Greater detail can be found by consulting [88]. In terms of the Hawking temperature, T_H, the absorption probability becomes

$$P_{\text{abs}} = 1 - \exp\left(-\frac{\varepsilon}{T_H}\right), \tag{7.15}$$

where ε is the energy of the re-inflating particles.

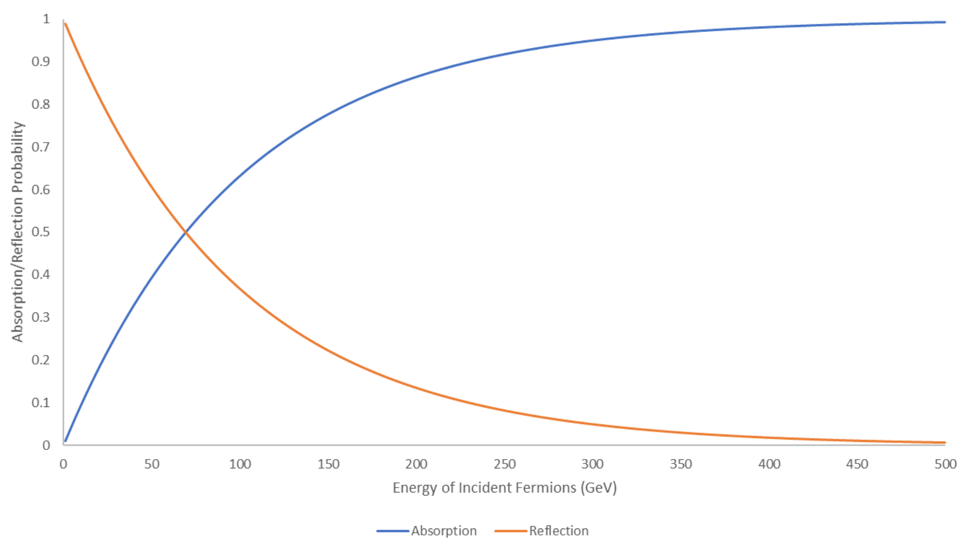

Figure 7.2: Plot of reflection & absorption probabilities as a function of energy for fermions incident upon a 100 GeV PBH. The reflection and absorption probabilities are equal when $\varepsilon = T_H \ln 2$ (about 70 GeV for a 100 GeV PBH).

From Figure 7.2, it is desirable that incident fermions arbitrarily have an energy of at least $5k_B T_H$ and therefore, an absorption probability of 0.9933.

7.3.2 *Position Uncertainty: The Effect on Absorption Probability*

If an incident fermion field of nearly infinite pseudorapidity is considered, the Heisenberg Uncertainty Principle, $Dx \cdot Dp \geq \frac{\hbar}{2}$ (where $\hbar$ is the reduced Planck's constant), significantly increases the required energy of the incident fermions for a given absorption probability. If the incoming fermions have an uncertainty in position of, for instance, $0.1R_S$, the corresponding uncertainty in energy is $DE = \frac{5\hbar c}{R_S} = 20\pi k_B T_H$. For a 1 attometer PBH, this corresponds to $\sim 1\,\mathrm{TeV}$.

In this scenario, in order to have a low reflection probability (< 0.1), incident fermions would need to have a minimum of $(20\pi + 5) k_B T_H \sim 67.8 k_B T_H$. For a reflection probability < 0.01, the required energy is $633.3 k_B T_H$. For a 100 GeV PBH, the incident fermion field would need an average energy of $\sim 63\,\mathrm{TeV}$ which is two orders of magnitude greater than the rest energy of the PBH[4].

7.3.3 *Incident Fermion Flux: Non-interaction*

Clearly, if a PBH were to increase in mass, the rate of energy absorption from incoming particles must exceed the energy loss rate by Hawking radiation. In the simplest approximation, the interaction between the incident radiation field and the Hawking radiation was neglected. However, this simplistic approach significantly underestimates the fermion energy requirement for absorption due to energy losses sustained from scattering and particle annihilation.

[4] This is approximately four times greater than the upper limit of the current energy capability of the Large Hadron Collider (LHC).

7.3.4 *Incident Fermion Flux: Interaction*

The non-interaction model for determining the minimum necessary flux for a PBH to retain its mass does not account for particle-particle interaction between the outgoing Hawking radiation and the incoming radiation field. The most elementary approach to particle interaction is to treat the entire Hawking radiation spectrum as photonic. However, the instantaneous Hawking radiation is composed of $p\bar{p}$, $e^{\pm}$, γ, and $\nu\bar{\nu}$, each particle species contributing substantially to the emergent flux and total power.

A black hole with angular velocity Ω, electric potential V, and surface gravity κ, which emits particles of spin s, charge q, axial quantum number $n\hbar$, absorption probability Γ_s, has a particle emission rate for particles with energies between E and E + dE, per degree of particle freedom given by:

$$\dot{N} = \frac{\Gamma_s dE}{2\pi\hbar}\left[\exp\left(\frac{E - n\hbar\Omega - qV}{\hbar\kappa/2\pi c}\right) - (-1)^{2s}\right]^{-1} \tag{7.16}$$

Since for a PBH, the electric potential goes to zero very rapidly, and most of its lifetime is spent with $\Omega = 0$, eq. (7.16) strongly resembles the thermal emission of a blackbody.

Photons, massless neutrinos, and very low mass neutrinos contribute very high Hawking fluxes at all PBH temperatures. Often, these particles are considered to tunnel quantum mechanically through the event horizon [91]. More specifically, virtual particle pairs are being spontaneously produced, by the gravitational field, in the region of the event horizon [92]. Particle annihilation is prevented if the virtual pair's wavelength (i.e., the separation of the particles) is approximately the Schwarzschild radius. The observed thermal radiation of a black hole is actually a positive-energy particle escaping to infinity after a classically prohibited negative-energy particle quantum mechanically tunnels through the event horizon to the black hole's interior.

The exponential dependency of $\dot{N}$ on the energy assures some contribution of massive species at all energies. A black hole will conserve all of the associated quantum numbers because it acts as a source of any massless gauge group [93], including the SU(3) color gauge field; thus, the emission of both Strongly Interacting Massive Particles (SIMPs) and Weakly Interacting Massive Particles (WIMPs) is expected for temperatures beyond several hundred MeV.

With the obvious exceptions of $p\overline{p}$ and $e^{\pm}$, massive particles are stable only on non-astrophysical timescales, which are nonetheless significantly longer than the time required to travel to the region where they would interact with the incident radiation. For instance, a neutron emitted from a 100 GeV PBH, has a lifetime of approximately 1 day. MacGibbon [43] has shown that when the decay of primary particles is considered, eq. (7.16) becomes

$$\frac{d\dot{N}_X}{dE_{\mathrm{TOT}}} = \sum_j \int_{\mathrm{E_{TOT}}}^{\infty} \frac{\Gamma_j(E,T)}{h}\left[\exp\left(\frac{E}{k_B T_H}\right) - (-1)^{2s_j}\right]^{-1} \cdot \frac{dg_{jX}(E,E_{TOT})}{dE_{TOT}} dE_{TOT}\ , \qquad (7.17)$$

where $\frac{dg_{jX}(E,E_{TOT})}{dE_{TOT}} dE_{TOT}$ is the relative number of particles of species X possessing energy E_{TOT} that are created by particle j with energy E, and $\frac{d\dot{N}_X}{dE_{\mathrm{TOT}}}$ is the instantaneous flux of particles in species X. The purpose of the sum of j is to account for all energy-carrying particle species and their concomitant degrees of freedom.

The de Broglie wavelength λ_B of an interacting particle (hence its effective "size") emitted with an energy equal to the Hawking temperature, is $8\pi^2 R_S$, where R_S is the Schwarzschild radius. If the emissions rate is greater than $\frac{c}{\lambda_B}$, interactions between emitted particles, irrespective of their species, would be expected. Consequently, a PBH would be surrounded by a high-density/high-opacity accretion cloud in the region surrounding the event horizon.

However, Oliensis has shown that less than 0.1% of the emitted particles in the lifetime of a PBH are interacting [94]. Therefore, a PBH's emitted particles are not self-interacting as a result of short-range forces prior to fragmentation. Furthermore, color is irrelevant to the short-range propagation of emitted particles. Thus, a dense cloud of emitted particles does not surround the PBH.

Additionally, relativistic jets of emitted particles are fragmented as a result of $q\bar{q}$ pairs produced in the region $r \sim 1$ of the PBH, with one quark tunneling back to the $r < 1$ region. The color field lines connecting the quark and anti-quark, located in the $r < 1$ and $r > 1$ regions, are compressed into a "conduit-like" length of spacetime. If there is constant linear energy density in the interior of the conduit, the potential energy between the quarks is proportional to their spatial separation. As their separation increases, the potential energy also increases to the value required to produce another $q\bar{q}$ pair, and the color conduit is hewn into two approximately equal length color conduits. This process will continue until the quark and gluon kinetic energies drop below the fragmentation threshold, at which point, color coupling will dominate. This signifies the end of fragmentation and the commencement of hadronization (the grouping of particles into color-singlet states) [95].

If an intense field of relativistic protons is incident upon the horizon of a PBH, multiple interactions with Hawking radiation will occur. Examined here are $p+\nu\bar{\nu}$, $p+p\bar{p}$, $p+e^{\pm}$, and $p+\gamma$ collisions, and their likely effect on the net flux of subsequent incident fermions. While an incident radiation field of any particle species could be considered, protons are selected, and their interactions with all of the emergent Hawking species are described.

Although neutrinos are often treated as non-interacting particles, neutrino-annihilation, neutrino-absorption, and neutrino-nucleon scattering can, in varying degrees, all be confidently expected at the energy levels considered here. Although the formation of an accretion cloud of emitted Hawking particles is not expected, an accretion veil, resulting from the interaction with incident fermions, is anticipated.

7.3.4.1. $\nu\bar{\nu}$ Absorption. Nucleonic absorption of neutrinos and anti-neutrinos results in momentum and energy transfers to the nucleons. Kneller et al. have determined the neutrino-antiproton and neutrino-neutron absorption cross sections to be [96]:

$$\sigma_{\nu n}^{\text{abs}} = \sigma_o\left(\frac{1+3g_A^2}{4}\right)\left(\frac{E_\nu+\Delta}{m_e^2}\right)^2\sqrt{1-\left(\frac{m_e}{E_\nu+\Delta}\right)^2}\,W_M \tag{7.18}$$

$$\sigma_{\bar{\nu}p}^{\text{abs}} = \sigma_o\left(\frac{1+3g_A^2}{4}\right)\left(\frac{E_\nu-\Delta}{m_e^2}\right)^2\sqrt{1-\left(\frac{m_e}{E_{\bar{\nu}}-\Delta}\right)^2}\,W_{\overline{M}}\,, \tag{7.19}$$

where g_A and Δ are the axial-vector coupling constant and the neutron-proton mass difference respectively, and W_M and $W_{\bar{M}}$ are the two weak magnetism corrections [97] given by

$$W_M = 1 + 1.1\frac{E_\nu}{m_n} \tag{7.20}$$

$$W_{\bar{M}} = 1 - 7.1\frac{E_{\bar{\nu}}}{m_n}. \tag{7.21}$$

The rates of total momentum and energy transfer from neutrinos materializing at (θ,φ), $F^{(\mathrm{abs})}$ and $W^{(\mathrm{abs})}$ respectively, per particle, to all nucleonic particles at position (r,z) are

$$F^{(\mathrm{abs})} = \int d\Omega_\nu \left[-\sin\theta\cos\phi\,\hat{i} + \cos\theta\,\hat{k}\right] \int dE_\nu \frac{b(r_\nu, E_\nu)}{4\pi} S_\nu(\theta_\nu,\phi_\nu) E_\nu \sigma_{\nu N}^{(\mathrm{abs})} \tag{7.22}$$

$$W^{(\mathrm{abs})} = \int d\Omega_\nu \int dE_\nu \frac{b(r_\nu, E_\nu)}{4\pi} S_\nu(\theta_\nu,\phi_\nu) E_\nu \sigma_{\nu N}^{(\mathrm{abs})}, \tag{7.23}$$

where $b(r_\nu, E_\nu)$ is the differential neutrino flux per unit area that derives from radial coordinate r_ν in the frame of the accretion disk.

The momentum transfer occurs in the $\hat{k}'$ direction. The basis vectors transformations are

$$\hat{i}' = -\cos\theta\cos\phi\,\hat{i} - \sin\theta\cos\theta\,\hat{j} - \sin\theta\,\hat{k}, \tag{7.24}$$

$$\hat{j}' = \sin\phi\,\hat{i} - \cos\phi\,\hat{j}, \tag{7.25}$$

and

$$\hat{k}' = -\sin\theta\cos\phi\,\hat{i} - \sin\theta\sin\phi\,\hat{j} + \cos\theta\,\hat{k}. \tag{7.26}$$

7.3.4.2. $\nu\bar{\nu}$ Annihilation. The energy density deposition rate $\frac{dL_{\nu\bar{\nu}}}{dV}$, for the annihilation of neutrino-antineutrino pairs into electron-positron pairs, is independent of the polar angle.

$$\begin{aligned}\frac{dL_{\nu\bar{\nu}}}{dV} &= \int\int d\Omega_\nu d\Omega_{\bar{\nu}} \int\int dE_\nu dE_{\bar{\nu}} \frac{b(r_\nu, E_\nu) b(r_{\bar{\nu}}, E_{\bar{\nu}})}{16\pi^2} S_\nu(\theta_\nu, \phi_\nu) S_{\bar{\nu}}(\theta_{\bar{\nu}}, \phi_{\bar{\nu}}) \\ &\times \frac{E_\nu + E_{\bar{\nu}}}{E_\nu E_{\bar{\nu}}} \left\{ E_\nu E_{\bar{\nu}} \left| \mathrm{v}_\nu - \mathrm{v}_{\bar{\nu}} \right| \sigma_{\nu\bar{\nu}} \right\}\end{aligned} \tag{7.27}$$

where $b(r_{\bar{\nu}}, E_{\bar{\nu}})$ is the differential neutrino flux per unit area that emerges from radial coordinate $r_{\bar{\nu}}$ in the frame of the accretion disk. $\left\{ E_\nu E_{\bar{\nu}} \left| \mathrm{v}_\nu - \mathrm{v}_{\bar{\nu}} \right| \sigma_{\nu\bar{\nu}} \right\}$ is a Lorentz invariant, which is most easily determined in the center of mass frame of the accretion disk, and then articulated in terms of *s*, the Mandelstam variable.

Herrera et al. have calculated the annihilation cross section, which allows eq. (7.27) to be evaluated [98].

$$E_\nu E_{\bar{\nu}} \left| \mathrm{v}_\nu - \mathrm{v}_{\bar{\nu}} \right| \sigma_{\nu\bar{\nu}} = \frac{\sigma_o s^2}{48 m_e^2} \sqrt{1 - \frac{4m_e^2}{s}} \left[2\left(C_V^2 + C_A^2\right) + \frac{4m_e^2}{s}\left(C_V^2 - 2C_A^2\right) \right] \tag{7.28}$$

where $C_V = \frac{1}{2} + 2\sin^2\theta_W$, $C_A = \frac{1}{2}$, $\sigma_o = \frac{4G_F^2 m_e^2}{\pi\hbar^4}$, and $\theta_W = \cos^{-1}\frac{m_W}{m_Z}$ is the Weinberg Angle. $S_\nu(\theta_\nu, \varphi_\nu) = \Theta(a_\nu - r_\nu) + \Theta(r_\nu - a_\nu)\sec\theta_\nu$ and $S_{\bar{\nu}}(\theta_{\bar{\nu}}, \varphi_{\bar{\nu}}) = \Theta(a_{\bar{\nu}} - r_{\bar{\nu}}) + \Theta(r_{\bar{\nu}} - a_{\bar{\nu}})\sec\theta_{\bar{\nu}}$ are the corrections to the neutrino and antineutrino differential number fluxes per unit area, respectively and which account for neutrino and antineutrino trapping occurring within the optically thick and optically thin zones of the disk. Θ is the Heaviside function, and a_ν and $a_{\bar{\nu}}$ are the neutrino and antineutrino radial boundaries, respectively.

For stellar mass black holes, a_ν and $a_{\bar{\nu}}$ have values from several 10s to several 100s of km [96]. Due to the significantly smaller radial boundaries in a PBH, neutrino and antineutrino trapping within the accretion disk is expected to be greatly reduced, and the contributions of $S_\nu\left(\theta_\nu, \varphi_\nu\right)$ and $S_{\bar{\nu}}\left(\theta_{\bar{\nu}}, \varphi_{\bar{\nu}}\right)$ are likely inconsequential.

7.3.4.3. $\nu\bar{\nu}$ Scattering. Momentum and energy transfer, due to the scattering of neutrinos and antineutrinos by protons within the incident fermion field, are given by

$$F = \int d\Omega_\nu \left[-\sin\theta\cos\phi\,\hat{i} + \cos\theta\,\hat{k}\right]\int dE_\nu \frac{b(r_\nu, E_\nu)}{4\pi} S_\nu(\theta_\nu, \phi_\nu)\int d\Omega'_\nu\, p_{k'} \frac{d\sigma}{d\Omega'_\nu} \qquad (7.29)$$

$$W = \int d\Omega_\nu \int dE_\nu \frac{b(r_\nu, E_\nu)}{4\pi} S_\nu(\theta_\nu, \phi_\nu)\int d\Omega'_\nu T \frac{d\sigma}{d\Omega'_\nu}, \qquad (7.30)$$

where $p_{k'} = \dfrac{E_\nu\left(E_\nu + M\right)\left(1-\cos\theta_{\nu'}\right)}{M + E_\nu\left(1-\cos\theta_{\nu'}\right)}$, and $T = \dfrac{E_\nu^2\left(1-\cos\theta_{\nu'}\right)}{M + E_\nu\left(1-\cos\theta_{\nu'}\right)}$.

The mass of the scattered particle, in this case a proton, is *M*. The neutrino is scattered at angle $\theta_{\nu'}$, measured with respect to basis vector $\hat{k}'$ (see Figure 7.3). The momentum transfer is always independent of the mass of the scattered particle and is approximately equal to the neutrino energy.

In the event that $M >> E_\nu$, the energy transfer is negligible. However, as Table 7.4 shows, the energy of emitted neutrinos and antineutrinos for a 100 GeV PBH is 2.829

GeV (~3 times the proton rest mass). Consequently, the energy transfer from $\nu\bar{\nu}$ scattering is not insignificant.

The differential cross section for neutrino-proton scattering is [99]:

$$\frac{d\sigma_{\nu p}}{d\Omega_\nu} = \frac{\sigma_o}{16\pi}\left(\frac{E_\nu}{m_e}\right)^2 \left[(C_V - 1)^2 + 3g_A^2 (C_A - 1)^2\right]\left(1 + \delta_p \cos\theta'_\nu\right), \tag{7.31}$$

where $\delta_p = \dfrac{(C_V - 1)^2 - g_A^2 (C_A - 1)^2}{(C_V - 1)^2 + 3g_A^2 (C_A - 1)^2}$.

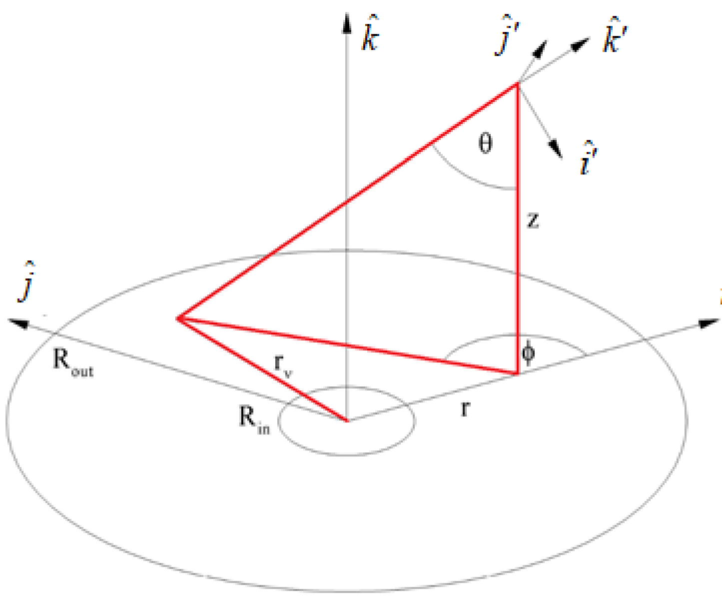

Figure 7.3: Basis vectors, distances and angles for neutrino absorption and scattering. The singularity is at the origin. R_{out} and R_{in} refer to the outer and inner accretion disk radii respectively. *i*' is within the same plane as θ. [96]

7.3.4.4. Critical Density. It is clear that the energy deposition resulting from neutrino-antineutrino annihilation into electron-positron pairs, as well as the scattering of neutrinos, will impede the flux of nucleons inbound to the PBH. Fryer & Mészáros [100] suggest the following approach to the problem of a differential mass element, beginning at infinity, approaching a stellar mass black hole. This approach is also valid for a fermion field incident upon a PBH. A region of the field with density ρ will experience a gravitational force F_g. It will further experience a force resulting from neutrino annihilation $F_{\nu\bar{\nu}}$ and from both scattering and absorption F_ν.

Since the fermion field emerges from infinity (i.e., $r >> 1$), the change in a mass element's kinetic energy between infinity and a height *z* is

$$\frac{1}{2}\rho v^2(z) = \int_z^\infty dz\left(F_g + F_\nu + F_{\nu\bar{\nu}}\right). \qquad (7.32)$$

The gravitational force is

$$F_G = \frac{-G_N M_{\mathrm{SK}}\rho}{z^2}. \qquad (7.33)$$

The force responsible for the neutrino-antineutrino annihilation acceleration is

$$F_{\nu\bar{\nu}} = \frac{1}{c}\frac{dL_{\nu\bar{\nu}}}{dV}. \qquad (7.34)$$

The force responsible for the acceleration due to both neutrino-antineutrino scattering and absorption is

$$F_\nu = n_n\left(F_n^{(\mathrm{abs})} + F_{n\nu} + F_{n\bar{\nu}}\right) + n_p\left(F_p^{(\mathrm{abs})} + F_{p\nu} + F_{p\bar{\nu}}\right) + n_e\left(F_{e\nu} + F_{e\bar{\nu}}\right), \qquad (7.35)$$

where n_i are the number densities. In the case of atomic matter falling into a black hole, $n_p = n_e$ and $\rho = \left(n_n + n_p\right)m_u$; m_u is the atomic mass unit.

Fryer & Mészáros [100] introduce a neutron fraction, *Y*, given by

$$Y = \frac{n_n}{n_n + n_p}. \quad (7.36)$$

Consequently, eq. (7.35) becomes

$$F_\nu = \frac{\rho}{m_u}\left[YF_n + (1-Y)(F_p + F_e)\right], \quad (7.37)$$

where F_n, F_p and F_e are the total momentum transfer rates.

Since F_G and F_ν are functionally dependent on ρ, there must exist a value of $\rho = \rho_0$ at which

$$\int_z^\infty dz\left(a_g + a_\nu + a_{\nu\bar{\nu}}\right) = 0 \quad (7.38)$$

$$\rho_0 = \frac{\int_z^\infty dz \frac{1}{c}\frac{dL_{\nu\bar{\nu}}}{dV}}{\int_z^\infty dz\left[\frac{G_N M_{SK}}{z^2} - \frac{YF_n + (1-Y)(F_p + F_e)}{m_u}\right]}. \quad (7.39)$$

If $\rho < \rho_0$, an incoming mass element will be ejected at a height greater than *z*. If $\rho = \rho_0$, an incoming mass element will be ejected at *z*. However, if $\rho > \rho_0$, the mass element will continue past *z*. Kneller et al. [96] have named the maximum value of ρ_0, the critical density ρ_*.

Material with a density greater than the critical density cannot be neutrino- or antineutrino-ejected at any value of *z* and is therefore accreted into the black hole.

In the case of a proton radiation field, incident upon a PBH, $F_n = F_e = 0$, $F_p = 1$, and $Y = 0$. Eqs. (7.37) and (7.39) reduce to

$$F_\nu = \frac{\rho}{m_u} \tag{7.40}$$

and

$$\rho_o = \frac{\int_z^\infty dz \frac{1}{c} \frac{dL_{\nu\bar{\nu}}}{dV}}{\int_z^\infty dz \left[\frac{G_N M_{\text{PBH}}}{z^2} - \frac{1}{m_u} \right]}, \tag{7.41}$$

respectively. Using the Schwarzschild radius and infinity as limits of integration guarantees that $p\nu$ and $p\bar{\nu}$ interactions will not prevent protons from being accreted into the PBH. Thus,

$$\rho_o = \frac{\int_{R_S}^\infty dz \frac{1}{c} \frac{dL_{\nu\bar{\nu}}}{dV}}{\int_{R_S}^\infty dz \left[\frac{G_N M_{\text{PBH}}}{z^2} - \frac{1}{m_u} \right]}. \tag{7.42}$$

7.3.4.5. pp and $p\bar{p}$ Scattering. An intense fermion radiation field will strongly resemble a highly collimated, incident beam of nearly infinite pseudorapidity protons, and will undergo hard scattering with the protons emerging as Hawking radiation. Since the effective radius of all of these protons is less than the Schwarzschild radius (and much less than the classical proton radius), the interaction is best represented as collisions between the constituent partons.

The cross-section calculation consists of terms containing the partonic scatter cross section $\hat{\sigma}$, and the parton density functions $f_{i,p}$, and is given by [101]

$$\sigma(pp \to X) = \sum_{i,j} \int dx_1 dx_2 \, f_{i,p}\left(x_1, \mu_F^2\right) f_{i,p}\left(x_2, \mu_F^2\right) \hat{\sigma}_{ij \to X}\left(x_1 x_2 s, \mu_R^2, \mu_F^2\right). \tag{7.43}$$

The sum over *i* and *j* is to account for all initial-state partons with longitudinal momentum fractions x_1 and x_2, capable of giving rise to the final state *X* whose center of mass energy is $\sqrt{x_1 x_2 s}$. μ_R^2 and μ_F^2 are the factorization scales, which are recovered from truncations of the expansion of the strong coupling constant, and which yield universal parton densities at a given resolution.

Parton-parton scattering is arguably by far, the most frequent hadron collision process that would occur between a fermion radiation field and Hawking radiation protons. Shortly after being collisionally created (and in many cases, prior to reaching the horizon), hard partons would continuously radiate low-energy collinear gluons as a *parton shower*.

If a high energy scattering of two protons occurs at a significant distance from the event horizon of the PBH, the emitted high-energy parton will reach distances from the proton constituents which are much larger than the constituents' effective radii; as a result, an increase in the QCD force would occur. Radiation of continuously softer gluons, at small angles relative to the initial parton, will likely continue.

When this occurs in a weak gravitational field (i.e., at $r > 1$), eventually, a non-perturbative transition would form color-neutral hadrons as a result of parton binding. A reasonably well-collimated hadron jet would ensue; its total energy and momentum would be comparable to the original scattered parton. If this process remains applicable in the vicinity of the horizon (i.e., $r \to 1$), then relatively little energy loss by incoming protons would be expected. Most of the incident energy would be transported by the posthadronisation hadronic jet. The acollinearity effect resulting from the emission of soft gluons reduces the probability of further collisions. However, if the extreme gravitation gradient in the $r \to 1$ region prevents parton binding, and consequently color-neutral hadrons do not form, an uncollimated parton shower could be accreted in the spacetime region surrounding the horizon.

The Compact Muon Solenoid experiment at the LHC produced hadron collisions with a double-differential inclusive jet cross section between approximately 10^{-2} and 10^{7} pb/GeV for $200 \le p_T\left(\text{GeV}\right) \le 1000$, $L = 34\ \text{pb}^{-1}$, $\sqrt{s} = 7\ \text{TeV}$, and $2.5 \le |y| < 1562.5$ [101].

The scattering picture for proton-antiproton collisions is exceptionally similar. The collision cross section is:

$$\sigma\left(p\bar{p} \to X'\right) = \sum_{i,j} \int dx_1 dx_2\, f_{i,p}\left(x_1, \mu_F^2\right) f_{i,\bar{p}}\left(x_2, \mu_F^2\right) \hat{\sigma}_{ij \to X'}\left(x_1 x_2 s, \mu_R^2, \mu_F^2\right), \tag{7.44}$$

In low-gravity environments, the cross sections for proton-antiproton collisions with $\sqrt{s} \gtrsim 100$ GeV are approximately equal [102]. Low energy ($\sqrt{s} \lessapprox 10$ GeV) proton-proton collisions have cross sections which are 2-3 times smaller than equivalent-energy proton-antiproton collision cross sections.

7.3.4.6. $pe^{\pm}$ *Scattering.* The above-discussed proton field will experience deep inelastic scattering with Hawking radiation electrons and positrons. This results in electron-quark fusion creating resonance peaks in the electron-proton collision cross sections, and potentially, hypothetical scalar leptoquark (LQ) isodoublet production. Considered here is the reaction:

$$e^{\pm} + q \rightarrow \gamma + LQ, \tag{7.45}$$

which comes from

$$e^{\pm} + p \rightarrow \gamma + LQ + X, \tag{7.46}$$

in which the LQ interacts with only the first-generation fermions.

The integrated cross section of the electron-proton collision is determined by convoluting the differential cross sections of the hard subprocesses with the related parton density functions [103]:

$$\sigma(s) = \int_{x_{\min}}^{1} dx q\left(x, Q^2\right) \int_{-1}^{1} d\cos\vartheta_\gamma \cdot \frac{d\hat{\sigma}\left(\hat{s}, \cos\vartheta_\gamma\right)}{d\cos\vartheta_\gamma} \cdot \Theta_{\text{cuts}}\left(E_\gamma, \vartheta_\gamma\right), \tag{7.47}$$

where q is a constituent quark of a targeting proton, $\hat{\sigma}$ is the cross section of eq. (7.46), $q\left(x, Q^2\right)$ is the quark distribution function, the 4-momentum transfer scale is $Q^2 = \hat{s}$, $\hat{s} = xs$, ϑ_γ is the photon emission angle relative to the proton beam, and $\Theta_{\text{cuts}}\left(E_\gamma, \vartheta_\gamma\right)$ accounts for the necessary kinematical cuts. Since eq. (7.45) is infrared divergent, $E_\gamma > E_\gamma^0 > 0$.

A Monte Carlo simulation with $E_\gamma^0 = 1\,\text{GeV}$ (equivalent to the $e^{\pm}$ energy radiated from a 10 GeV PBH), a photon emission angle cut of $\vartheta_\gamma^{\min} < \vartheta_\gamma < \vartheta_\gamma^{\max}$, a center of mass energy of 1740 GeV (corresponding to a 7.6 TeV proton beam), an electron energy of 100 GeV (much greater than the $e^{\pm}$ energy radiated from any considered PBH), and an integrated luminosity of 1 fb^{-1} [103] does not imply that the formation of leptoquarks would dissipate significant energy of incident protons. Even less proton field energy should be dispelled toward leptoquark formation when incident upon a 100 GeV PBH because the center of mass energy for a ~7.6 TeV proton field would be ~320 GeV.

7.3.4.7. $p\gamma$ Scattering. $p\gamma$ scattering in the vicinity of a PBH is likely to be diffractive and in the form of $\gamma p \to \gamma X$. Perturbative calculations of the scattering cross section at large *t* and extreme energies $\left(W^2 >> |t| >> \Lambda_{\mathrm{QCD}}^2\right)$ exceed the $\frac{J}{\Psi}$ photoproduction cross section and are therefore considered here. The complete scattering cross section is [104]

$$\frac{d\sigma(\gamma q \to \gamma q)}{dt} = \frac{\left|A_{(+,+)}\right|^2 + \left|A_{(+,-)}\right|^2}{16\pi s^2}, \tag{7.48}$$

where the amplitudes $A_{(+,+)}$ and $A_{(+,-)}$ are

$$A_{(+,+)} = i\frac{6}{9}\alpha_{em}\alpha_s^2 \frac{4\pi}{3}\frac{s}{|t|}\int d\nu \frac{\nu^2}{\left(\frac{1}{4}+\nu^2\right)^2}\left(\frac{\frac{11}{4}+3\nu^2}{1+\nu^2}\right)\left(\frac{\tanh(\pi\nu)}{\pi\nu}\right)\left(\frac{s}{|t|}\right)^{\omega(\nu)} \tag{7.49}$$

and

$$A_{(+,-)} = i\frac{6}{9}\alpha_{em}\alpha_s^2 \frac{4\pi}{3}\frac{s}{|t|}\int d\nu \frac{\nu^2}{\left(\frac{1}{4}+\nu^2\right)^2}\left(\frac{\frac{1}{4}+\nu^2}{1+\nu^2}\right)\left(\frac{\tanh(\pi\nu)}{\pi\nu}\right)\left(\frac{s}{|t|}\right)^{\omega(\nu)}. \tag{7.50}$$

$$\omega(\nu) = \frac{3\alpha_s}{\pi}\left[2\Psi(1) - \Psi\left(\frac{1}{2}+i\nu\right) - \Psi\left(\frac{1}{2}-i\nu\right)\right] \tag{7.51}$$

Saddle point approximations for eqs. (7.49) and (7.50) yield

$$A_{(+,+)} = \frac{528}{27} i\alpha_{em}\alpha_s^2 \frac{s}{|t|}\left(\frac{\pi}{7\varsigma(3)\eta}\right)4^{\eta} \tag{7.52}$$

and

$$A_{(+,-)} = \frac{48}{27} i\alpha_{em}\alpha_s^2 \frac{s}{|t|}\left(\frac{\pi}{7\varsigma(3)\eta}\right)^{\frac{3}{2}} 4^{\eta}, \tag{7.53}$$

where

$$\eta \equiv \frac{6}{\pi}\alpha_s \ln\left(\frac{s}{|t|}\right), \tag{7.54}$$

and $\varsigma(\nu)$ is the Riemann zeta function; *t* is the squared momentum transfer. A more detailed explanation can be found in [104]. A Vector Dominance Model numerical simulation performed by Ivanov and Wusthoff [104] showed

$$\frac{d\sigma(\gamma)}{dt} \approx 7.5nb\exp\left(-5.3|t| \text{ GeV}^{-2}\right). \tag{7.55}$$

For the case of Hawking photons emitted from a 100 GeV PBH which scatter off an incident 2 TeV proton field, extrapolation of the Ivanov and Wusthoff simulation data yields a cross section of approximately 8.2 pb. If a 7.6 TeV proton field (as considered in the $p\gamma$ Scattering section) is incident, the cross section is approximately 3.6 pb.

7.3.4.8. Interaction Summary. The above analyses of interaction processes and scattering cross sections of incident fermions and PBH Hawking radiation have phenomenologically shown scattering cross sections that are significantly smaller than the available Schwarzschild targeting cross section $\left(4\pi R_S^2\right)$. For TeV proton fields incident upon a 100 GeV PBH, the Schwarzschild targeting cross section is four orders of magnitude larger than the proton-gamma-ray interaction cross section.

However, Hawking particle fluxes range from $10^{26} – 10^{28}$ GeV^{-1}·s^{-1} for a 100 GeV PBH (Table 7.3). If equivalent incident fluxes are isotropically distributed across 2π sr of the horizon, the interaction cross section can increase volumetrically by as much as 26-28 orders of magnitude, yielding a "volumetric" cross section of potentially 100 Tb - 10 Pb. In this event, a [relatively] enormous accretion cloud would surround the PBH. The approximately equivalent stellar scale would be an accretion disk 30,000 AU - 300,000 AU in radius surrounding a $10M_\odot$ black hole[5].

7.4 Extrapolation to Planck-scale PBHs

While the flux of Hawking radiation from Planck-scale PBHs is uncertain, if a Hawking spectrum exists, it can be taken to consist of particles with the Planck energy $\sqrt{\frac{\hbar c^5}{8\pi G_N}} \sim 2.43\times10^{18}\ \mathrm{eV}$. At the Planck time prior to evaporation, the PBH temperature is the Planck temperature $T_P = \sqrt{\frac{\hbar c^5}{G_N k_B^2}} \sim 1.42\times10^{32}\ \mathrm{K}$. In this context, eq. (7.15) becomes

$$P_{\text{abs}} = 1 - \exp\left(-\frac{\varepsilon}{T_P}\right). \tag{7.56}$$

However, it is not entirely clear that a Hawking spectrum will exist for a Planck-sized PBH because Hawking radiation is, of course, a semi-classically derived quantity. Without a full quantum approach, it is unclear whether the role of gravitons, which account for only ~2% of the Hawking radiation energy at the attometer scale [43], would

[5] These radii are the distances from the sun to the Spherical Oort Cloud and Outer Oort Cloud, respectively.

be significant at the Planck scale. The lack of a complete quantum theory of gravity precludes a definitive conclusion.

Since no incident particles can have energy in excess of the Planck energy, the maximum absorption probability from eq. (7.56), discounting the interaction with Hawking radiation, is $1-\exp(-1) \sim 0.63$.

While the final evaporation state of a PBH remains unresolved, the expected time required for a Planck-sized black hole to evaporate is the Planck time. Therefore, only photons reaching the horizon at the Planck time would have a non-zero probability of being absorbed before total evaporation.

Although it is unclear if Hawking radiation would be produced by a Planck-sized PBH, if Hawking radiation does persist until final PBH evaporation, then all particles reaching the horizon would first have to traverse the emergent Hawking radiation efflux which would likely be exclusively Planck-energy gamma rays. If the incident particles are fermions, then the intense parton showers from previous collisions, and energy dissipation from scattering and annihilation of many incoming particles would be expected. Thus, much of the incoming radiation, even particles with the Planck energy, will be subject to a reduction in energy by means of collisions and scattering with both the expelled Hawking radiation and the resulting quark- and gluon-rich accretion cloud. Therefore, in this interactive model, it is not expected that many particles could arrive in the vicinity of the PBH horizon with the Planck energy.

However, even if Hawking radiation shuts down by the time the PBH reaches the Planck scale, and even if the sparseness of the expelled Hawking flux is significant [87] allowing the incoming radiation to arrive with the Planck energy, all incoming particles would still be incident upon a horizon with a Schwarzschild radius rapidly approaching the Planck length. Therefore, even the non-interactive absorption probability would certainly be less than 1. Although, since the absorption probability is asymptotic toward zero, absorption of incident particles by the PBH cannot be entirely ruled out. Thus, even though relatively low energy particles have an exceedingly negligible chance of being absorbed by a PBH approaching the Planck scale, the absorption probability is not exactly zero. Consequently, for their Planck time lifetimes, Planck-sized PBHs best approximate white holes, in so far as their near 1 scattering probability is concerned. However, a totally opaque collisionally-produced accretion cloud will not occur, particularly if there is a cessation of Hawking radiation at the Planck length and if the expelled Hawking shower is sparse. Therefore, a state of "absolute whiteness" of PBHs is just not possible.

7.5 Summary

The Hawking radiation spectrum of attometer PBHs has been described, and the non-interactive absorption probability of incident fermions was discussed. Although the non-interactive absorption probability of incident fermions by a PBH is not insignificant, the probability of a fermion incident on the horizon being absorbed is substantially smaller when the interaction with Hawking radiation is considered.

When the Schwarzschild radius of a PBH is extrapolated to the Planck length, even incident fermions with the Planck energy have only an extremely negligible chance of absorption due to any degree of opacity of the surrounding accretion cloud and the need to cross the intervening distance in the Planck time and be incident upon a target of the Planck length. Subsequently, as PBHs evaporate and their Schwarzschild radii approach the Planck length, they asymptotically mimic white holes. However, the scattering-probability-equal-to-one characteristic of a white hole is never actually achieved by a PBH.

The consequence of Hawking radiation not being emitted at the precise location of the event horizon of a Schwarzschild PBH [87] is unlikely to alter the upshot of the argument that as PBHs approach the Planck scale, they increasingly mimic white holes, but never actually achieve total whiteness. A more confident picture of pp, $p\bar{p}$, $pe^{\pm}$, $p\gamma$, and $p\nu\bar{\nu}$ interactions involving quark-gluon scattering in the purlieu of the horizon of a Planck-sized or near Planck-sized PBH awaits further developments in Quantum Gravity.

REFERENCES

[1] "On the Electrodynamics of Moving Bodies," *Annalen der Physik,* vol. 17, pp. 891-921, 1905.

[2] W. Thomson, *Wave Theory Of Light (A Lecture Delivered At The Academy Of Music),* Philadelphia, PA, 1884.

[3] R. Lévi, "Théorie de l'action universelle et discontinue," *Phys. Radium,* vol. 8, no. 4, pp. 182-198, 1927.

[4] D. Amati, M. Ciafaloni and G. Veneziano, "Classical and Quantum Gravity Effects from Planckian Energy Superstring Collisions," *International Journal of Modern Physics A,* vol. 3, no. 7, pp. 1615-1661, 1988.

[5] D. Amati, M. Ciafaloni and G. Veneziano, "Higher-order gravitational deflection and soft bremsstrahlung in planckian energy superstring collisions," *Nuclear Physics B,* vol. 3, no. 31, pp. 550-580, 1990.

[6] D. Amati, M. Ciafaloni and G. Veneziano, "Superstring collisions at planckian energies," *Physics Letters B,* vol. 197, no. 1-2, pp. 81-88, 1987.

[7] D. J. Gross and P. F. Mende, "String theory beyond the Planck scale," *Nuclear Physics B,* vol. 3, no. 4, pp. 407-454, 1988.

[8] W. Pauli, Wissenschaftlicher Briefwechsel mit Bohr, Einstein, Heisenberg u.a., K. v. Meyenn, Ed., 1940.

[9] J. Kowalski–Glikman, "Introduction to Doubly Special Relativity," *arxiv.org/pdf/hep-th/0405273*, 29 May 2004.

[10] J. Magueijo and L. Smolin, "Generalized Lorentz invariance with an invariant energy scale," *Phys. Rev. D,* vol. 67, no. 044017, 2003.

[11] J. Cortes and J. Gamboa, "Quantum Uncertainty in Doubly Special Relativity," *Phys. Rev. D,* 2005.

[12] A. N. Tawfik and A. M. Diab, "Review on Generalized Uncertainty Principle," *arXiv:1509.02436 [physics.gen-ph],* 2015.

[13] G. Amelino-Camelia, "DOUBLY-SPECIAL RELATIVITY: FIRST RESULTS AND KEY OPEN PROBLEMS," *International Journal of Modern Physics D,* vol. 11, no. 10, pp. 1643-1669, 2002.

[14] F. Scardigli, "Generalized uncertainty principle in quantum gravity from micro-black hole gedanken experiment," *Physics Letters B,* vol. 452, no. 1-2, pp. 39-44, 1999.

[15] A. Einstein, *Jahrbuch der Radioaktivit¨at und Elektronik,* vol. 4, no. 411, 1907.

[16] M. Planck, *Ann. Physik,* vol. 26, no. 1, 1908.

[17] H. Ott, *Z. Physik,* vol. 175, no. 70, 1963.

[18] H. Arzelies, *Nuovo Cim.,* vol. 35, no. 792, 1965.

[19] C. Møller, *Det. Kong. Danske Videnskab. Selskab. Mat.-Fys. Medd.,* vol. 36, no. 1, 1967.

[20] P. Landsberg, *Nature,* vol. 212, no. 571, 1966.

[21] P. Landsberg, *Nature,* vol. 214, no. 903, 1967.

[22] P. Landsberg and K. John, *Ann. Phys.,* vol. 56, no. 299, 1970.

[23] P. Landsberg, *Europ. J. Phys.,* vol. 2, no. 203, 1981.

[24] M. van Laue, "Die Relativitaetstheorie," *Vieweg,* vol. I, 1951.

[25] R. Tolman, Relativity, Thermodynamics and Cosmology, New York: Dover , 1987.

[26] M. Requardt, "Thermodynamics meets Special Relativity – or what is real in Physics?," *arXiv:0801.2639 [gr-qc],* 2008.

[27] M. Przanowski and J. Tosiek, 2011. [Online]. Available: arXiv:1010.5701v2. [Accessed 4 November 2013].

[28] E. Bormashenko, "Entropy of Relativistic Mono-Atomic Gas and Temperature Relativistic Transformation in Thermodynamics," *Entropy,* vol. 9, pp. 113-117, 2007.

[29] D. Cubero, J. Casado–Pascual, J. Dunkel, P. Talkner and P. Hanggi, *Phys. Rev. Lett.,* vol. 99, 2007.

[30] M. Kardar, Statistical Physics of Particles, New York: Cambridge University Press, 2007.

[31] S. Costa and G. Matsas, "Temperature and relativity," *Physics Letters A*, vol. 209, pp. 155-159, 1995.

[32] P. Landsberg and G. Matsas, "Laying the ghost of the relativistic temperature transformation," *Physics Letters*, vol. A223, p. 401–403, 1996.

[33] P. Landsberg and G. Matsas, "The impossibility of a universal relativistic temperature transformation," *Physica A Statistical Mechanics and its Applications*, vol. 340, p. 92–94, 2004.

[34] R. Aldrovandi and J. Gariel, "On the riddle of the moving thermometers," *Physics Letters A*, vol. 170, pp. 5-10, 1992.

[35] K. Schwarzschild, "Über das Gravitationsfeld eines Massenpunktes nach der Einsteinschen Theorie," *Sitzungsberichte der Königlich Preussischen Akademie der Wissenschaften,* vol. 7, pp. 189-196, 1916.

[36] S. Hawking, "Black hole explosions?," *Nature,* vol. 248, pp. 30-31, 1974.

[37] Y. Zel'dovitch and I. Novikov, "The Hypothesis of Cores Retarded During Expansion and the Hot Cosmological Model," *Soviet Astronomy,* vol. 10, no. 4, pp. 602-603, 1966.

[38] T. Harada, C. Yoo and K. Khori, "Threshold of primordial black hole formation," *Physical Review D,* vol. 88, no. 8, p. 084051, 2013.

[39] A. Kashlinsky, "LIGO gravitational wave detection, primordial black holes and the near-IR cosmic infrared background anisotropies," *The Astrophysical Journal,* vol. 823, no. 2, p. L25, 2016.

[40] H. Niikura, M. Takada, N. Yasuda and et al., "Microlensing constraints on primordial black holes with Subaru/HSC Andromeda observations," *Nature Astronomy,* vol. 3, pp. 524-534, 2019.

[41] J. Scholtz and J. Unwin, "What If Planet 9 Is a Primordial Black Hole?," *Phys. Rev. Lett.,* vol. 125, p. 051103, 2020.

[42] J. MacGibbon and B. Webber, "Quark and gluon jet emission from primordial black holes: The instantaneous spectra," *Phys. Rev. D,* vol. 41, pp. 3052-3079, 1990.

[43] J. MacGibbon and B. Webber, "Quark- and gluon-jet emission from primordial black holes. II. The emission over the black-hole lifetime," *Physical Review D.,* vol. 44, no. 2, pp. 376-392, 1991.

[44] I. Novikov, *Soviet Encyclopedia,* p. 180, 1988.

[45] "Kruskal–Szekeres coordinates," April 2021. [Online]. Available: www.wikipedia.org. [Accessed June 2021].

[46] N. McGill, "The Apparent Shape of Rapidly Moving Objects in Special Relativity," *Contemp. Phys.,* vol. 9, no. 1, pp. 33-48, 1968.

[47] W. Mückenheim, "Is Lorentz Contraction Observable?," *Annales de la Fondation Louis de Broglie* , vol. 17, no. 3, pp. 351-354, 1992.

[48] J. Terrell, "The Terrell Effect," *Am. J. Phys.,* vol. 57, no. 1, pp. 9-10, 1989.

[49] E. Baird, "Ruler-Changes and Relative Velocity," *arXiv:physics/9807015v2 [physics.ed-ph],* August 1998.

[50] L. Barbado, C. Barceló, L. Garay and G. Jannes, "The trans-Planckian problem as a guiding principle," *arXiv:1109.3593v2 [gr-qc],* November 2011.

[51] S. Giddings, "Black hole production in TeV-scale gravity, and the future of high energy physics," *In the Proceedings of Snowmass. arXiv:0110127 [hep-ph],* 2001.

[52] M. H. Johnson and E. Teller, "Intensity changes in the Doppler effect," in *Proc. Natl. Acad. Sci.*, 1982.

[53] T. K. Nakamura, "Lorentz Transform of Black Body Radiation Temperature," *EPL,* vol. 88, no. 2, October 2009.

[54] E. Veitsman, "Stefan-Boltzmann's Law under Relativistic Conditions; Generalized Case," *Universal Journal of Physics and Application,* vol. 4, no. 1, pp. 380-391, 2013.

[55] M. Przanowski, "Heat,temperature and relativity," *Acta Physicae Superficierum*, vol. XI, no. 43, 2009.

[56] K. Mosengeil, *Ann. Physik,* vol. 22, no. 876, 1907.

[57] W. Pauli, *Relativitatstheorie, Teubner,* 1921.

[58] M. Laue, *Die Relativitatstheorie, Friedrich Vieweg und Sohn,* 1921.

[59] P. T. Landsberg and G. E. Matsas, "Laying the ghost of the relativistic temperature transformation," *arXiv:physics/9610016v1 [physics.gen-ph],* October 1996.

[60] P. Landsberg, *Europ. J. Phys.,* vol. 2, no. 208, 1981.

[61] T. K. Nakamura, "Covariant Thermodynamics of an Object with Finite Volume," 30 April 2005. [Online]. Available: arXiv:physics/0505004v1 [physics.class-ph]. [Accessed 6 September 2016].

[62] G. Rybicki and A. Lightman, Radiative Processes in Astrophysics, John Wiley & Sons, 1979.

[63] T. Bracewell and E. Conklin, "An observer moving in the 3 k radiation field," *Nature,* vol. 219, pp. 1343-1344, 1968.

[64] G. Henry, R. Feduniak, J. Silver and M. Peterson, "Distribution of blackbody cavity radiation in a moving frame of reference," *Phys. Rev.,* vol. 176, no. 5, p. 1451–1455, 1968.

[65] P. Peebles and D. Wilkinson, "Comment on the anisotropy of the primeval fireball," *Phys. Rev.,* vol. 174, no. 5, p. 2168, 1968.

[66] H. Weaver, "The Visibility of Stars Without Optical Aid," *Publications of the Astronomical Society of the Pacific,* vol. 59, no. 350, p. 233, 1947.

[67] G. A. de Parga, A. Á. Vargas and B. López-Carrera, "On a Self-Consistency Thermodynamical Criterion for Equations of the State of Gases in Relativistic Frames," *Entropy,* vol. 2013, no. 15, pp. 1271-1288, April 2013.

[68] W. Widger and M. Woodall, "Integration of the Planck blackbody radiation function," *Bulletin of the Am. Meteorological Society,* vol. 57, no. 10, pp. 1217-1219, October 1976.

[69] H. F. Weaver, "The Visibility of Stars without Optical Aid," *Publications of the Astronomical Society of the Pacific,* vol. 59, no. 350, pp. 232-243, 1947.

[70] E. P. Johnson and N. R. Bartlett, "Effect of Stimulus Duration on Electrical Responses of the Human Retina," *Journal of the Optical Society of America,* vol. 46, no. 3, pp. 167-170, 1956.

[71] B. E. Schaefer, "Astronomy and the Limits of Vision," *Vistas in Astronomy,* vol. 36, no. 4, p. 311–361, 1993.

[72] D. Hughes, "On Seeing Stars Especially up Chimneys," *Quarterly Journal of the Royal Astronomical Society,* vol. 24, no. 3, pp. 246-257, 1983.

[73] B. E. Schaefer, "Glare and Celestial Visibility," *Publications of the Astronomical Society of the Pacific,* vol. 103, no. 665, pp. 645-660 , 1991.

[74] P. Hallett, "Quantum efficiency of dark–adapted human vision," *J Opt Soc Am A,* vol. 4, pp. 2330-2335, 1987.

[75] O. Packer and D. R. Williams, The Science of Color, S. K. Shevell, Ed., Kidlington Oxford: Optical Society of America, 2003.

[76] C. Starr, C. A. Evers and L. Starr, Biology: Concepts and Applications, Thomson Brooks/Cole, 2006.

[77] N. Balasanyan and V. Mkrtchian, "Blackbody radiation drag on a relativistically moving mirror," *arXiv:0907.2311v1,* jULY 2009.

[78] Z. Wu, "Inverse Temperature 4-vector in Special Relativity," [Online]. Available: arXiv:0804.3827v4. [Accessed 12 November 2013].

[79] C. Møller, The Theory of Relativity, Oxford : Oxford University Press, 1972.

[80] L. Landau and E. Lifshitz, Fluid Mechanics, Oxford: Pergamon Press, 1959.

[81] L. Landau and E. Lifshitz, Theory of Elasticity, Oxford: Pergamon Press, 1970.

[82] S. Weinberg, Gravitation and Cosmology: Principles and Applications of the General Theory of Relativity, New York: John Wiley & Sons, Inc., 1972.

[83] C. Møller, Thermodynamics in the Special and the General Theory of Relativity, Academic Press, 1968, pp. 202-221.

[84] A. Staruszkiewicz, *Acta Phys. Polon.,* vol. 29, no. 249, 1966.

[85] H. Callen and G. Horwitz, *Am. J. Phys.,* vol. 39, no. 938, 1971.

[86] L. Crane and S. Westmoreland, "ARE BLACK HOLE STARSHIPS POSSIBLE?," *arXiv:0908.1803 [gr-qc]* , 12 August 2009 Last Accessed: 13th October 2013.

[87] M. Visser, "Thermality of the Hawking Flux," *arXiv:1409.7754v3 [gr-qc],* May 2015.

[88] R. Sini and V. Kuriakose, "Absorption cross section and Emission spectra of Schwarzschild black hole in Dirac field.," *Mod. Phys. Lett.,* vol. A, no. 23, pp. 2867-2879, 2008.

[89] R. Siri, N. Varghese and V. Kuriakose, "Absorption Cross-Section of Reissner-Nordstrom and Schwarzschild-De Sitter Extremal Black Hole," *IJMPA,* no. 23, pp. 4011-4021, 2008.

[90] V. P. Frolov and I. D. Novikov, Black Hole Physics: Basic Concepts and New Developments, Kluwer Academic Publishers, 1997, p. 398.

[91] S. Hawking, *Sci. Am.,* vol. 236, no. 34, 1977.

[92] N. Birrell and P. Davies, "Quantum Fields in Curved Space," *Cambridge University Press,* p. 263, 1982.

[93] M. Perry, *Phys. Lett.,* vol. 71B, no. 234, 1977.

[94] J. Oliensis and T. Hill, *Phys. Lett.,* vol. 143B, no. 92, 1984.

[95] F. Halzen and A. Martin, Quarks and Leptons: An Introductory Course in Modern Particle Physics, New York: Wiley, 1984.

[96] J. Kneller, G. McLaughlin and R. Surman, "Neutrino Scattering, Absorption and Annihilation above the accretion disks of Gamma Ray Bursts," *arXiv:astro-ph/0410397v1* , 2008 Last Accessed: 13th October 2013.

[97] C. Horowitz, "Weak magnetism for antineutrinos in supernovae," *arXiv:astro-ph/0109209,* vol. 65, 9 October 2001 Last Accessed: 13th October 2013.

[98] M. Herrera and S. Hacyan, *ApJ,* vol. 336, no. 539, 1989.

[99] A. Burrows, S. Reddy and T. A. Thompson, "NEUTRINO OPACITIES IN NUCLEAR MATTER," *arXiv:astro-ph/0404432,* 2004 Last Accessed: 13th October 2013.

[100] C. Fryer and P. Mészáros, *ApJ,* vol. 588, no. L25, 2003.

[101] J. M. Butterworth, G. Dissertori and G. P. Salam, "Hard Processes in Proton-Proton Collisions at the Large Hadron Collider," *arXiv:1202.0583* , 2 February 2012 Last Accessed: 13th October 2013.

[102] R. Godbole, A. Grau, G. Pancheri and Y. Srivastava, "Hunting for asymptotia at LHC," *Phys. Rev. D.,* vol. 72, no. 076001, 2005.

[103] V. Ilyin, A. Pukhov and V. Savrin, "Single leptoquark production associated with hard photon emission in ep collisions at high energies," *arXiv:hep-ph/9503401v2 Last Accessed: 13th October 2013,* 17 May 1995.

[104] D. Y. Ivanov and M. Wusthoff, "Hard diffractive Photon-Proton Scattering at large t," *Eur. Phys. J*, vol. C8, pp. 107-114, 1999.